# “Structural analysis and aggregation of Alzheimer’s disease related pyroglutamate-modified amyloid-β”

Inaugural-Dissertation

zur Erlangung des Doktorgrades

der Mathematisch-Naturwissenschaftlichen Fakultät

der Heinrich-Heine-Universität Düsseldorf

vorgelegt von

**Christina Dammers**

aus Würselen

Düsseldorf, September 2015

aus dem Institut für Physikalische Biologie

der Heinrich-Heine-Universität Düsseldorf

Gedruckt mit der Genehmigung der
Mathematisch-Naturwissenschaftlichen Fakultät der

Heinrich-Heine-Universität Düsseldorf

Referent: Prof. Dr. Dieter Willbold

Korreferent: Prof. Dr. Henrike Heise

Tag der mündlichen Prüfung: 21.10.2015

## Table of Contents

## List of figures

## Abbreviations

| | |
|---|---|
| aa | amino acid |
| AD | Alzheimer's disease |
| Aβ | amyloid-β |
| apoE4 | apolipoprotein E4 |
| APP | amyloid precursor protein |
| BBB | blood brain barrier |
| CD | circular dichroismus |
| CSF | cerebrospinal fluid |
| CT | computed tomography |
| ELISA | enzyme linked immunosorbent assay |
| fAD | familiar Alzheimer's disease |
| LPR | lipoprotein receptor-related protein |
| MRI | magnetic resonance imaging |
| NFT | neurofibrillary tangles |
| NMR | nuclear magnetic resonance |
| pE | pyroglutamate |
| pEAβ | pyroglutamate-modified amyloid-β |
| PET | positron emission tomography |
| PHF | paired helical filament |
| PiB | Pittsburgh compound B |
| PSEN | presenilin |
| QC | glutaminyl cyclase |
| sAD | sporadic Alzheimer's disease |
| SEC | size exclusion chromatography |
| sFIDA | surface based fluorescence intensity distribution assay |
| SFs | straight filaments |
| TEM | transmission electron microscopy |
| TFE | 2,2,2-trifluoroethanol |
| ThT | thioflavin-T |

## Zusammenfassung

Die Alzheimer-Krankheit ist eine neurodegenerative Erkrankung, deren Symptome durch eine fortschreitende Abnahme der kognitiven Funktionen gekennzeichnet sind. Sie gilt als Hauptursache für Demenz. Toxische extrazelluläre Amyloid-β (Aβ) Plaques gehören zur Pathologie der Alzheimer Krankheit. N-terminal modifiziertes Pyroglutamat Aβ (pEAβ) gilt als eine wichtige Spezies im Gehirn von Alzheimer-Erkrankten.

Im Rahmen dieser Arbeit wurde eine reproduzierbare Methode für die Expression und Reinigung rekombinanter Pyroglutamat-modifizierter Amyloid-β (pEAβ) Peptide entwickelt. Es war möglich, die N-Terminal modifizierten Peptide sowohl in mit als auch ohne $^{13}$C- und $^{15}$N-Isotopenanreicherung zu gewinnen. Die durch die Umsetzung zu Pyroglutamat chemische Änderung der Peptide wurde mittels RP-HPLC und Massenspektrometrie überprüft. pEAβ(3-40) und pEAβ(3-42) wurden auf ihr Aggregationsverhalten hin untersucht und zeigten eine für amyloidogene Peptide typische sigmoidale Aggregationskinetik. Mittels heteronuklearer multidimensionaler NMR Spektroskopie war es möglich die Resonanzen des Proteinrückgrates unter annähernd physiologischen Bedingungen zuzuordnen und mit dem nicht-modifiziertem Aβ zu vergleichen.

Der strukturelle Unterschied zwischen Aβ und den Pyroglutamat-modifizierten Varianten wurde weiterhin in Gegenwart des sekundärstrukturinduzierendem Lösungsmittels Trifluorethanol (TFE) charakterisiert. Im Gegensatz zu Aβ(1-40) und Aβ(1-42) bilden beide korrespondierenden pEAβ-Peptide in TFE mikroskopisch sichtbare gedrehte Fibrillen und große amyloidogene Aggregate aus. Außerdem zeigen die pEAβ Peptide eine sigmoidale Aggregationskinetik unter Bedingungen bei denen die nicht-modifizierten Aβ peptide keine fibrillären Strukturen ausbildet. Zirkulardichroismus (CD) Daten zeigen, dass die Tendenz zur Bildung von β-Faltblättern in TFE für pEAβ im Vergleich zum nicht-modifiziertem Aβ stark erhöht ist. So wurde mittels CD beobachtet, dass pEAβ, unter Bedingungen bei denen der Aβ ausschließlich α-helikale Strukturen zeigt, β-Faltblätter bildet. Die Sekundärstrukturanalyse auf Basis der NMR Daten zeigte allerdings ausschließlich lösliche jedoch instabile α-helikale Monomere, welche innerhalb weniger Stunden aggregierten. Es ist möglich, dass pEAβ TFE induzierte transiente α-Helices bildet, die einen Übergangszustand zu β-Faltblättern und daraus folgenden Fibrillen darstellen. Da die Bildung zu Pyroglutamat die chemische Verschiebung der N-Terminalen Aminosäuren bis zu Histidin13 / Histidin14 beeinflusst, gibt es Grund zu der Annahme, dass der veränderte Aminoterminus die TFE-induzierte Aggregation begünstigt oder sogar initiiert.

Es konnten Einblicke bezüglich des strukturellen Unterschiedes basierend auf der N-terminalen Modifizierung zu Pyroglutamat gemacht werden. Die Charakterisierung der pEAβ Peptide und ihr erhöhtes Aggregationspotenzial ist ein wichtiger Schritt für die Erforschung der Alzheimer-Demenz - vor allem im Hinblick auf die Entwicklung neuer Biomarker und therapeutischer Ansätze.

Aus diesem Grunde wurde rekombinantes pEAβ(3-42) genutzt, um das Aβ-bindende D-enantiomere Peptid D3 und sein tandem-Derivat D3D3 *in vitro* zu charakterisieren. Zusätzliche *in vivo* Studien zeigten die Wirksamkeit beider D-Peptide in pEAβ(3-42) exprimierenden transgenen Mäusen. D3 und D3D3 konnten die im Zusammenhang mit pEAβ induzierte Fortschreitung des neurodegenerativen Phänotyps signifikant verzögern und sind somit vielversprechende Kandidaten für eine medikamentöse Behandlung der Alzheimer-Demenz.

## Abstract

Alzheimer's disease (AD) is a neurodegenerative disorder characterized by a progressive decline of cognitive functions and has become the main cause for dementia in the elderly. Toxic extracellular amyloid-β (Aβ) plaques belong to the pathology of AD. N-terminally truncated pyroglutamate-modified Aβ (pEAβ) has been identified as a major compound of Aβ species in AD brains.

The first well working expression and purification system for reproducible production of pEAβ isoforms is presented within this thesis. pEAβ(3-40) and pEAβ(3-42) were obtained in natural abundance as well as $^{13}C$ and $^{15}N$ isotopically enriched in qualities and quantities to perform reproducible biophysical studies. The chemical state of the purified protein was evaluated by RP-HPLC and formation of pyroglutamate was verified by mass spectroscopy. Recombinant pEAβ(3-40) and pEAβ(3-42) were characterized by ThT assay and showed typical sigmoidal aggregation kinetics. Heteronuclear multidimensional NMR spectroscopy was performed to assign sequence specific backbone resonances of the pEAβ peptides under near-physiological conditions at neutral pH.

The structural difference between Aβ and the pyroglutamate-modified variant was investigated in the presence of the helix inducing co-solvent trifluoroethanol (TFE). In contrast to Aβ(1-40) and Aβ(1-42), both corresponding pEAβ peptides build twisted fibrils and large amyloidogenic aggregates in aqueous TFE solution shown by transmission electron microscopy (TEM). Aggregation kinetics of pEAβ variants were drastically increased compared to the non-modified Aβ as monitored by ThT assays. Although analysis of secondary structure obtained by NMR data suggests, that Aβ as well as pEAβ form mainly soluble monomers characterized by α-helices in two regions connected by a flexible linker, these monomers were shown to be unstable and prone to aggregate resulting in an accumulation into fibrils. Additional NMR and CD data indicate an increased tendency to build β-sheet structures for pEAβ(3-42) and pEAβ(3-40) in TFE when compared to the corresponding non-truncated variant under exactly the same conditions. There is evidence that pEAβ(3-42) builds TFE-induced transient α-helices as a precursor to β-sheet formation and fibrillation in the presence of TFE. Moreover, the pyroglutamate modification affects the N-terminal amino acid residues up to H13/H14 what are in fact roughly 30 % of the overall amino acids indicating that the altered N-terminus promotes TFE-induced aggregation.

Based on this study, we could expose the knowledge of the structural difference of pyroglutamate-modified Aβ peptides and their aggregation behavior. However, there is need to further characterize and define the altered properties of pEAβ peptides especially with regard to its usage as new biomarkers and therapeutic approaches.

Recombinant pEAβ(3-42) was used to characterized the effect of D3 and its head to tail tandem derivative D3D3 *in vitro*. Additionally *in vivo* studies in a pEAβ(3-42) expressing transgenic mouse model indicated the efficiency of D3 and D3D3. Treatment with both peptides showed to significantly slow down pEAβ-related progression of the neurodegenerative phenotype of transgenic mice. Thus, the D-enantiomeric peptides D3 and D3D3 are promising candidates for treatment and therapy of AD.

# 1 Introduction

## 1.1 Alzheimer's disease

More than a 100 years ago, Alzheimer's disease (AD) was discovered for the first time as a presenile dementia in 1906 by the German psychiatric Alois Alzheimer (Alzheimer 1907). AD is defined as a neurodegenerative disorder characterized by a progressive decline of cognitive functions.

AD is a common disease and the risk for any person of developing is approximately 10 - 12 % (Bird 1993, last revision 2014, Alzheimer's Association 2015). In 2013, nearly 44 million people suffered from dementia and 4.6 million new cases were predicted to arise every year reaching 81.1 million by 2040 (Prince *et al.* 2013, Alzheimer's Disease International 2015). AD has become the main cause of dementia with an accounting up to 70 %, which makes it an emerging social health issue (Anand *et al.* 2012, Galimberti *et al.* 2012, Alzheimer's Association 2015). AD is most common in Western Europe with North America close behind and is known to be the most represented disability in the elderly. It is mainly diagnosed in people whose ages are over 65 and the prevalence increases stepwise up to 50 % at the age of 85 (Weuve *et al.* 2014, Zhao *et al.* 2014). Interestingly, independent of age, the estimated lifetime risk for AD is almost doubled for woman (Alzheimer's Association 2015).

### 1.1.1 Familiar and sporadic Alzheimer's disease

AD has been classified into two types: First, the gene-related familiar Alzheimer's disease (fAD) affecting less than 1 % of all AD patients (Eckert *et al.* 2003). 95 % of all fAD cases are late-onset starting at an age above 65 and the remaining 5 % are early-onset starting at an age below 65 (Woo *et al.* 2011). Mutations in the amyloid precursor protein (APP), presenilin (PSEN) 1 and PSEN2 genes play a central role in early-onset autosomal AD by altering APP processing or increasing production and therefore aggregation and accumulation of the AD related protein amyloid-β (Aβ) (Bertram *et al.* 2010). Apolipoprotein E4 (apoE4) was identified as the top late-onset gene with extremely high confidence linked to late-onset fAD and sporadic AD (sAD), the second type of AD. sAD represents the majority of all AD cases and is mostly influenced by non-genetic environmental factors and only partly by genetics (Duara *et al.* 1993, Gatz *et al.* 2006, Bird 2008). No particular cause could be determined for sporadic AD so far, but it is resumed

to be a multifactorial disease including the influence of genetic factors, vascular changes, head injury, low educational levels, diabetes mellitus or metabolic disorders (Iqbal *et al.* 2010, Morris *et al.* 2014, Reitz *et al.* 2014). However, the process of aging has been identified as the biggest risk factor (Iqbal *et al.* 2010, Imtiaz *et al.* 2014). The combination of these risk factors with the presence of apoE4 raises the risk for late-onset AD and age-related cognitive decline (Caselli *et al.* 2011).

### 1.1.2 Clinical course of Alzheimer's disease

The clinical course of AD is differentiated into three stages: preclinical AD, the stage of mild cognitive impairment and severe dementia. The symptoms of AD vary among individuals and the progression of the disease. One of the initial symptoms is the decreased ability to remember new information resulting in a decline of memory, apathy and depression (Alzheimer's Disease International 2014, Alzheimer's Association 2015). Later symptoms include poor judgment and impaired communication as well as disorientation and confusion. In final stages of the disease, individuals experience difficulties in speaking, swallowing and walking (Alzheimer's Association 2015). Typically, clinical duration of AD lasts for eight to ten years (Bird 1993, last revision 2014). The patient's death results from general inanition, malnutrition and pneumonia rather than from AD itself due to the symptoms of severe dementia (Alzheimer's Association 2015). According to the Alzheimer's association, one in three elderly people dying in a given year have been diagnosed with dementia making AD to a highly topical issue in an aging society (Alzheimer's Disease International 2013, Alzheimer's Association 2015).

Although no clear symptoms are present in preclinical AD, pathological changes occur such as first deposits of Aβ and/or the tau protein in the cerebrospinal fluid (CSF) in the brain which could be already measurable (Budson and Solomon 2012; Sperling and Johnson 2013; Riedel 2014). Recent reports indicate that these changes are likely to occur more than 20 years before the first noticeable clinical symptoms indicating mild cognitive impairment.

## 1.2 Neuropathology

As shown in figure 1a, the brains of AD patients are distinguished from healthy brains by an extensive decrease in overall brain volume based on the shrinkage and loss of neuronal processes (Huang *et al.* 2012). Another macroscopic characteristic in AD brains is the cerebral atrophy present in the hippocampus and the cortex which is increased sixfold compared to healthy normal aging individuals (Fox *et al.* 2000, Fotuhi *et al.* 2009).

AD is characterized by two pathological hallmarks, the intracellular neurofibrillary tangles (NFT) consisting of insoluble hyperphosphorylated tau and the extracellular amyloid plaques built by amyloid-β deposits (Figure 1b) (McKhann *et al.* 1984). Additional evidenced for AD are selective neuronal degeneration, neurotransmitter deficits and inflammations (Mucke 2009).

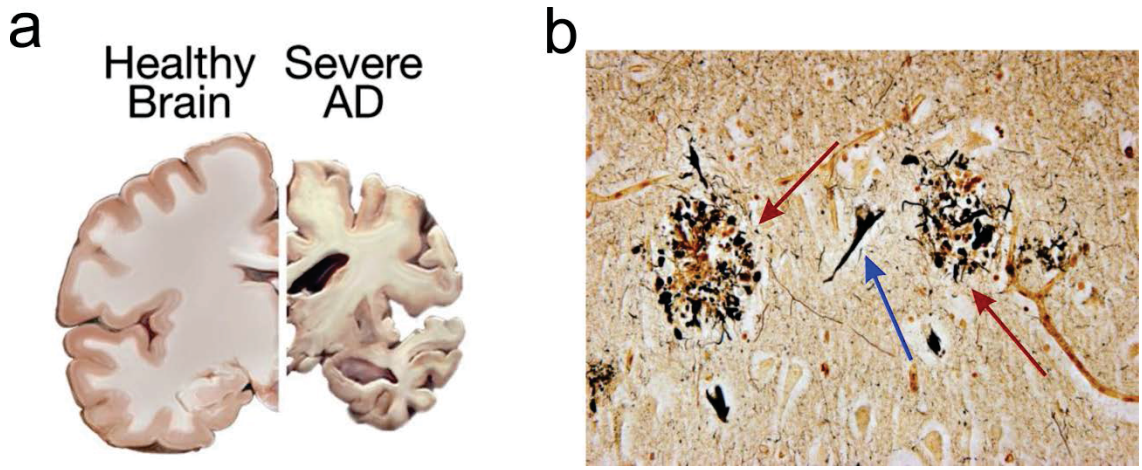


**Figure 1 Neuropathology of Alzheimer's disease**. (A) Brain of a healthy individual compared to the brain of an AD patient with severe dementia where the total brain volume is significantly shrunken (National Institute of Aging 2015). (B) Photomicrograph of the temporal cortex of an AD patient (modified Bielschowski stain; original magnification, 400×). Two senile plaques (red arrows) with a neurofibrillary tangle (blue arrow) between them are shown (modified according to (Perl 2010)).

### 1.2.1 Intracellular neurofibrillary tangles

NFT's are consisting of insoluble forms of the tau protein generated by alternative splicing of the microtubule-associated protein tau. The intrinsically unstructured protein normally binds to microtubules for stabilization of the axonal transport of neurons and interacts with the plasma membrane and nucleic acids (Avila *et al.* 2004, Zilka *et al.* 2009). Although phosphorylation-modified tau protein stabilizes the axonal microtubules in the central nervous system, further post-translational modifications particularly hyperphosphorylation as well as nitration and glycosylation were identified to be involved in tau misfolding and aggregation (Flaherty *et al.* 2000, Mendieta *et al.* 2005, Haas 2012). In AD, 40% of tau is hyperphosphorylated resulting in a changed conformation. Abnormal phosphorylated tau loses its biological activity, dissociates from microtubule and is prone to self-assembly (Chen *et al.* 2004, Mendieta *et al.* 2005). The more NFT are built, the less soluble tau remains for microtubule binding resulting in impaired stability and disrupted axonal transport (Trojanowski *et al.* 2005, Xu *et al.* 2010). Misfolded tau reduces microtubule

binding and therefore axonal trafficking is decreased contributing to neuropathology (Haas 2012). Tau self-assemblies form straight filaments (SFs) and/or paired helical filaments (PHF) accumulating to intracellular fibrils leading to NFT, which incidence is significantly correlated with the severity of AD. It has been shown, that β-sheets are the most dominant structure in PHFs (Zhao *et al.* 2014); electron microscopy revealed the appearance of two strands with a repeat of 75-80 nm and a width of 10-22 nm twisting around each other (Crowther *et al.* 1985, Friedhoff *et al.* 2000).

### 1.2.2 Extracellular plaques

The second characteristic pathology of AD besides intracellular NFTs are toxic extracellular deposits. These amyloid plaques are mainly composed of Aβ with an overall size ranging from 5 to 200 µM in diameter. Amyloid plaques are mainly located in *cortex cerebri, hippocampus* and in the limbic system of AD patients (Hutton *et al.* 1997). Nonetheless, these extracellular plaques can be found in low density in persons not suffering from AD symptoms (Selkoe 1997). Amyloid plaques are differed into two types: the senile plaques, also called neuritic plaques, and diffuse plaques. Diffuse plaques consist of amorphous, non-fibrillar structures of Aβ-deposits and are supposed to be the precursor of other amyloid plaques. Senile plaques contain Aβ fibrils mixed with non-fibrillar accumulations of the peptide. Moreover, microglia and astrocytes can be found in senile but not in diffuse plaques (Selkoe 1999). Senile plaques are furthermore classified into compact plaques mainly consisting of Aβ fibrils with a dense central core and non-compact so called primitive plaques without any core (Cruz *et al.* 1997, Dickson 1997). The classical senile plaque is a few microns in diameter and consists of a compact core and an outer zone with Aβ, active astrocytes and microglia and degenerative axons (Dickson 1997).

## 1.3 Amyloid-β

Extracellular amyloid plaques result from the aggregation of Aβ, generated by the cleavage of the APP by secretases. Although several studies have identified the biological and physiological relevance of APP in neurite outgrowth modulation, copper homeostasis regulation and synaptic transmission, formation and activity, its precise function is still not defined (Bellingham *et al.* 2004, Herard *et al.* 2006, Priller *et al.* 2006, Hoe *et al.* 2009). Under physiological conditions, APP is processed by α-secretases inside the Aβ domain leading to the formation of non-amyloidogenic fragments (Weidemann *et al.* 1989, Turner *et al.* 2003). In AD, Aβ is generated by the cleavage of APP via β- and γ-secretases

(Figure 2). The β-secretase cleaves extracellularly at a specific position of Aβ whereas the γ-secretase has multiple cleavage sites within the APP sequence resulting in Aβ peptides varying in their C-terminal length and their susceptibility to aggregate (Haass *et al.* 1993, De Strooper 2010). Additional heterogeneity is based on posttranslational modifications mediated by amino peptidases, glutaminyl cyclases, isomerases or modifications including isomerization, phosphorylation or metal-induced oxidation (Milton 2001, Dong *et al.* 2003, De Strooper 2010, Kumar *et al.* 2011). The main variants Aβ(1-40) and Aβ(1-42) were identified to be neurotoxic in AD as well as in Down-Syndrome (Mann *et al.* 1990, Murphy *et al.* 1990, Beyreuther *et al.* 1993).

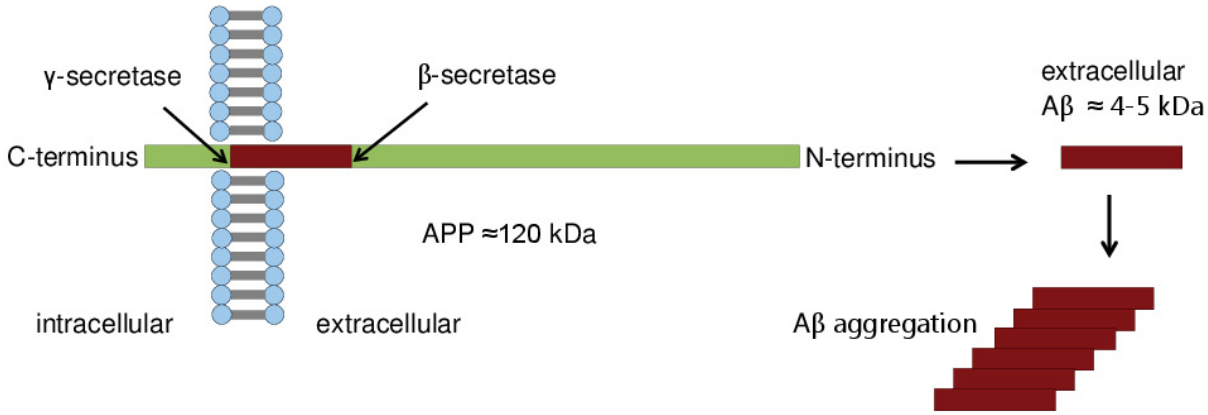


**Figure 2 Amyloidogenic processing of APP and formation of Aβ.** The transmembrane protein APP is extracellularly cleaved by β-secretase and by γ-secretase within the membrane. Generated extracellular Aβ varying in length due to heterogeneity accumulates and starts to aggregate.

The most long-standing explanation of AD development is the amyloid cascade hypothesis. According to this hypothesis, the aggregation of Aβ arises from an imbalance between Aβ clearance and production. The level of Aβ is drastically increased due to mutations or risk factors resulting in Aβ oligomerization (Figure 3). The central amyloidogenic step of the oligomerization process is the transition from unstructured elements into β-sheet rich structures before accumulation into diffuse plaques. Those soluble non-fibrillary assemblies of Aβ (dimers, trimers and larger oligomers) and not insoluble fibrils found in plaques or monomeric Aβ are viewed as the main disease-causing species with the most possessing neurotoxicity (Shankar *et al.* 2008, Benilova *et al.* 2012, Zhao *et al.* 2012, Zhao *et al.* 2014). It was shown, that Aβ oligomers impair synaptic functions by inhibiting the long-term potentiation in the hippocampus and astrocytes and microglia are activated (Lambert *et al.* 1998, Haass *et al.* 2007). Senile plaques and neuritic inflammation occur leading to oxidative stress with the effect of altering tau-targeting kinases resulting in hyperphosphorylated tau proteins that

accumulate into NFT's. Thus, the accumulation of NFT's and degenerative neurons are seen as a result of amyloid plaque formation (Hardy *et al.* 1992). Neuronal and neuritic dysfunctions finally lead to cell death and consequently (severe) dementia (Hardy *et al.* 1992, Hardy *et al.* 2002, Haass *et al.* 2007).

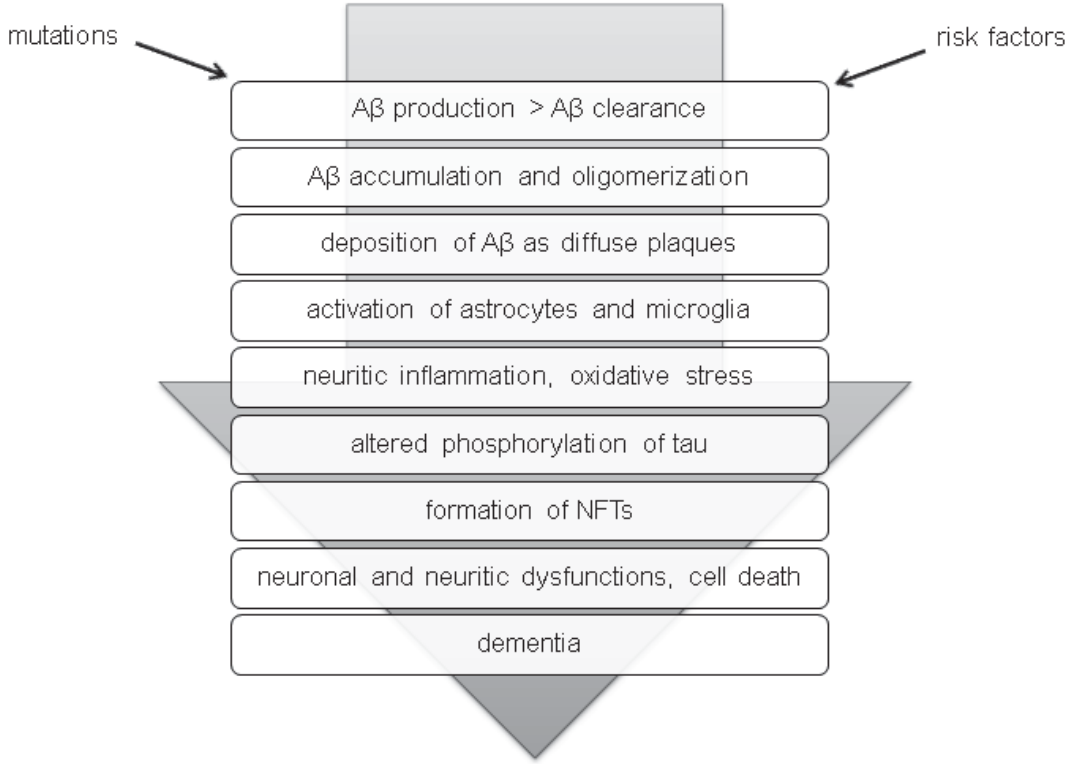


**Figure 3 Amyloid cascade hypothesis.** According to this hypothesis, the imbalance between Aβ production and clearance leading to accumulation is seen as the main hallmark leading to dementia. Aβ oligomers are classified as the most toxic species (modified according to (Hardy *et al.* 1992, Hardy *et al.* 2002)).

## 1.4 Amyloid-β isoforms

*In vivo* and *in vitro* analysis of several amyloid deposits in AD have disclosed various Aβ species, differing in length as well as in C- and N-terminal modifications (Masters *et al.* 1985, Prelli *et al.* 1988, Miller *et al.* 1993). C-terminal modified isoforms, such as Aβ(1-15/16), Aβ(1-37/38/39) and Aβ(1-43), play a central role in in AD pathogenesis (Wiltfang *et al.* 2002, Welander *et al.* 2009, Portelius *et al.* 2012). However, a significant proportion of N-terminally truncated Aβ variants have been discovered in AD brains such as Aβ(n-40/42) with n ranges from 2 to 11 (Bouter *et al.* 2013, Zhao *et al.* 2014). The toxicity of these aggregates was demonstrated to correlate with the predominance of N-truncated Aβ species over the full-length non-modified Aβ (Piccini *et al.* 2005, Guntert *et al.* 2006).

Pyroglutamate-modified Aβ (pEAβ) has been demonstrated to be the predominant isoform amongst them (Saido *et al.* 1995, Gunn *et al.* 2010, Jawhar *et al.* 2011). pEAβ(3-42), bearing N-terminal pyroglutamate at position 3, was revealed to be the major N-truncated component of intracellular, extracellular and vascular Aβ deposits in AD brain tissue (Harigaya *et al.* 2000, Portelius *et al.* 2010, Wirths *et al.* 2010).

### 1.4.1 Discovery and prevalence of pyroglutamate amyloid-β

In 1986, Selkoe and collaborators firstly revealed that the N-terminus of Aβ might be blocked as they were not able to obtain N-terminal sequences from purified plaques without the use of proteases (Selkoe *et al.* 1986). Other groups did not succeed neither in gaining N-terminal sequences of plaque cores by the use of other methods (Gorevic *et al.* 1986). Mori *et al.* described the presence of N-terminally pyroglutamate-modified Aβ in brain samples with an incidence of 15-20 %. Pyroglutamate amino peptidases were used to unravel the N-terminus, which is resistant to other peptidases that are used for Edman degradation, because of the formation of an intra lactam ring (Mori *et al.* 1992). Afterwards, pEAβ(3-x) and pEAβ(11-x) were detected and shown to be involved in the formation of the central core of amyloid aggregates (Naslund *et al.* 1994, Saido *et al.* 1995). This led to the hypothesis that pEAβ deposition may play a central role in initiating the aggregation of the full length Aβ (Hartig *et al.* 2010, Sullivan *et al.* 2011). pEAβ(3-x) was proven to be present in equivalent or larger amounts than full-length Aβ in senile plaques and it was also found in diffuse plaques, one of the earliest depositions of amyloid aggregates as well as in soluble amyloid peptides as the most dominant fraction underlying that pEAβ seems to precede amyloid plaque formation (Saido *et al.* 1995, Iwatsubo *et al.* 1996, Russo *et al.* 1997). Kuo and coworkers have shown, that senile plaques from individuals suffering from AD contain on average 51 % of pEAβ(3-x), while the percentage in vascular amyloid depositions is only about 11 % (Kuo *et al.* 1997). Levels of pEAβ ending with position 42 were found to be always higher than C-terminal shortened species (Hosoda *et al.* 1998, Harigaya *et al.* 2000). pEAβ(3-42) represents 25 % of the total Aβ in senile plaques (Harigaya *et al.* 2000). Recent studies showed, that aggregated or oligomerized pEAβ(3-x) is an abundant pathological species in neuronal lysosomes and neuroglia obtained from human brain tissue (De Kimpe *et al.* 2013). Further, the intracellular amount of pEAβ(3-x) increases with age (Bayer *et al.* 2011).

### 1.4.2 Generation of pyroglutamate amyloid-β

Formation of pyroglutamate-modified Aβ(3-x) requires the removal of the first two amino acids (aa) D1 and A2 leading to the N-terminal aa E3 by an unknown mechanism (Figure 4) (Jawhar *et al.* 2011). In general, Aβ(1-x) is released after the cleavage of APP, which is catalyzed by β- and γ-secretases. In 1995, Saido and collaborators hypothesized the presence of peptidases cleaving the first two aa to expose E3 (Saido *et al.* 1995). More recently, Sevalle *et al.* suggested that the cleavage of the initial N-terminal aa are triggered by aminopeptidase A (Sevalle *et al.* 2009). In contrast, Aβ(11-x) starting N-terminal exposed E11 is generated by an alternative cleavage of APP in the *trans*-Golgi network (Huse *et al.* 2002). Post-translational pyroglutamate formation is then catalyzed by the enzyme glutaminyl cyclase (QC) targeting the exposed N-terminal amino group of E3/E11 for intra-E lactam ring formation by dehydration (Figure 4) (Schilling *et al.* 2003, Schilling *et al.* 2004).

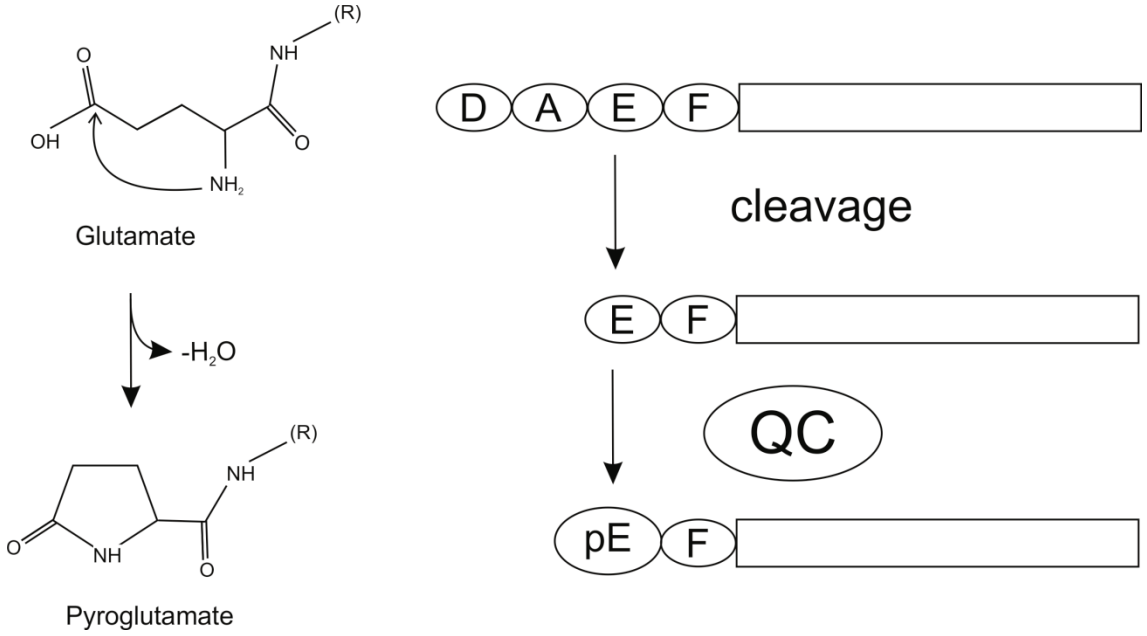


**Figure 4 Generation of pEAβ *in vivo.*** The N-terminal aa aspartate (D1) and alanine (A2) are cleaved off by an unknown mechanisms leading to N-aminoterminal glutamic acid (E3). E3 can be converted to pyroglutamate (pE) due to the formation of an intramolecular lactam ring by dehydration catalyzed by the enzyme glutaminyl cyclase (QC) (modified according to (Jawhar *et al.* 2011)).

Although N-terminal pE formation from E is a preferred enzymatic reaction (Twardzik *et al.* 1972), it can also be achieved non-enzymatically under mild acidic conditions and increased temperature (Chelius *et al.* 2006). The amino group attacks the carboxyl side chain group due to a nucleophile substitution for pyroglutamate-formation under the release of water. Intra-molecular lactam ring formation with an N-terminal Q residue instead of E is much faster for both the enzymatic and the non-enzymatic reaction (Schilling *et al.* 2008). The mechanism of pyroglutamate formation remains identical by replacing E with Q, but the lactam ring generation is no longer obtained by dehydration but under the release of ammoniac (Figure 5)

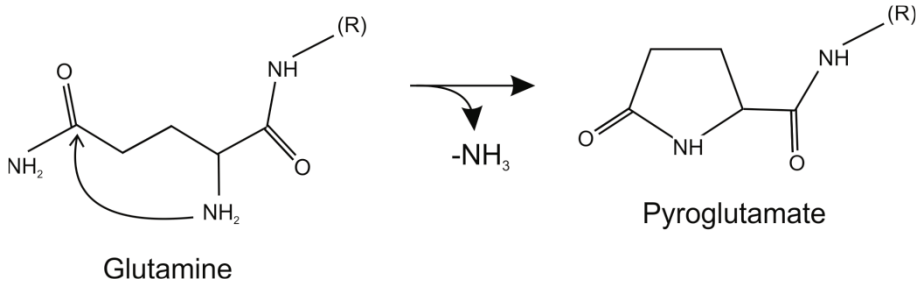


**Figure 5 Conversion to pyroglutamate based on N-terminal glutamine.** N-aminoterminal glutamine can be converted to pyroglutamate due to the formation of an intramolecular lactam ring according to a nucleophile attack under the release of ammoniac.

### 1.4.3 Biophysical properties of pyroglutamate amyloid-β

Conversion to pEAβ results in altered biophysical and biochemical characteristics with severe pathological consequences. There is evidence, that pEAβ self-assembles and accumulates because of its limited degradation (Saido *et al.* 1996). Formation of the intramolecular lactam ring increases its resistance to degradation by amino peptidases and therefore the stability of the peptide (Saido *et al.* 1996). Since the formation of pyroglutamate results in the loss of two negative and one positive charge, the hydrophobicity of pEAβ(3-x) is increased (Jawhar *et al.* 2011). pEAβ was shown to form β-sheet structures more readily and has an enhanced aggregation propensity compared to the full-length peptide demonstrating it to be a potential seeding species of Aβ oligomerization and accumulation (He *et al.* 1999, Schilling *et al.* 2006, D'Arrigo *et al.* 2009, Schlenzig *et al.* 2012). Compared to the non-modified Aβ(1-x), pEAβ(3-x) possesses an up to 250-fold accelerated aggregation kinetic - independent of the C-terminal length (Schilling *et al.* 2006). Our group performed previously structural analysis on pEAβ(3-40) and Aβ(1-40) using solution state nuclear magnetic resonance (NMR).

These studies indicate that the pyroglutamate-modified variant has an increased tendency to form β-sheet rich structures under exactly the same conditions (Sun *et al.* 2012).

Russo *et al.* suggested pEAβ to be more toxic to neurons and astrocytes than the corresponding full-length peptide (Russo *et al.* 2001). Aβ mixtures containing pEAβ as found in AD brains were further claimed to increase cell membrane permeability resulting in raised neuroblastoma cell death (Piccini *et al.* 2005). In general, the formation to pEAβ leads to an enhanced toxicity which might be due to the higher aggregation propensity and the longer bioavailability of pEAβ oligomers, since they are more resistance to degradation.

## 1.5 Diagnosis of Alzheimer's disease

Diagnosis of AD is limited since definite AD diagnosis can only be observed *post mortem* by autopsied neuropathological findings that are based on the identification of SP and NFT (McKhann *et al.* 1984, Bird 1993, last revision 2014). This leads to a "probably AD" clinical diagnosis *in vivo* in accordance to the symptoms, which are highly dependent on the progression of the disease and are thus impeding diagnosis in the early stages of AD (Jack *et al.* 2011). Clinical diagnosis is accurate in 71 – 88 % of all cases (Bird 1993, last revision 2014, Beach *et al.* 2012). Methods for morphological and functional imaging such as magnetic resonance imaging (MRI), positron emission tomography (PET) and computed tomography (CT) support the diagnosis but are expensive (Fox *et al.* 2001, Laske *et al.* 2015). In 2014, new criteria for AD diagnosis were published considering neurodegeneration quantified by PET and brain atrophy quantified by MRI. Levels of the total Aβ(1-42) and phosphorylated tau in the CSF and Aβ-plaques quantified by PET are a pathophysiological hallmark of AD (Dubois *et al.* 2014).

The most studied and validated PET tracer for identification of Aβ-aggregation is the Pittsburgh compound B (PiB), a neutral derivate of the dye thioflavin-T (ThT) which binds to extracellular aggregated Aβ (Klunk *et al.* 2004). The signal obtained by visualizing Aβ using PiB as a tracer is more than twofold higher in AD patients than in healthy controls (Edison *et al.* 2007). The uptake of PiB *in vivo* was demonstrated to correlate with the level of Aβ in AD brain tissue taken at autopsy (Svedberg *et al.* 2009). However, PiB has low affinity to soluble or non-fibrillar Aβ and does not bind to NFTs (Lockhart *et al.* 2007, Ikonomovic *et al.* 2008). Thus, new tracers for the detection of tau fibrillary pathology were developed supporting PET based diagnosis of AD (Chien *et al.* 2014, Okamura *et al.* 2014).

A promising approach for early diagnosis of AD is the detection of Aβ aggregates using surface based fluorescence intensity distribution assay (sFIDA) (Funke *et al.* 2007, Funke *et al.* 2010). The principle of sFIDA is similar to a sandwich enzyme-linked immunosorbent assay (ELISA) with the advantage to correlate well with the number and size of Aβ oligomers in the sample. Recent results have shown a higher readout for AD patients compared to healthy controls giving this immunoassay reliability as a new diagnostic tool for early AD diagnosis (Wang-Dietrich *et al.* 2013).

## 1.6 Therapeutic strategies of Alzheimer's disease

Up-to-date, no drug is available that cures AD. Current therapies stabilize the symptoms but are not able to modify the progression of the disease; most patients die within a decade after being diagnosed (Panza *et al.* 2009). Several therapeutic strategies targeting different pathophysiological mechanisms of AD progression exist.

Since neuronal dysfunction starts early in AD, one symptomatic treatment is the modulation of neurotransmission by identifying cholinesterase inhibitors or receptor antagonisms to improve short-term cognitive functions and to control psychosis and mood disturbance (Lawrence *et al.* 1998, Anand *et al.* 2014). Other options are the modulation of intracellular signaling cascades or cellular calcium homeostasis, oxidative stress reduction and anti-inflammatory therapy (Anand *et al.* 2014). Tau based therapies are dealing with the inhibition of tau hyperphosphorylation by inhibiting kinases, stabilizing microtubules, blocking tau aggregation with vaccination or tau binding molecules or enhancing tau clearance by targeting chaperones (Morris *et al.* 2011, Huang *et al.* 2012).

### 1.6.1 Amyloid-β targeting strategies

The amyloid cascade hypothesis has become the most-researched conceptual framework of AD and several studies have focused on interrupting it. One approach is Aβ targeted immunotherapy. Aβ vaccination is separated into active and passive immunization. It was shown, that active immunization against Aβ resulted in an antibody response and reduction of Aβ plaque load in patients. However, trials had to be stopped in phase II because of immunopathological side effects due to an induction of cell-mediated immune response (Gilman *et al.* 2005, Holmes *et al.* 2008, Lemere *et al.* 2010).

The movement of Aβ between the central nervous system and periphery is regulated by apolipoproteins (Fan *et al.* 2009). ApoE4 increases the crossing of Aβ from brain to blood by a receptor mediated transport using the low-density lipoprotein receptor-related protein

(LPR) (Zlokovic 2004). LPR expression decreases with age leading to a declined efflux of Aβ and thus accumulations in the brain (Shibata *et al.* 2000). One strategy is to increase Aβ passage through the blood brain barrier (BBB) resulting in a reduced amyloid deposition in the brain (Anand *et al.* 2014).

APP processing secretases are targeted in order to decrease the production of Aβ. In the non-pathogenic pathway, APP is cleaved by α- and γ-secretases leading to non-toxic products. Replacing α-secretases by alternate β-secretases result in amyloidogenic processing (Huang *et al.* 2012, Mullane *et al.* 2013, Anand *et al.* 2014). Several drugs have been designed to inhibit β- and γ-secretases in combination with augmenting the α-secretase - with difficulties to specifically inhibit the pathogenic cleavage of APP without affecting alternative physiological important substrates (Citron 2010, De Strooper *et al.* 2010, Golde *et al.* 2011).

Some proteases that are known to degrade Aβ plaques do exist such as plasmin, neprilysin, insulin degrading enzyme, metalloproteinase and a few other proteases (Nalivaeva *et al.* 2012). The concentration and activity of these enzymes decline within the progression of AD and may contribute to Aβ accumulation (Anand *et al.* 2014). Some studies focusing on increasing neprisilyn have shown to reduce amyloid pathology in mouse models (Marr *et al.* 2003, Spencer *et al.* 2008, Blurton-Jones *et al.* 2014).

### 1.6.2 D-enantiomeric peptides for decreasing amyloid-β aggregation

Within the last years, a number of studies have been performed with Aβ targeting D-peptides to prevent aggregation and subsequent toxicity (Kumar *et al.* 2014). D-aa are the stereoisomers of naturally occurring L-aa. Peptides containing D-aa can mimic naturally occurring peptides without being a binding ligand for proteases. Thus, they are more resistant than their L-enantiomeric counterpart and unlikely to provoke immunogenicity, which makes them more suitable for therapeutics (Kumar *et al.* 2014). A number of D-peptides containing F and L at second and third position were screened with a pentapeptide library and identified to bind Aβ and thus prevent fibril formation (Tjernberg *et al.* 1996). Hayward and coworkers investigated a cholyl-modified D-pentapeptide capable of inhibiting fibril formation and thus preventing cytotoxicity (Findeis *et al.* 1999). The group by Doig investigated a D-peptide with additionally introduced N-methylation and cyclohexylglycines binding to Aβ and thus promotes the aggregation into large non-fibrillar and non-cytotoxic aggregates (Kokkoni *et al.* 2006). Short D-enantiomeric peptides

could be a great possibility for early therapeutic intervention due to their increased protease resistance and selectivity.

## 1.7 D3

Our group has previously selected Aβ binding D-peptides by mirror image phage display. Randomized peptides were screened against D-enantiomeric Aβ(1-42) and then synthesized into their D-enantiomeric form for binding to the physiological L-Aβ(1-42). The 12mer peptide D3 with the sequence RPRTRLHTHRNR was found to be a suitable candidate for AD therapy (Wiesehan *et al.* 2008). D3 was shown to inhibit the formation of toxic Aβ oligomers by driving aggregation towards amorphous non-toxic aggregates (Funke *et al.* 2010). The peptide promotes disassembly of pre-formed Aβ aggregates, increases cell viability in PC12 cells and reduces the level of amyloid plaques and thus improves the pathology and behavior in APP/PS1 transgenic mice (van Groen *et al.* 2008, van Groen *et al.* 2012, van Groen *et al.* 2013). Moreover, D3 did not initiate any immune response or inflammatory and indicated its capability to cross the BBB (van Groen *et al.* 2009, van Groen *et al.* 2013). Therefore, D3 represents a potential drug candidate in the modulation of Aβ aggregation.

pEAβ got more and more in focus because it plays a central role in seeding Aβ aggregation and since it is known to be one of the dominant isoforms in senile plaques (Gunn *et al.* 2010, Jawhar *et al.* 2011). Therefore, it is necessary to test drugs also for their effect to bind pEAβ. D3 was shown to be effective *in vitro* and *in vivo* by specifically targeting Aβ and thus to decrease amyloid formation (Wiesehan *et al.* 2008, van Groen *et al.* 2013). Its ability to target pEAβ and to inhibit fibril formation needs to be analyzed in transgenic pEAβ expressing mice. The TBA2.1 mouse model expresses AβE3Q-42 (E is replaced to Q to facilitate pE formation, see 1.4.2) which is then posttranslational modified to pEAβ(3-42) (Alexandru et al. 2011). Thus, this mouse model allows studies of the effect of D3 and its tandem derivative D3D3 regarding pEAβ(3-42) mediated pathology *in vivo*

.

# 2 Objective

A deeper understanding of the molecular mechanisms of pEAβ formation, aggregation and its structure may provide new insights into the difference compared to Aβ and its role in AD. However, large amounts of pEAβ are needed for such studies. Within this study, a method for reproducible expression and purification of recombinant pEAβ(3-40) and pEAβ(3-42) in natural abundance as well as stable isotopically enriched, should be established. The production is based on Aβ(E3Q-40/42) mutants leading to quantitative and more rapid pEAβ formation compared to the Aβ(E3-40/42) wild type. The chemical and conformational states of the purified proteins should be characterized biophysically under different conditions.

Furthermore, structural difference and altered biochemical properties of pEAβ should be investigated and compared to the corresponding non-modified Aβ. The main problem is the fast aggregation kinetics and the low solubility which impedes such studies drastically. It was shown that Aβ builds α-helical structures in solutions containing TFE enable to facilitate structural studies. Structural analysis and aggregation of pEAβ was further investigated by solution state NMR spectroscopy. Three dimensional experiments for backbone and side chain assignments provide chemical shift data for secondary structure analysis. CD spectroscopy confirms the secondary structure prediction of pEAβ and Aβ under different conditions. ThT assays monitoring the aggregation kinetics of pEAβ compared to non-truncated Aβ as well as size exclusion chromatography (SEC) and TEM images expose the difference in aggregation due to the formation to pyroglutamate and its resulting altered biochemical properties.

Recombinant pEAβ will be used to characterize the previously identified D-enantiomeric peptides D3 and D3D3 regarding their potency to prevent fibril formation. The potency of D3 and D3D3 in Aβ-directed therapy will be tested *in vivo* in a pEAβ(3-42) expression transgenic mouse model. Ideally, new insights might be drawn regarding the altered biochemical properties and resulting pathological consequences and the structural difference between pEAβ and Aβ.

# 3 Manuscripts

**(1) Purification and characterization of N-terminal pyroglutamate-modified amyloid-β variants and structural analysis by solution NMR spectroscopy**

Christina Dammers, Lothar Gremer, Philipp Neudecker, Hans-Ulrich Demuth, Melanie Schwarten and Dieter Willbold

Journal: PLOS ONE

Impact Factor: 3.53 (2013/2014)

Contributions: 90 %, experimental design, performance and data analysis of cloning, protein expression, purification and biophysical studies, manuscript writing

**(2) Structural analysis and aggregation of pyroglutamate Aβ(3-40) in triflouroethanol**

Christina Dammers, Lothar Gremer, Kerstin Reiß, Antonia N. Klein, Philipp Neudecker, Rudolf Hartmann, Na Sun, Hans-Ulrich Demuth, Melanie Schwarten and Dieter Willbold

Journal: PLOS ONE

Impact Factor: 3.53 (2013/2014)

Contributions: 85 %, protein production, experimental design, performance and analysis of ThT assays, TEM and NMR and CD spectroscopy, manuscript writing

**(3) pEAβ(3-42) undergoes amyloid formation via an α-helical intermediate as revealed by 3D NMR spectroscopy**

Christina Dammers, Kerstin Reiß, Lothar Gremer, Tamar Ziehm, Justin Lecher, Melanie Schwarten and Dieter Willbold

Journal: Journal of Biological Chemistry (under review)

Impact Factor: 4.57

Contributions: 80 %, protein production, experimental design, performance and data analysis of CD spectroscopy, TEM, ThT assays and NMR spectroscopy, manuscript writing

**(4) Aβ-directed therapy interferes successfully with pEAβ(3-42) induced degenerative phenotype in transgenic mice**

Tina Dunkelmann, Kerstin Teichmann, Markus Tusche, Christina Dammers, Dagmar Jürgens, Karl-Josef Langen, Hans-Ulrich Demuth, Nadim Jon Shah, Janine Kutzsche, Antje Willuweit and Dieter Willbold

Journal: Nature Communications (to be submitted)
Impact Factor: 11.47 (2014)

Contributions: 20 %, production of recombinant protein, experimental design of *in vitro* studies

## 3.1 Purification and characterization of recombinant N-terminally pyroglutamate modified amyloid-β variants and structural analysis by solution NMR spectroscopy

Christina Dammers, Lothar Gremer, Philipp Neudecker, Hans-Ulrich Demuth, Melanie Schwarten and Dieter Willbold

Journal: PLOS ONE

Impact Factor: 3.53 (2013/2014)

Contributions: 90 %, experimental design, performance and data analysis of cloning, protein expression, purification and biophysical studies, manuscript writing

PLOS | ONE

RESEARCH ARTICLE

# Purification and Characterization of Recombinant N-Terminally Pyroglutamate-Modified Amyloid-β Variants and Structural Analysis by Solution NMR Spectroscopy

**Christina Dammers[1], Lothar Gremer[1,2], Philipp Neudecker[1,2], Hans-Ulrich Demuth[3], Melanie Schwarten[1], Dieter Willbold[1,2]***

**1** Institute of Complex Systems (ICS-6) Structural Biochemistry, Forschungszentrum Jülich, 52425 Jülich, Germany, **2** Institut für Physikalische Biologie, Heinrich-Heine-Universität Düsseldorf, 40225 Düsseldorf, Germany, **3** Fraunhofer Institute for Cell Therapy and Immunology, Dep. Molecular Drug Biochemistry and Therapy, 06120 Halle (Saale), Germany

* d.willbold@fz-juelich.de



OPEN ACCESS

**Citation:** Dammers C, Gremer L, Neudecker P, Demuth H-U, Schwarten M, Willbold D (2015) Purification and Characterization of Recombinant N-Terminally Pyroglutamate-Modified Amyloid-β Variants and Structural Analysis by Solution NMR Spectroscopy. PLoS ONE 10(10): e0139710. doi:10.1371/journal.pone.0139710

**Editor:** Michael Massiah, George Washington University, UNITED STATES

**Received:** July 3, 2015

**Accepted:** September 16, 2015

**Published:** October 5, 2015



**Data Availability Statement:** All relevant data are within the paper.

**Funding:** The authors gratefully acknowledge support of CD from the International NRW Research School BioStruct, granted by the Ministry of Innovation, Science and Research of the State North Rhine-Westphalia, the Heinrich-Heine-University of Düsseldorf, and the Entrepreneur Foundation at the Heinrich-Heine-University of Düsseldorf. DW was supported by grants from the "Portfolio Technology and Medicine", the "Portfolio Drug Research" and the

## Abstract

Alzheimer's disease (AD) is the leading cause of dementia in the elderly and is characterized by memory loss and cognitive decline. Pathological hallmark of AD brains are intracellular neurofibrillary tangles and extracellular amyloid plaques. The major component of these plaques is the highly heterogeneous amyloid-β (Aβ) peptide, varying in length and modification. In recent years pyroglutamate-modified amyloid-β (pEAβ) peptides have increasingly moved into the focus since they have been described to be the predominant species of all N-terminally truncated Aβ. Compared to unmodified Aβ, pEAβ is known to show increased hydrophobicity, higher toxicity, faster aggregation and β-sheet stabilization and is more resistant to degradation. Nuclear magnetic resonance (NMR) spectroscopy is a particularly powerful method to investigate the conformations of pEAβ isoforms in solution and to study peptide/ligand interactions for drug development. However, biophysical characterization of pEAβ and comparison to its non-modified variant has so far been seriously hampered by the lack of highly pure recombinant and isotope-enriched protein. Here we present, to our knowledge, for the first time a reproducible protocol for the production of pEAβ from a recombinant precursor expressed in *E. coli* in natural isotope abundance as well as in uniformly [*U*-$^{15}$N]- or [*U*-$^{13}$C, $^{15}$N]-labeled form, with yields of up to 15 mg/l *E. coli* culture broth. The chemical state of the purified protein was evaluated by RP-HPLC and formation of pyroglutamate was verified by mass spectroscopy. The recombinant pyroglutamate-modified Aβ peptides showed characteristic sigmoidal aggregation kinetics as monitored by thioflavin-T assays. The quality and quantity of produced pEAβ40 and pEAβ42 allowed us to perform heteronuclear multidimensional NMR spectroscopy in solution and to sequence-specifically assign the backbone resonances under near-physiological conditions. Our results suggest that the presented method will be useful in obtaining cost-effective high-quality recombinant pEAβ40 and pEAβ42 for further physiological and biochemical studies.

Helmholtz-Validierungsfonds of the Impuls und Vernetzungs-Fonds der Helmholtzgemeinschaft. The funders had no role in study design, data collection and analysis, decision to publish, or preparation of the manuscript.

**Competing Interests**: The authors have declared that no competing interests exist.

## Introduction

Alzheimer's disease (AD) is a neurodegenerative disorder characterized by progressive decline of cognitive functions and has become the main cause for dementia in the elderly [1, 2]. Pathological hallmarks of AD are intracellular neurofibrillary tangles and the accumulation of extracellular amyloid plaques [3, 4]. Amyloid-β (Aβ), the major component of these amyloid plaques, is produced by cleavage of the amyloid precursor protein through β- and γ-secretases, generating various Aβ isoforms varying in length [5–9]. Besides Aβ isoforms starting with the amino acid (aa) D at position 1 (D1), a significant amount of N-terminally truncated Aβ variants is deposited in the brains of AD patients [10, 11], whereby pyroglutamate (pE)-modified Aβ species were described as the major isoforms [12–15]. Up to 20% of the total Aβ are reported to bear a pE residue at the N-terminus [16]. N-terminally truncated pEAβ(3-x) species, with the first two N-terminal aa D1 and A2 being absent, are dominant isoforms in AD brains [17, 18] and are present in up to equivalent amounts compared to full-length Aβ(1-x) in senile plaques [19–21]. The intracellular amount of pEAβ increases with age and it is predominantly found in lysosomes of neurons and neuroglia [22]. pEAβ plays a central role in triggering neurodegeneration and lethal neurological deficits [23, 24]. Thus, N-terminally modified Aβ isoforms represent highly desirable therapeutic targets and became more important in the recent years [15, 25–27].

Aβ(3-x) can be generated by the removal of the first two aa (D1 and A2) from Aβ(1-x) or by alternative splicing, leading to the N-terminal aa E3. The enzyme glutaminyl cyclase (QC) catalyzes intra-E lactam ring formation involving the N-terminal amino group of E3 and its γ-carboxyl group by dehydration leading to pEAβ [28, 29]. Although N-terminal pE formation is a preferred enzymatic reaction [30], it can also be achieved non-enzymatically [31]. This reaction is accelerated with an N-terminal Q residue as a substrate instead of E [32].

The conversion results in altered biophysical and biochemical properties since: (1) pEAβ shows higher hydrophobicity due to the formation of the N-terminal pE lactam ring and the loss of three charges resulting in increased aggregation propensity [12, 19]. (2) The blocked N-terminus leads to higher stability since it is inaccessible for degradation by aminopeptidases. (3) pEAβ shows faster aggregation kinetics with up to 250-fold acceleration and (4) is also more neurotoxic as compared with corresponding non-N-terminally truncated Aβ species independent of their C-terminal lengths [24, 33–36].

A deeper understanding of the molecular mechanisms of pEAβ formation, aggregation and its structure may provide new insights into the difference compared to Aβ and its role in AD. Structural data from NMR spectroscopy could extend the knowledge of pEAβ pathogenicity and will give information about ligand interactions for rational drug design. However, large amounts of pEAβ are needed for such studies. Principally, peptides up to 100 amino acid residues can be prepared chemically by solid phase synthesis, but when it comes to isotope-enriched peptides this strategy becomes very costly and constant biological activity is not guaranteed since there are often differences in purity between the batches [37].

Here, we report a method for reproducible expression and purification of recombinant pEAβ(3–40) and pEAβ(3–42) with natural isotope abundance, as well as uniformly [$U$-$^{15}$N] or [$U$-$^{13}$C, $^{15}$N]-labeled protein with yields up to 15 mg/l culture based on a previously published protocol for Aβ by Finder, Glockshuber and coworkers [37]. To avoid time and cost consuming enzymatic pE formation by QC, we applied conditions for nonenzymatic pE formation on Aβ (E3Q-x) mutants leading to complete and more rapid pEAβ formation compared to the Aβ (E3-x) species. The chemical and conformational states of the purified pEAβ proteins were characterized biophysically by mass spectrometry, thioflavin-T (ThT) assay and solution NMR spectroscopy.

## Results and Discussion

### Cloning, expression and purification of the mutants Aβ(E3Q-40/42)

The fusion constructs Aβ(E3Q-40) and Aβ(E3Q-42) are based on the recombinant Aβ(1–42) *E. coli* derived construct published by Finder, Glockshuber and coworkers [37] consisting of a $His_6$-tag, a solubilizing fusion partner $(NANP)_{19}$, established previously [38], followed by a TEV protease recognition and cleavage site and the Aβ sequence 3-40/42. E3 was replaced by Q in order to improve the non-enzymatic reaction to pE (Method A in S1 File). The protease recognition site thus is now modified to ENLYFQ↓Q, where the arrow indicates the cleavage site, leading to Q3 as the N-terminal aa in the resulting Aβ constructs. Typically, the TEV protease recognition and cleavage site contains a G or a S C-terminal of the TEV protease cut, but as proven previously, an exchange of G or S to Q leads to 90% cleavage efficiency [39]. Thus Q becomes the first aa (Q3) of the cleavage product, which is readily susceptible to non-enzymatic pE formation under mild acidic and elevated temperature conditions. To show the applicability and advantage of this mutation for non-enzymatic pEAβ conversion, we additionally produced Aβ(3–42) starting at the N-terminal position with the original E instead of Q, which *in vivo* is the primary substrate for QC and is catalytically converted to pEAβ but can also be modified non-enzymatically [28]. We found that Aβ(3–42) converted to pEAβ significantly slower than Aβ(E3Q-42) with Q at the N-terminal position.

Expression of the fusion constructs in *E. coli* BL21 (DE3) pLysS was obtained at a high cell density of $OD_{600nm} \geq 1.2$. Reducing the temperature after induction to 30°C and expression overnight resulted in a large amount of fusion protein accumulated in inclusion bodies (Fig 1a). Denaturing conditions were necessary to solubilize these inclusion bodies. The first purification step was an IMAC in 8 M GdmCl. One-step washing of the IMAC column with 20 mM imidazole and subsequent elution with 500 mM imidazole was performed to isolate the fusion protein and to remove most of non-specifically bound impurities as analyzed by analytical RP-HPLC (Fig 1b). Typical retention time of fusion Aβ(E3Q-40) was 5 min and 7 min for fusion Aβ(E3Q-42). The fusion proteins were further purified using preparative RP-HPLC and lyophilized from aqueous ACN resulting in pure fusion protein determined via SDS-PAGE according to Laemmli [40] (Fig 1c, Method B in S1 File). The following yields per l of cell culture were obtained as shown in Table 1: 200 ± 5 mg for fusion Aβ(E3Q-40/42) and fusion Aβ(3–42) in natural abundance, 25 ± 3 mg for [$U$-$^{15}$N] fusion Aβ(E3Q-40/42) and 20 ± 3 mg for [$U$-$^{13}$C, $^{15}$N] fusion Aβ(E3Q-40/42).

Next, the lyophilized fusion proteins were analyzed for efficient TEV protease cleavage. It turned out, that high molar ratios of TEV protease were necessary to balance the modified cleavage site, i.e. ENLYFQ↓Q, instead of ENLYFQ↓G/S. Enhanced cleavage reaction was achieved by lowering the incubation temperature to 4°C by decreasing the aggregation of the cleaved Aβ with remaining fusion protein (Method C in S1 File). Most of the fusion Aβ(E3Q-40/42) were cleaved within 7 h, as proven by analytical RP-HPLC (Fig 2a and 2b). Retention-time of cleaved Aβ(E3Q-40) was approximately 8.9 min and 12.2 min for Aβ(E3Q-42). After overnight incubation, cleaved Aβ(E3Q-42) and Aβ(3–42) precipitated during the reaction completely, whereas around 50% of Aβ(E3Q-40) stayed in solution. Precipitates were resolved in 8 M GdmCl for further purification. Chromatograms of preparative HPLC indicate that there was still some fusion protein remaining (Fig 2c) which could be removed by adjusting the gradient as described in the Materials and Methods section. Cleaved Aβ was separated from the fusion-tag and TEV protease and lyophilized. As the fusion-tag accounts for 70% of the total fusion protein, a maximum of 30 mg target protein per 100 mg fusion protein is theoretically obtainable with 100% cleavage efficiency. In total, approximately 20 mg purified cleaved Aβ(E3Q-40/42) per 100 mg fusion protein were received.

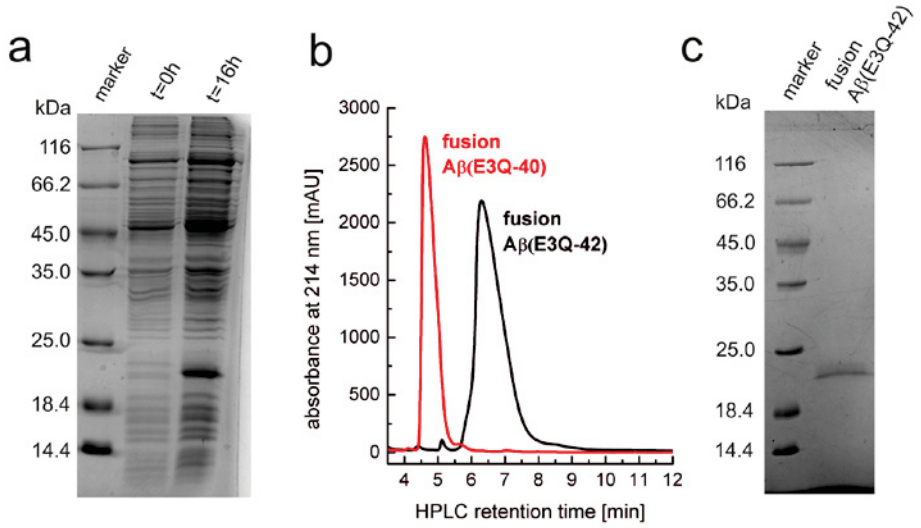


**Fig 1. Expression and purification of fusion Aβ(E3Q-42) protein in *E. coli* BL21 (DE3) pLysS.** (a) 15% Tris/Glycine-SDS-PAGE analysis of the lysates before IPTG induction (t = 0 h) and after IPTG induction leading to expression of fusion Aβ(E3Q-42) (t = 16 h after induction) at 30°C. (b) Analytical RP-HPLC of IMAC purified fusion Aβ(E3Q-40) (red) and fusion Aβ(E3Q-42) (black) with typical retention times of 5 and 7 min, respectively. (c) 15% Tris/Glycine-SDS-PAGE of IMAC and RP-HPLC purified fusion Aβ(E3Q-42).

doi:10.1371/journal.pone.0139710.g001

## Conversion to pEAβ40 and pEAβ42

It is known, that N-terminal pE formation from E is a preferred enzymatical reaction [30], but also can be achieved non-enzymatically under mild acidic conditions and increased temperature [31]. However, both enzymatic and non-enzymatic intra-molecular lactam formation with an N-terminal Q residue instead of E is much faster [32]. For this reason, we decided to use the mutant Aβ(E3Q) for spontaneous pE formation and compared it with a construct bearing E3 at the N-terminus. The reaction schemes for the conversion to pE from N-terminal E by dehydration or from N-terminal Q by subtraction of ammonia are shown in Fig 3d. Purified Aβ (E3Q-40), Aβ(E3Q-42) and Aβ(3–42) were dissolved in acetate buffer at pH 3.5 and incubated at 45°C for spontaneous pE formation (Method D in S1 File). Reaction was observed with analytical RP-HPLC at the start of the reaction, after 3 h and after 24 h incubation, respectively (Fig 3a and 3b). Due to the loss of the positively charged hydrophilic amino group, the pE-modified peptides get more hydrophobic resulting in a longer retention time on RP-HPLC. For Aβ(E3Q-40)and Aβ(E3Q-42), the initial peptide peaks eluting at 8.2 or 12.6 min decreased

**Table 1. Yields of intermediates and final purified pEAβ peptides in mg per l culture broth.**

| | Natural abundant [mg/l] | [*U*-$^{15}$N] labeled [mg/l] | [*U*-$^{13}$C,$^{15}$N] labeled [mg/l] |
|---|---|---|---|
| fusion Aβ(E3Q-40) | 205 | 28 | 23 |
| Aβ(E3Q-40) | 42 | 5 | 4.5 |
| pEAβ40 | 15 | 2.3 | 2 |
| fusion Aβ(E3Q-42) | 200 | 24 | 20 |
| Aβ(E3Q-42) | 41 | 4.8 | 4 |
| pEAβ42 | 14 | 2.1 | 1.8 |

doi:10.1371/journal.pone.0139710.t001

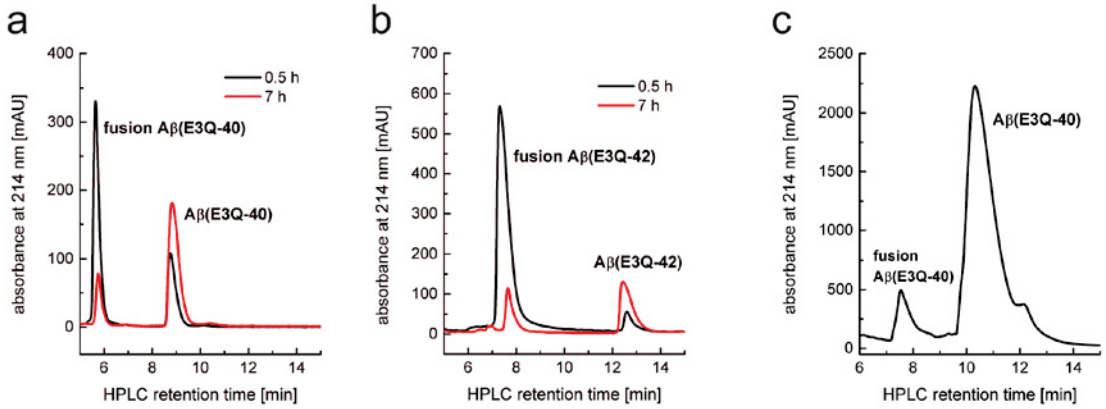


**Fig 2. Analytical RP-HPLC of TEV protease cleavage reaction of Aβ(E3Q-40) (a) and Aβ(E3Q-42) (b).** The peptides were applied on an analytical Zorbax SB-300 C8 column and eluted with 30% ACN and 0.1% TFA at 80°C. Black lines indicate analysis after 0.5 h and red lines after 7 h TEV cleavage reaction at 4°C. Peaks for the fusion proteins decreased while peaks indicating cleaved Aβ(E3Q-40) or Aβ(E3Q-42) were increasing. (c) Semi-preparative RP-HPLC of TEV-cleaved fusion Aβ(E3Q-40) to separate Aβ(E3Q-40) from remaining fusion protein.

doi:10.1371/journal.pone.0139710.g002

over time while new peaks eluting at 9.5 or 15 min emerging due to pE conversion of Aβ(E3Q-40) and Aβ(E3Q-42) appeared. MALDI-mass spectrometry (see below) proved the conversion to the corresponding pE-modified variants. An incubation time of 24 h was appropriate to convert most of Aβ(E3Q-40/42) to pEAβ40 and pEAβ42, respectively, as observable by RP-HPLC analytics (Fig 3a and 3b).

Conversion was proven by comparing a non-pE-converted sample of [*U*-$^{15}$N]-Aβ(E3Q-40) with [*U*-$^{15}$N]-pEAβ40 using MALDI-mass spectrometry (Fig 3e, Method F in S1 File). The calculated averaged mass of [*U*-$^{15}$N]-Aβ(E3Q-40) is 4194 Da and 4176 Da for [*U*-$^{15}$N]-pEAβ40. Major peaks differing in 18 Da mass were visible, which corresponds to the loss of $^{15}NH_3$. However, the exact mass of both peptides were 2 Da less than calculated based on the fact that the purified protein is not monoisotopic, but at least 95% of all nitrogen atoms are $^{15}$N isotopes. Non-enzymatic conversion of Aβ(3–42) containing the N-terminal E3 to pEAβ42 showed a pronounced decreased efficiency under exactly the same conditions, i.e. 24 h incubation time at 45°C incubation temperature with sodium acetate, pH 3.5, as buffer condition. Only approximately 55% were non-enzymatically converted to pEAβ42 after 24 h incubation time (Fig 3c). Although the incubation time was increased up to 3 days, an improvement of the E to pE conversion was not observable, most likely as a consequence of aggregation. Thus, we proved that the E3Q mutation facilitates and increases the yield of the final pEAβ significantly.

Since pEAβ precipitated completely during conversion the cleavage products were dissolved in 8 M GdmCl for preparative RP-HPLC purification. In this last purification step, it was possible to eliminate remaining impurities like non-pE-converted Aβ(E3Q-40/42). The purity of final pEAβ40 and pEAβ42 was checked by analytical RP-HPLC and by Tris/Tricine-SDS-PAGE [41] and determined to be more than 95% pure (Fig 4a–4c). Final yields of natural abundant pEAβ40 and pEAβ42 were 15 mg/l culture and 14 mg/l culture, respectively. Yields for isotope enriched pEAβ were approximately 2 mg/l culture as shown in Table 1.

## Biophysical characterization of pEAβ40 and pEAβ42

Formation of amyloid-aggregates of various amyloidogenic proteins can be easily monitored by the commonly applied ThT assay [42]. Therefore, this assay was used to characterize the

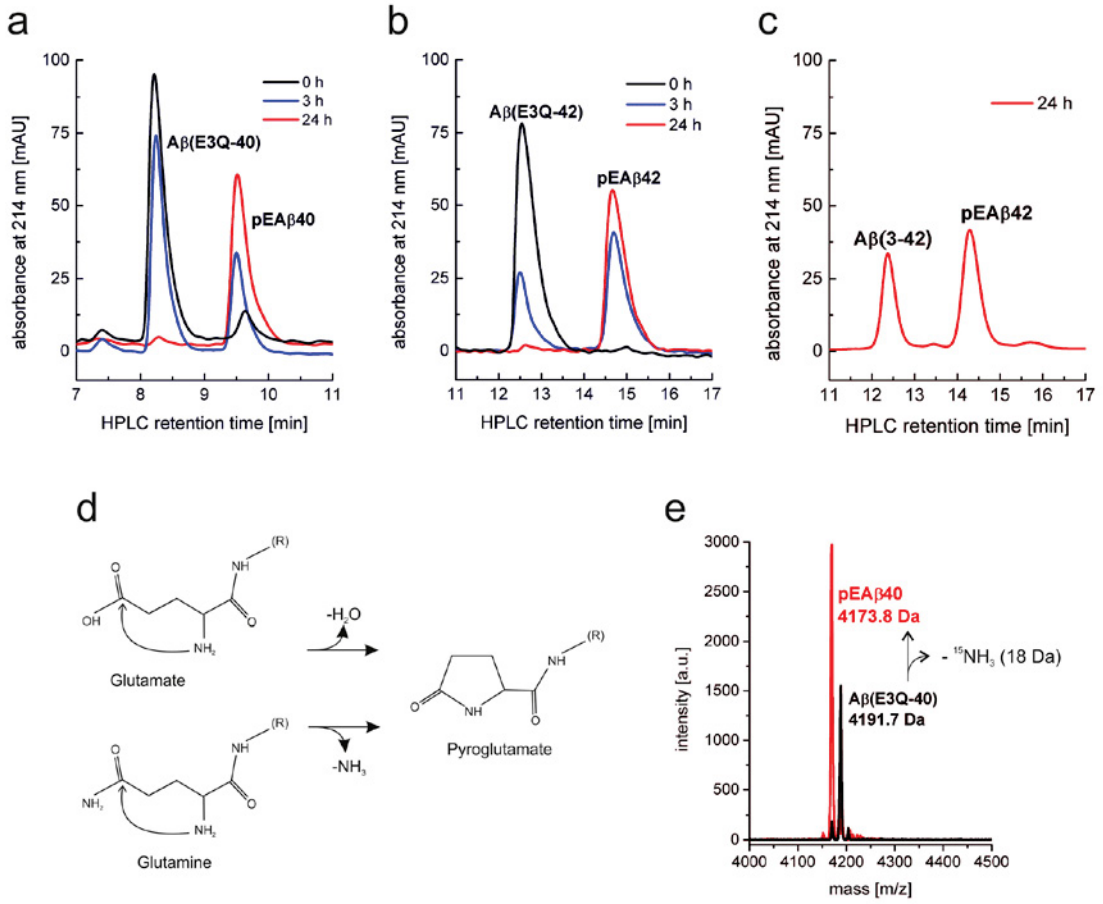


**Fig 3. Non-enzymatic pyroglutamate (pE) formation by acidic and elevated temperature conditions of Aβ(E3Q-40) (a), Aβ(E3Q-42) (b) and wild type Aβ(3–40) (c).** Peptides were incubated at 45°C in sodium acetate buffer pH 3.5 for 24 h. Conversion was observed by analytical RP-HPLC with an analytica Zorbax SB-300 C8 column in 30% ACN/ 0.1% TFA at 80°C. Peaks for non-modified peptides decreased while peaks for the pEAβ variants appeared at a longer retention time. (d) Reaction scheme of the conversion of N-terminal E3 or N-terminal Q3 to pE. (e) Mass spectrometry of [*U*-$^{15}$N]Aβ(E3Q-40) compared to N-terminally modified [*U*-$^{15}$N]pEAβ40. Molecular mass of the peptides differs in 18 Da due to the loss of the $^{15}NH_3$ group.

doi:10.1371/journal.pone.0139710.g003

aggregation kinetics of recombinant pEAβ. Aggregation kinetics of 10 μM solutions of pEAβ40 and pEAβ42 were performed in near-physiological aqueous solution (sodium phosphate buffer, pH 7.4) at 37°C (Method G in S1 File). Both recombinant pE-modified Aβ peptides showed the typical properties of Aβ aggregation, i.e. a distinct lag phase, an elongation phase and a stationary phase over a 12 h incubation period (Fig 5). Compared to pEAβ40, pEAβ42 started to aggregate much faster, already before measurement was started, and reaches its stationary phase after 4 h. In contrast, at this time point (4 h) pEAβ40 just starts to overcome its lag phase monitored by ThT assay. Maximum ThT fluorescence intensity for pEAβ40 was observed after 10 h. The observed different aggregation kinetics of pEAβ40 and pEAβ42 can be explained by the fact, that the increased C-terminal length in pEAβ42 compared to pEAβ40 but also, in comparison to wild type Aβ(1-40/42) data, N-terminal deletions enhance aggregation [33, 43].

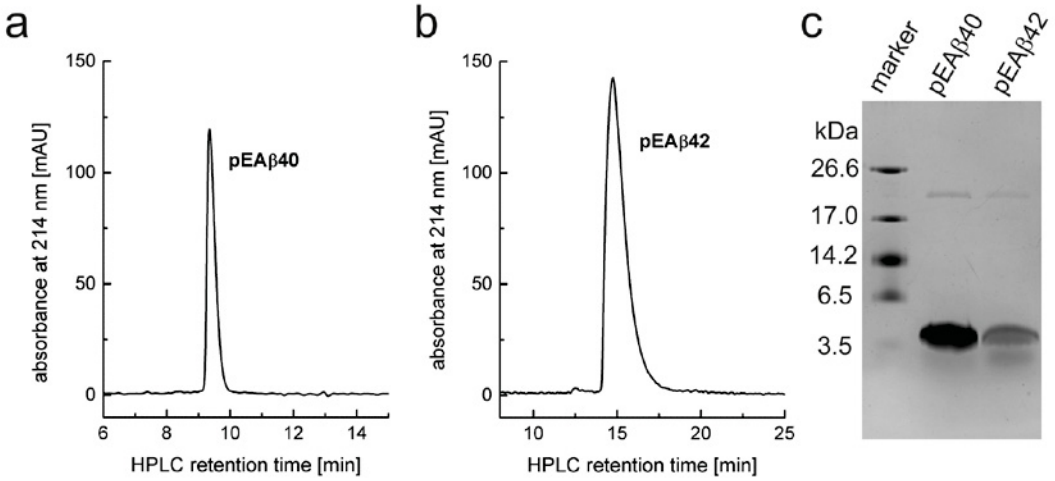


**Fig 4. Analytics of final purified pEAβ.** Analytical RP-HPLC of pEAβ40 (a) and pEAβ42 (b) after final purification and corresponding analysis of the proteins by Tris/Tricine-SDS-PAGE (c). The characteristic RP-HPLC retention times are approximately 9.5 min for pEAβ40 and 15 min for pEAβ42.

doi:10.1371/journal.pone.0139710.g004

pEAβ40 and pEAβ42 were further analyzed by solution NMR spectroscopy. 2D and 3D NMR data were obtained at concentrations varying from 25 to 70 μM in aqueous solution at pH 7.4 and at 5°C (Method H in S1 File). No changes in chemical shifts could be detected within three days for pEAβ40 and pEAβ42. The NMR assignments were accomplished using BEST-TROSY HNCA+ experiments [44] for pEAβ40 and pEAβ42. Fig 6a displays an overlay of $^{1}$H,$^{15}$N-HSQCs of pEAβ40 compared with the non-converted Aβ(E3Q-40). The loss of two signals from the γ-amino group due to deamination upon lactam ring formation as well as a shift of F4 and the appearance of a new signal of the pE3 peptide bond is the main difference.

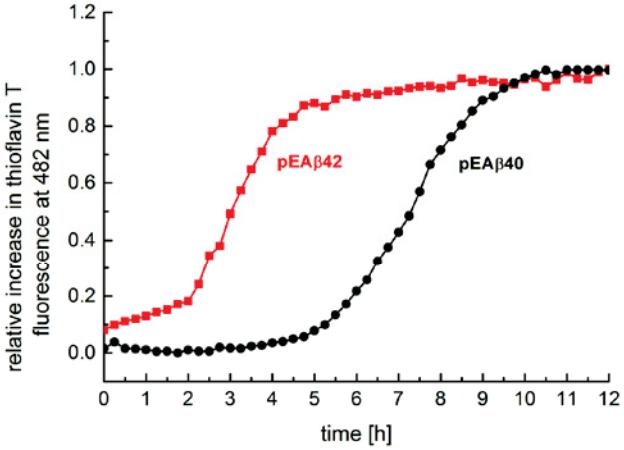


**Fig 5. ThT assay of 10 μM recombinant pEAβ40 and pEAβ42.** Experiments were performed in 10 mM sodium phosphate buffer pH 7.4 at 37°C. Binding of ThT (10 μM final concentration) to Aβ fibrils was determined by fluorescence at an extinction of 440 nm and emission at 492 nm.

doi:10.1371/journal.pone.0139710.g005

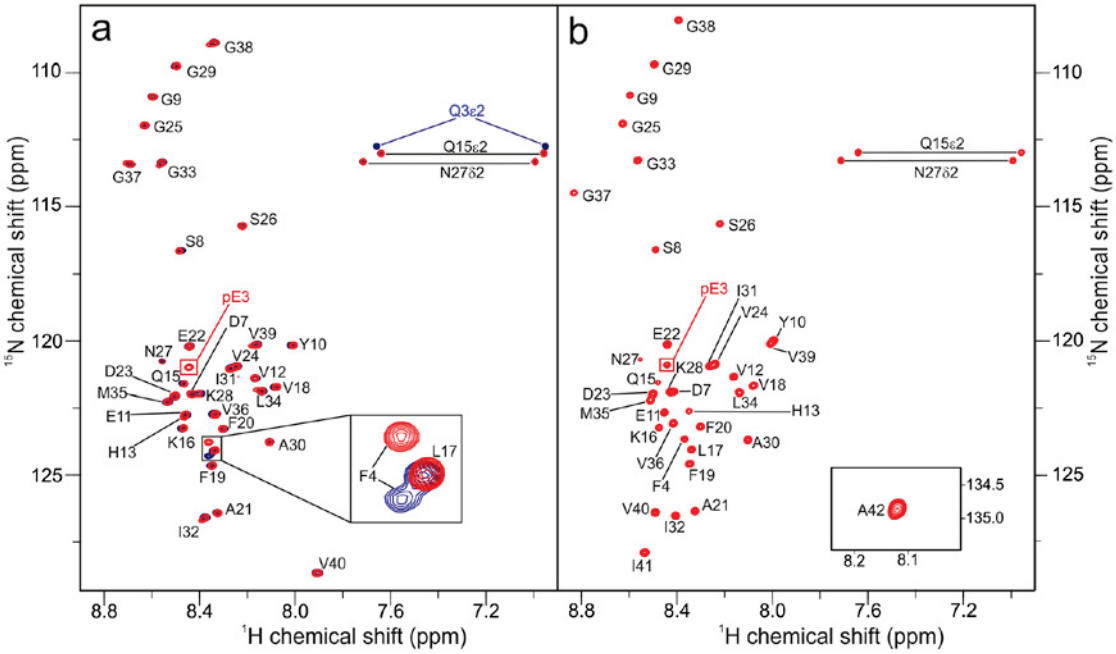


**Fig 6. $^{1}$H,$^{15}$N-HSQC spectra of Aβ(E3Q-40) (blue) and pEAβ40 (red) (a) or of pEAβ42 (b).** NMR spectra were recorded from 25 μM protein samples solved in 10 mM sodium phosphate buffer pH 7.4 at 5°C on a 600 MHz Bruker spectrometer. Note that in (a) "blue" signals derived from Aβ(E3Q-40) are overlaid with "red" signals from pEAβ40. Therefore "blue" signals are not visible, if identical in shift and intensity to "red" signals.

doi:10.1371/journal.pone.0139710.g006

The spectra of pEAβ42 showed analogous results, the signals for the N-terminal amino group and the γ-amino group of Q3 are missing and a signal derived from the intramolecular pE3 lactam group appears (Fig 6b). However, compared with spectra of recombinant Aβ(1–40) and Aβ(1–42) under similar conditions published previously [45–47], the $^{1}$H,$^{15}$N-HSQC NMR spectra of pEAβ40 and pEAβ42 differ slightly from Aβ(1-40/42). Although in both pEAβ species the N-terminal amino acid pE3 and the neighboring F4 are clearly visible, interestingly, R5 and H6 are missing not only in the pE modified peptides but also in the non-converted mutant E3Q, maybe due to the histidine-water proton exchange of H6 at neutral pH. Line-broadening and thus the disappearance of histidine signals were already described [48]. The intermediate acid-base proton exchange rate as well as the different tautomers of H6 might also affect the signal of the neighboring residue R5. D7 is shifted to lower frequency but from residue S8 on till the C-terminus, both NMR spectra for wild type Aβ(1-40/42) and for pEAβ40/42 are nearly identical.

## Conclusion

The described expression and purification system allows, for the first time, reproducible production of pEAβ in natural abundance and isotope-enriched in quantities up to 15 mg/l culture and overcomes the yield and costs limitations to perform reproducible biophysical studies. The purified pEAβ peptides (pEAβ40 and pEAβ42) showed elevated aggregation kinetics compared to Aβ(1–40) or Aβ(1–42), but, nonetheless, the monomeric states were suitable for biophysical studies at 5°C for at least three days. Moreover, it was possible to produce [*U*-$^{13}$C,$^{15}$N] pEAβ40

and pEAβ42 in high quality and quantity to perform high resolution NMR spectroscopy in solution state and to assign sequence specific signals of pEAβ40 and pEAβ42 under physiological conditions.

## Supporting Information

**S1 File.** Method A. Cloning of recombinant plasmid encoding Aβ(E3Q-40/42) fusion protein. Method B. Expression and purification of Aβ fusion proteins. Method C. Cleavage of the fusion protein and purification of Aβ. Method D. Conversion to pEAβ40 and pEAβ42. Method E. pEAβ sample preparation. Method F. Mass spectrometry. Method G. Thioflavin-T assay. Method H. NMR spectroscopy.
(DOCX)

## Acknowledgments

The plasmid encoding the Aβ(1–42) sequence was a generous gift from Prof. Dr. Rudolf Glockshuber (ETH Zürich). We thank Dr. Sabine Metzger (IUF, Düsseldorf) for recording mass spectra. Dr. Kerstin Reiß, Dr. Justin Lecher, Dr. Matthias Stoldt and Maren Thomaier (ICS-6, Forschungszentrum Jülich) are highly acknowledged for scientific advices.

## Author Contributions

Conceived and designed the experiments: CD LG PN HUD MS DW. Performed the experiments: CD LG MS PN. Analyzed the data: CD LG MS PN. Wrote the paper: CD MS LG PN DW.

## References

1. Soto C. Plaque busters: strategies to inhibit amyloid formation in Alzheimer's disease. Mol Med Today. 1999; 5: 343–350. PMID: 10431167
2. Palop JJ, Mucke L. Epilepsy and cognitive impairments in Alzheimer disease. Arch Neurol. 2009; 66: 435–440. doi: 10.1001/archneurol.2009.15 PMID: 19204149
3. Selkoe DJ. Alzheimer's disease: genotypes, phenotypes, and treatments. Science. 1997; 275: 630–631. PMID: 9019820
4. Huang Y, Mucke L. Alzheimer mechanisms and therapeutic strategies. Cell. 2012; 148: 1204–1222. doi: 10.1016/j.cell.2012.02.040 PMID: 22424230
5. Selkoe DJ. Physiological production of the beta-amyloid protein and the mechanism of Alzheimer's disease. Trends Neurosci. 1993; 16: 403–409. PMID: 7504355
6. Weidemann A, Konig G, Bunke D, Fischer P, Salbaum JM, Masters CL, et al. Identification, biogenesis, and localization of precursors of Alzheimer's disease A4 amyloid protein. Cell. 1989; 57: 115–126. PMID: 2649245
7. Kang J, Lemaire HG, Unterbeck A, Salbaum JM, Masters CL, Grzeschik KH, et al. The precursor of Alzheimer's disease amyloid A4 protein resembles a cell-surface receptor. Nature. 1987; 325: 733–736. PMID: 2881207
8. De Strooper B. Proteases and proteolysis in Alzheimer disease: a multifactorial view on the disease process. Physiol Rev. 2010; 90: 465–494. doi: 10.1152/physrev.00023.2009 PMID: 20393191
9. De Strooper B, Vassar R, Golde T. The secretases: enzymes with therapeutic potential in Alzheimer disease. Nat Rev Neurol. 2010; 6: 99–107. doi: 10.1038/nrneurol.2009.218 PMID: 20139999
10. Naslund J, Schierhorn A, Hellman U, Lannfelt L, Roses AD, Tjernberg LO, et al. Relative abundance of Alzheimer A beta amyloid peptide variants in Alzheimer disease and normal aging. Proc Natl Acad Sci U S A. 1994; 91: 8378–8382. PMID: 8078890
11. Roher AE, Lowenson JD, Clarke S, Woods AS, Cotter RJ, Gowing E, et al. beta-Amyloid-(1–42) is a major component of cerebrovascular amyloid deposits: implications for the pathology of Alzheimer disease. Proc Natl Acad Sci U S A. 1993; 90: 10836–10840. PMID: 8248178

12. Jawhar S, Wirths O, Bayer TA. Pyroglutamate amyloid-beta (Abeta): a hatchet man in Alzheimer disease. J Biol Chem. 2011; 286: 38825–38832. doi: 10.1074/jbc.R111.288308 PMID: 21965666

13. Sullivan CP, Berg EA, Elliott-Bryant R, Fishman JB, McKee AC, Morin PJ, et al. Pyroglutamate-Abeta 3 and 11 colocalize in amyloid plaques in Alzheimer's disease cerebral cortex with pyroglutamate-Abeta 11 forming the central core. Neurosci Lett. 2011; 505: 109–112. doi: 10.1016/j.neulet.2011.09.071 PMID: 22001577

14. Gunn AP, Masters CL, Cherny RA. Pyroglutamate-Abeta: role in the natural history of Alzheimer's disease. Int J Biochem Cell Biol. 2010; 42: 1915–1918. doi: 10.1016/j.biocel.2010.08.015 PMID: 20833262

15. Perez-Garmendia R, Gevorkian G. Pyroglutamate-Modified Amyloid Beta Peptides: Emerging Targets for Alzheimer s Disease Immunotherapy. Curr Neuropharmacol. 2013; 11: 491–498. doi: 10.2174/1570159X11311050004 PMID: 24403873

16. Mori H, Takio K, Ogawara M, Selkoe DJ. Mass spectrometry of purified amyloid beta protein in Alzheimer's disease. J Biol Chem. 1992; 267: 17082–17086. PMID: 1512246

17. Portelius E, Bogdanovic N, Gustavsson MK, Volkmann I, Brinkmalm G, Zetterberg H, et al. Mass spectrometric characterization of brain amyloid beta isoform signatures in familial and sporadic Alzheimer's disease. Acta Neuropathol. 2010; 120: 185–193. doi: 10.1007/s00401-010-0690-1 PMID: 20419305

18. Güntert A, Dobeli H, Bohrmann B. High sensitivity analysis of amyloid-beta peptide composition in amyloid deposits from human and PS2APP mouse brain. Neuroscience. 2006; 143: 461–475. PMID: 17008022

19. Saido TC, Iwatsubo T, Mann DM, Shimada H, Ihara Y, Kawashima S. Dominant and differential deposition of distinct beta-amyloid peptide species, A beta N3(pE), in senile plaques. Neuron. 1995; 14: 457–466. PMID: 7857653

20. Harigaya Y, Saido TC, Eckman CB, Prada CM, Shoji M, Younkin SG. Amyloid beta protein starting pyroglutamate at position 3 is a major component of the amyloid deposits in the Alzheimer's disease brain. Biochem Biophys Res Commun. 2000; 276: 422–427. PMID: 11027491

21. Kuo YM, Emmerling MR, Woods AS, Cotter RJ, Roher AE. Isolation, chemical characterization, and quantitation of A beta 3-pyroglutamyl peptide from neuritic plaques and vascular amyloid deposits. Biochem Biophys Res Commun. 1997; 237: 188–191. PMID: 9266855

22. De Kimpe L, van Haastert ES, Kaminari A, Zwart R, Rutjes H, Hoozemans JJ, et al. Intracellular accumulation of aggregated pyroglutamate amyloid beta: convergence of aging and Abeta pathology at the lysosome. Age (Dordr). 2013; 35: 673–687.

23. Wirths O, Breyhan H, Cynis H, Schilling S, Demuth HU, Bayer TA. Intraneuronal pyroglutamate-Abeta 3–42 triggers neurodegeneration and lethal neurological deficits in a transgenic mouse model. Acta Neuropathol. 2009; 118: 487–496. doi: 10.1007/s00401-009-0557-5 PMID: 19547991

24. Meissner JN, Bouter Y, Bayer TA. Neuron Loss and Behavioral Deficits in the TBA42 Mouse Model Expressing N-Truncated Pyroglutamate Amyloid-beta3-42. J Alzheimers Dis. 2015; 45: 471–482. doi: 10.3233/JAD-142868 PMID: 25547635

25. Venkataramani V, Wirths O, Budka H, Hartig W, Kovacs GG, Bayer TA. Antibody 9D5 recognizes oligomeric pyroglutamate amyloid-beta in a fraction of amyloid-beta deposits in Alzheimer's disease without cross-reactivity with other protein aggregates. J Alzheimers Dis. 2012; 29: 361–371. doi: 10.3233/JAD-2011-111379 PMID: 22232007

26. Acero G, Manoutcharian K, Vasilevko V, Munguia ME, Govezensky T, Coronas G, et al. Immunodominant epitope and properties of pyroglutamate-modified Abeta-specific antibodies produced in rabbits. J Neuroimmunol. 2009; 213: 39–46. doi: 10.1016/j.jneuroim.2009.06.003 PMID: 19545911

27. Wirths O, Erck C, Martens H, Harmeier A, Geumann C, Jawhar S, et al. Identification of low molecular weight pyroglutamate A{beta} oligomers in Alzheimer disease: a novel tool for therapy and diagnosis. J Biol Chem. 2010; 285: 41517–41524. doi: 10.1074/jbc.M110.178707 PMID: 20971852

28. Schilling S, Hoffmann T, Manhart S, Hoffmann M, Demuth HU. Glutaminyl cyclases unfold glutamyl cyclase activity under mild acid conditions. FEBS Lett. 2004; 563: 191–196. PMID: 15063747

29. Schilling S, Niestroj AJ, Rahfeld JU, Hoffmann T, Wermann M, Zunkel K, et al. Identification of human glutaminyl cyclase as a metalloenzyme. Potent inhibition by imidazole derivatives and heterocyclic chelators. J Biol Chem. 2003; 278: 49773–49779. PMID: 14522962

30. Twardzik DR, Peterkofsky A. Glutamic acid as a precursor to N-terminal pyroglutamic acid in mouse plasmacytoma protein (protein synthesis-initiation-immunoglobulins-pyrrolidone carboxylic acid). Proc Natl Acad Sci U S A. 1972; 69: 274–277. PMID: 4400295

31. Chelius D, Jing K, Lueras A, Rehder DS, Dillon TM, Vizel A, et al. Formation of pyroglutamic acid from N-terminal glutamic acid in immunoglobulin gamma antibodies. Anal Chem. 2006; 78: 2370–2376. PMID: 16579622

32. Schilling S, Wasternack C, Demuth HU. Glutaminyl cyclases from animals and plants: a case of functionally convergent protein evolution. Biol Chem. 2008; 389: 983–991. doi: 10.1515/BC.2008.111 PMID: 18979624

33. Schilling S, Lauber T, Schaupp M, Manhart S, Scheel E, Bohm G, et al. On the seeding and oligomerization of pGlu-amyloid peptides (in vitro). Biochemistry. 2006; 45: 12393–12399. PMID: 17029395

34. D'Arrigo C, Tabaton M, Perico A. N-terminal truncated pyroglutamyl beta amyloid peptide Abetapy3-42 shows a faster aggregation kinetics than the full-length Abeta1-42. Biopolymers. 2009; 91: 861–873. doi: 10.1002/bip.21271 PMID: 19562755

35. Russo C, Salis S, Dolcini V, Venezia V, Song XH, Teller JK, et al. Amino-terminal modification and tyrosine phosphorylation of [corrected] carboxy-terminal fragments of the amyloid precursor protein in Alzheimer's disease and Down's syndrome brain. Neurobiol Dis. 2001; 8: 173–180. PMID: 11162251

36. Bayer TA, Wirths O. Focusing the amyloid cascade hypothesis on N-truncated Abeta peptides as drug targets against Alzheimer's disease. Acta Neuropathol. 2014; 127: 787–801. doi: 10.1007/s00401-014-1287-x PMID: 24803226

37. Finder VH, Vodopivec I, Nitsch RM, Glockshuber R. The recombinant amyloid-beta peptide Abeta1-42 aggregates faster and is more neurotoxic than synthetic Abeta1-42. J Mol Biol. 2010; 396: 9–18. doi: 10.1016/j.jmb.2009.12.016 PMID: 20026079

38. Luhrs T, Ritter C, Adrian M, Riek-Loher D, Bohrmann B, Dobeli H, et al. 3D structure of Alzheimer's amyloid-beta(1–42) fibrils. Proc Natl Acad Sci U S A. 2005; 102: 17342–17347. PMID: 16293696

39. Kapust RB, Tozser J, Copeland TD, Waugh DS. The P1' specificity of tobacco etch virus protease. Biochem Biophys Res Commun. 2002; 294: 949–955. PMID: 12074568

40. Laemmli UK. Cleavage of structural proteins during the assembly of the head of bacteriophage T4. Nature. 1970; 227: 680–685. PMID: 5432063

41. Schagger H, von Jagow G. Tricine-sodium dodecyl sulfate-polyacrylamide gel electrophoresis for the separation of proteins in the range from 1 to 100 kDa. Anal Biochem. 1987; 166: 368–379. PMID: 2449095

42. Bolder SG, Sagis LM, Venema P, van der Linden E. Thioflavin T and birefringence assays to determine the conversion of proteins into fibrils. Langmuir. 2007; 23: 4144–4147. PMID: 17341102

43. Pike CJ, Overman MJ, Cotman CW. Amino-terminal deletions enhance aggregation of beta-amyloid peptides in vitro. J Biol Chem. 1995; 270: 23895–23898. PMID: 7592576

44. Gil-Caballero S, Favier A, Brutscher B. HNCA+, HNCO+, and HNCACB+ experiments: improved performance by simultaneous detection of orthogonal coherence transfer pathways. J Biomol NMR. 2014; 60: 1–9. doi: 10.1007/s10858-014-9847-x PMID: 25056271

45. Weber DK, Sani MA, Gehman JD. A routine method for cloning, expressing and purifying Abeta(1–42) for structural NMR studies. Amino Acids. 2014; 46: 2415–2426. doi: 10.1007/s00726-014-1796-x PMID: 25027618

46. Rezaei-Ghaleh N, Andreetto E, Yan LM, Kapurniotu A, Zweckstetter M. Interaction between amyloid beta peptide and an aggregation blocker peptide mimicking islet amyloid polypeptide. PLoS One. 2011; 6: e20289. doi: 10.1371/journal.pone.0020289 PMID: 21633500

47. Hou L, Shao H, Zhang Y, Li H, Menon NK, Neuhaus EB, et al. Solution NMR studies of the A beta(1–40) and A beta(1–42) peptides establish that the Met35 oxidation state affects the mechanism of amyloid formation. J Am Chem Soc. 2004; 126: 1992–2005. PMID: 14971932

48. Day RM, Thalhauser CJ, Sudmeier JL, Vincent MP, Torchilin EV, Sanford DG, et al. Tautomerism, acid-base equilibria, and H-bonding of the six histidines in subtilisin BPN' by NMR. Protein Sci. 2003; 12: 794–810. PMID: 12649438

## Supporting Information

### S1 Cloning of recombinant plasmid encoding Aβ(E3Q-40/42) fusion protein

Cloning was based on a plasmid encoding wildtype Aβ(1-42) as a fusion protein with an N-terminal $His_6$-tag, a solubilizing fusion partner $(NANP)_{19}$ and a modified tobacco etch virus protease (TEV) recognition site, which was kindly provided by Finder, Glockshuber and coworkers (1). Firstly, codons for D1 and A2 were deleted (Δ1/2) leading to the Aβ(3-42) construct. The following mutation of the encoding DNA sequence of E3 to Q (E3Q) leads to Aβ(E3Q-42) intended for increasing nonenzymatic conversion to pE. In addition, codons for the aa 41 and 42 (Δ41/42) were deleted to obtain the shortened variant ending with V40, i.e. Aβ(E3Q-40).

The oligonucleotides for deletion of codons for D1 and A2 and for codon mutation of E3 to Q were obtained (HPLC-grade) from Eurofins (Ebersberg, Germany) and the oligonucleotides to delete codons for I41 and A42 were obtained from BioTeZ (Berlin, Germany).

Δ1/2 forward: 5'-`CTG AAA ACC TGT ATT TCC AGG AGT TCC GTC ATG ATT CAG`-3'

Δ1/2 reverse: 5'-`CTG AAT CAT GAC GGA ACT CCT GGA AAT ACA GGT TTT CAG`-3'

E3Q forward: 5'-`GAA AAC CTG TAT TTC CAG CAG TTC CGT CAT GAT TCA G`-3'

E3Q reverse: 5'-`GTG AAT CAT GAC GGA ACT GCT GGA AAT ACA GGT TTT C`-3'

Δ41/42 forward: 5'-`GGT GGG TGG TGT TGT CTA ATA GTA AAG CTT G`-3'

Δ41/42 reverse: 5'-`CAA GCT TTA CTA TTA GAC AAC ACC ACC CAC C`-3'

Constructs for Δ1/2 and E3Q mutation were cloned using QuikChange Lightning Multi Site-Directed Mutagenesis Kit (Agilent, Böblingen, Germany). Amplification conditions were 30 cycles of 20 sec at 95 °C for denaturing, 30 sec at 55 °C for annealing and 2 min at 65 °C for elongation with *Pfu* ultra HF polymerase. Δ41/42 mutation of the E3Q construct was cloned with GeneArt® Site-Directed Mutagenesis PLUS System (Invitrogen Life Technology, Darmstadt, Germany) using 18 cycles of 50 sec at 95 °C for denaturing, 50 sec at 60 °C for annealing and 5 min at 68 °C for elongation with *Pfu* ultra HF polymerase. The amplified DNA was directly used for *Dpn*I digestion of the parental strain. *Escherichia coli* XL10 cells were transformed with the PCR product and grown clones were picked and sequenced by Seqlab (Göttingen, Germany).

## S2 Expression and purification of Aβ fusion proteins

For expression of Aβ(E3Q-40/42) and wildtype Aβ(3-42) fusion proteins in natural abundance, a single colony of freshly transformed *E. coli* BL21 (DE3) pLysS cells was used to inoculated LB overnight starter-cultures (10 g/l tryptone, 5 g/l yeast extract and 5 g/l NaCl containing 100 mg/l ampicillin and 34 mg/l chloramphenicol). Main cultures of 1 l TB medium (12 g/l tryptone, 24 g/l yeast extract and 17 mM $KH_2PO_4$ and 72 mM $K_2HPO_4$ containing 100 mg/l ampicillin and 34 mg/l chloramphenicol) were inoculated with starter-cultures (1:100) and incubated at 37 °C until an $OD_{600\ nm}$ of 2.0 was reached. Protein expression was induced by adding isopropyl β-D-1-thiogalactopyranoside (IPTG) to a final concentration of 1 mM. The cells were incubated overnight at 30 °C and 160 rpm and then harvested by centrifugation (5,000 x g, 30 min). Cell pellets were resuspended in 5-10 ml lysis buffer (8 M guanidine hydrochloride (GdmCl)-NaOH, 300 mM NaCl, 30 mM Tris-HCl, 10 mM imidazole, pH 7.9) per gram wet weight, stirred for 2 h at 4 °C and then sonicated under ice cooling (3 x 1min, 50 % power, 5 mm micro-tip, Branson sonifier 250). Cell extract was clarified by centrifugation (50,000 x g, 45 min).

Uniformly [*U*-$^{15}$N]- and [*U*-$^{13}$C, $^{15}$N]-Aβ(E3Q-40/42) fusion proteins were expressed from cultures grown in M9 minimal media (2) with 1 g/l $^{15}NH_4Cl$ and 2.5 g/l unlabeled or [*U*-$^{13}$C]-glucose being the sole nitrogen and carbon sources, respectively. Cultures were grown as described above for expression in natural abundance, with the difference that a starter-culture in non-isotope enriched M9 minimal media was prepared and used to inoculate 1 l main culture to an $OD_{600\ nm}$ of 0.1. The cells were then grown to an $OD_{600\ nm}$ of 1.2 and protein expression was performed overnight as described above.

The cell lysate was purified using immobilized metal affinity chromatography (IMAC) with 2 ml of $Ni^{2+}$-NTA agarose (Qiagen, Hilden, Germany) per g of processed cells. The resin was equilibrated with lysis buffer and the cell extract was applied. After washing with 10 column volumes (CV) of lysis buffer, non-specifically bound protein was removed with 5 CV of lysis buffer including 20 mM imidazole. The fusion protein was eluted with 3 CV of 500 mM imidazole in lysis buffer and stored at -20 °C until further use. The eluate was checked by analytical reversed-phase high performance liquid chromatography (RP-HPLC) using a Zorbax SB-300 C8 column (5 µ, 4.6 mm x 250 mm, Agilent, Böblingen, Germany) connected to an Agilent 1200 Infinity system in 30 % acetonitrile (ACN) containing 0.1 % trifluoroacetic acid (TFA) at 80 °C and a flow-rate of 1 ml/min. Absorbance was measured at 214 nm. Data were recorded and analyzed with the program ChemStation (Agilent, Böblingen, Germany).

Further purification was performed via RP-HPLC using a semi-preparative Zorbax SB-300 C8 column (5 µ, 9.4 mm x 250 mm, Agilent, Böblingen, Germany) equilibrated with 20 % ACN/ 0.1 % TFA heated at 80 °C. IMAC purified fusion protein was directly loaded onto the column with a flow-rate of 4 ml/min. The column was washed for 12 min with 20 % ACN/ 0.1 % TFA and the fusion protein was then eluted with an isocratic step to 32 % ACN/ 0.1 % TFA and lyophilized.

**S3 Cleavage of the fusion protein and purification of Aβ**

The $His_6$-tag and the solubilizing fusion partner $(NANP)_{19}$ were cleaved from the fusion protein using TEV protease. Lyophilized fusion protein was resuspended in protease compatible buffer including 30 mM Tris-HCl, 1 mM EDTA, pH 8.0 and 3 mM dithiotreithol (DTT). 1 mg TEV protease per 8 mg fusion protein was added leading to a molar ratio around 0.06 equivalents relative to the fusion protein. Standard concentration of fusion protein was around 3-4 mg/ml. The cleavage reaction was performed at 4 °C for 20 h and was observed by analytical RP-HPLC isocratically with of 30 % ACN/ 0.1 % TFA at 80 °C. Since cleaved Aβ(E3Q-42) precipitated completely and Aβ(E3Q-40) partially during the reaction, the reaction mixture was centrifuged (16,000 x g, 20 min), the precipitate was dissolved in lysis buffer and both, supernatant and resuspended pellet, were reanalyzed by analytical RP-HPLC. Aβ containing fractions were purified on semi-preparative RP-HPLC (details see above). For Aβ(E3Q-42), the Zorbax SB300 C-8 column was equilibrated in 28 % ACN/ 0.1 % TFA and after sample loading washed for 12 min isocratically under equilibration conditions, then the target protein was eluted in an isocratic step with 35 % ACN/ 0.1 % TFA within 10 min. For Aβ(E3Q-40), the column was equilibrated with 30 % ACN/ 0.1 % TFA and protein was eluted isocratically with the same eluent. Pooled fractions containing Aβ(E3Q-40/42) were lyophilized and stored at -20 °C.

**S4 Conversion to pEAβ40 and pEAβ42**

Non-enzymatic conversion of Aβ(E3Q-40/42) to pEAß40 or pEAß42 was performed by incubation in mild acidic and elevated temperature condition. Therefore, lyophilized protein was dissolved in 30 mM sodium acetate, pH 3.5 (adjusted with acetic acid) to a concentration of 0.25 mg/ml and incubated at 45 °C with gentle stirring for 24 h. Conversion to pEAβ was analyzed by analytical RP-HPLC isocratically (see above) with 30 % ACN/ 0.1 % TFA at 80 °C and a flow-rate of 1 ml/min. Converted pEAβ40 and pEAβ42 precipitated completely during chemical reaction, therefore the reaction mixture was centrifuged (16,000 x g, 20 min) and the protein pellet was resuspended in lysis buffer. Purification of pEAβ was performed by semi-preparative RP-HPLC using the same

conditions applied for the purification of unconverted Aβ(E3Q-40/42), respectively, and lyophilized.

**S5 pEAβ sample preparation**

Lyophilized pEAβ40 or pEAβ42 was dissolved in hexafluoroisopropanol (HFIP) and incubated at room temperature (RT) for at least three days to monomerize. Concentration was determined using a pEAβ40 calibration curve obtained by RP-HPLC. For this, 1 mg pEAβ40 was dissolved in 8 M GdmCl-NaOH pH 7.9 and diluted to final concentrations varying from 0 µM to 240 µM. The dilution series was applied on analytical Zorbax SB-300 C8 column in 30 % ACN/ 0.1 % TFA and eluted isocratically. A linear calibration curve was estimated due to the known concentration of pEAβ and the depended peak area detected at 214 nm. Based on this, all adjacent concentrations for recombinant pEAβ were calculated. Aliquots of 1 mg and specific aliquots for following experiments were prepared, lyophilized and stored at -20 °C until further use.

**S6 Mass spectrometry**

Mass spectrometry was performed using a high performance matrix-assisted laser desorption time of flight mass spectrometer (Voyager MALDI-TOF). Data were recorded between 1,000 and 15,000 m/z in positive-ion mode at the Leibniz-Institut für Umweltmedizinische Forschung (IUF, Düsseldorf, Germany).

**S7 Thioflavin-T assay**

Lyophilized pEAβ40 or pEAβ42 was dissolved in 10 mM $H_3PO_4$-NaOH, pH 7.4 and 10 µM ThT to a final concentration of 25 µM. Aggregation assays were performed using black non-binding 96-well plates (Sigma-Aldrich, Germany) at 37 °C. Wells were filled with samples to a total volume of 100 µl and each reaction was performed fivefold. Fluorescence was monitored with a microplate reader (PolarStar Optima, BMG, Offenburg, Germany) at excitation and emission wavelength of 440 and 492 nm, respectively, in bottom-reading mode every 15 min with 30 s shaking prior to reading. Fluorescence of the buffer excluding pEAβ was subtracted to correct for background.

**S8 NMR spectroscopy**

Lyophilized pEAβ was directly dissolved in 10 mM $H_3PO_4$-NaOH, pH 7.4 and 10 % $D_2O$ by vortexing. Sample concentrations varied between 25 and 50 µM. NMR spectra were acquired using a cryoprobe-equipped Bruker 600 MHz spectrometer at 5 °C in 5 mm

standard NMR tubes. Chemical shift assignments were made using standard $^{1}H,^{15}N$-HSQC and BEST-TROSY HNCA+ (3) experiments and spectra were processed with NMRPipe (4) and analyzed using CCPNmr Analysis (5). $^{1}H$ chemical shifts were referenced with respect to external DSS in $D_2O$, $^{13}C$ and $^{15}N$ chemical shifts were referenced indirectly according to their gyromagnetic ratios (6, 7).

## References (Supporting Information)


1. Finder VH, Vodopivec I, Nitsch RM, Glockshuber R. The recombinant amyloid-beta peptide Abeta1-42 aggregates faster and is more neurotoxic than synthetic Abeta1-42. J Mol Biol. 2010;396: 9-18.

2. Maniatis T, Fritsch EF, Sambrook J. Molecular cloning : a laboratory manual. Cold Spring Harbor, N.Y.: Cold Spring Harbor Laboratory; 1982. x, 545 p. p.

3. Gil-Caballero S, Favier A, Brutscher B. HNCA+, HNCO+, and HNCACB+ experiments: improved performance by simultaneous detection of orthogonal coherence transfer pathways. J Biomol NMR. 2014;60: 1-9.

4. Delaglio F, Grzesiek S, Vuister GW, Zhu G, Pfeifer J, Bax A. NMRPipe: a multidimensional spectral processing system based on UNIX pipes. J Biomol NMR. 1995;6: 277-293.

5. Vranken WF, Boucher W, Stevens TJ, Fogh RH, Pajon A, Llinas M, et al. The CCPN data model for NMR spectroscopy: development of a software pipeline. Proteins. 2005;59: 687-696.

6. Wishart DS, Bigam CG, Yao J, Abildgaard F, Dyson HJ, Oldfield E, et al. 1H, 13C and 15N chemical shift referencing in biomolecular NMR. J Biomol NMR. 1995;6: 135-140.

7. Markley JL, Bax A, Arata Y, Hilbers CW, Kaptein R, Sykes BD, et al. Recommendations for the presentation of NMR structures of proteins and nucleic acids--IUPAC-IUBMB-IUPAB Inter-Union Task Group on the standardization of data bases of protein and nucleic acid structures determined by NMR spectroscopy. Eur J Biochem. 1998;256: 1-15.

## 3.2 Structural analysis and aggregation propensity of pEAβ(3-40) in aqueous triflouroethanol

Christina Dammers, Lothar Gremer, Kerstin Reiß, Antonia N. Klein, Philipp Neudecker, Rudolf Hartmann, Na Sun, Hans-Ulrich Demuth, Melanie Schwarten and Dieter Willbold

Journal: PLOS ONE

Impact Factor: 3.53 (2013/2014)

Contributions: 90 %, protein production, experimental design, performance and analysis of ThT assays, TEM and NMR and CD spectroscopy, manuscript writing

PLOS | ONE

RESEARCH ARTICLE

# Structural Analysis and Aggregation Propensity of Pyroglutamate Aβ(3-40) in Aqueous Trifluoroethanol

**Christina Dammers[1], Lothar Gremer[1,2], Kerstin Reiß[1], Antonia N. Klein[1], Philipp Neudecker[1,2], Rudolf Hartmann[1], Na Sun[1], Hans-Ulrich Demuth[3], Melanie Schwarten[1], Dieter Willbold[1,2]***

**1** Institute of Complex Systems (ICS-6) Structural Biochemistry, Forschungszentrum Jülich, 52425, Jülich, Germany, **2** Institut für Physikalische Biologie, Heinrich-Heine-Universität Düsseldorf, 40225, Düsseldorf, Germany, **3** Fraunhofer Institute for Cell Therapy and Immunology, Department of Drug Design and Target Validation, 06120, Halle (Saale), Germany

* d.willbold@fz-juelich.de



OPEN ACCESS

**Citation:** Dammers C, Gremer L, Reiß K, Klein AN, Neudecker P, Hartmann R, et al. (2015) Structural Analysis and Aggregation Propensity of Pyroglutamate Aβ(3-40) in Aqueous Trifluoroethanol. PLoS ONE 10(11): e0143647. doi:10.1371/journal.pone.0143647

**Editor:** Surajit Bhattacharjya, Nanyang Technological University, SINGAPORE

**Received:** September 25, 2015

**Accepted:** November 6, 2015

**Published:** November 23, 2015



**Data Availability Statement:** All relevant data are within the paper and its Supporting Information files.

**Funding:** We gratefully acknowledge support of CD from the International NRW Research School BioStruct, granted by the Ministry of Innovation, Science and Research of the State North Rhine-Westphalia, the Heinrich Heine University of Düsseldorf, and the Entrepreneur Foundation at the Heinrich Heine University of Düsseldorf. DW was supported by grants from the "Portfolio Technology and Medicine", the "Portfolio Drug Research" and the Helmholtz-Validierungsfonds of the "Impuls und

## Abstract

A hallmark of Alzheimer's disease (AD) is the accumulation of extracellular amyloid-β (Aβ) plaques in the brains of patients. N-terminally truncated pyroglutamate-modified Aβ (pEAβ) has been described as a major compound of Aβ species in senile plaques. pEAβ is more resistant to degradation, shows higher toxicity and has increased aggregation propensity and β-sheet stabilization compared to non-modified Aβ. Here we characterized recombinant pEAβ(3–40) in aqueous trifluoroethanol (TFE) solution regarding its aggregation propensity and structural changes in comparison to its non-pyroglutamate-modified variant Aβ (1–40). Secondary structure analysis by circular dichroism spectroscopy suggests that pEAβ(3–40) shows an increased tendency to form β-sheet-rich structures in 20% TFE containing solutions where Aβ(1–40) forms α-helices. Aggregation kinetics of pEAβ(3–40) in the presence of 20% TFE monitored by thioflavin-T (ThT) assay showed a typical sigmoidal aggregation in contrast to Aβ(1–40), which lacks ThT positive structures under the same conditions. Transmission electron microscopy confirms that pEAβ(3–40) aggregated to large fibrils and high molecular weight aggregates in spite of the presence of the helix stabilizing co-solvent TFE. High resolution NMR spectroscopy of recombinantly produced and uniformly isotope labeled [*U*-$^{15}$N]-pEAβ(3–40) in TFE containing solutions indicates that the pyroglutamate formation affects significantly the N-terminal region, which in turn leads to decreased monomer stability and increased aggregation propensity.

## Introduction

The pathology of Alzheimer's disease (AD) is characterized by the presence of intracellular neurofibrillary tangles consisting of accumulated hyperphosphorylated tau protein and extracellular plaques containing amyloid-β (Aβ) as major component [1, 2]. Aβ is derived by

Vernetzungs-Fonds der Helmholtzgemeinschaft". The funders had no role in study design, data collection and analysis, decision to publish, or preparation of the manuscript.

**Competing Interests**: The authors have declared that no competing interests exist.

processing of the amyloid precursor protein by β- and γ-secretases [3, 4]. Multiple possible cleavage positions of γ-secretase combined with various posttranslational modifications of the cleaved products result in different Aβ isoforms with heterogeneity in length as well as N- and C-terminal sequences [5, 6]. Pyroglutamate-modified Aβ (pEAβ) peptides have been reported to be the dominant component of all N-terminal truncated Aβ variants in AD plaques as up to 20% of the total Aβ are pEAβ variants [7–9]. pEAβ deposits in the brains of presymptomatic AD patients [10] and was shown to play a dominant role in plaque formation and to provoke neurodegeneration in mouse models [11, 12]. Formation of pEAβ is based on N-terminal truncation leading to N-terminal E3 or E11 and subsequent cyclization of the accessible E amino group with the side chain carboxy group leading to pyroglutamate. *In vivo* it was suggested the cyclization is catalyzed by the enzyme glutaminyl cyclase [13, 14]. pEAβ starting at position 3 (pEAβ(3-x)) represents the major fraction of N-pyroglutamate modified Aβ species in intracellular, extracellular and vascular accumulations in AD brains [15–18]. The cumulative deposition of pEAβ in AD brains coincides with increased protease-stability since the pyroglutamate modified N-terminus is inaccessible to aminopeptidases [19, 20]. The loss of two negative charges (side chain carboxyl groups of D1 and E3) and one positive charge (E3 amino group) at physiological pH result in higher hydrophobicity of pEAβ(3-x) [19, 21]. Aggregation of pEAβ (3-x) is up to 250-fold accelerated [22] and its neurotoxicity is enhanced [23, 24] when compared with the corresponding wild type Aβ species independent of the C-terminal length.

Structural analysis of pEAβ monomers is essential to uncover its aggregation mechanism and to reveal, why it is more prone to self-assembly than Aβ wild type. In a previous NMR study, we analyzed pEAβ(3–40) in aqueous buffer conditions at neutral pH and compared it with given Aβ(1–40) data [25]. Most chemical shifts were nearly identical except of the very N-terminal region and both peptides were shown to be unstructured.

Since structural studies of Aβ peptides are often limited due to their high aggregation tendency, solvent conditions need to be carefully chosen. α-helical Aβ monomers are predominantly formed in micelles [26], hexafluoroisopropanol (HFIP)/water [27] and 2,2,2-trifluoroethanol (TFE)/water [28] mixtures. In a previous NMR study we compared pEAβ(3–40) with Aβ(1–40), both chemically synthesized with natural carbon and nitrogen isotope abundance, in aqueous solution containing 40% TFE [29]. The results indicated that both Aβ isoforms formed α-helical structures in two regions (aa 14–22 and aa 30–36) connected by a flexible and disordered linker. However, pEAβ(3–40) exhibited a decreased helix propensity in agreement with its higher hydrophobicity and faster aggregation kinetics.

Here, we analyzed the solvent conditions for the transition of pEAβ(3–40) from TFE-induced α-helices to β-sheets by gradually lowering the TFE concentrations. We expand the data by investigations of recombinantly produced [$U$-$^{15}$N]-pEAβ(3–40) regarding structure and aggregation in 20% TFE, where Aβ(1–40) is still in a predominantly α-helical monomeric state, while pEAβ(3–40) forms a β-sheet dominated secondary structure, starts to aggregate and forms large fibrils.

## Materials and Methods

### Peptides and sample preparation

Expression and purification of uniformly isotope labeled [$U$-$^{15}$N]-pEAβ(3–40) and [$U$-$^{15}$N]-Aβ(1–40) as well as non-labeled pEAβ(3–40) were performed as described recently [25, 30]. Synthetic non-labeled Aβ(1–40) was purchased from Bachem (Heidelberg, Germany). Samples were prepared in Protein LowBinding tubes (Eppendorf AG, 230 Hamburg, Germany). The Aβ peptides were dissolved in HFIP (1,1,1,3,3,3,-hexafluoro-2-propanol, Sigma-Aldrich,

Hannover, Germany) and monomerized for 3 days at room temperature. Samples were lyophilized and stored at -20°C.

### CD spectroscopy

Lyophilized peptides were dissolved in aqueous buffer containing different TFE concentrations (20–25% TFE in 50 mM potassium phosphate, pH 2.8) to a final concentration of 25 μM. UV CD measurements were performed in 1 mm path-length cuvettes at 20°C. CD spectra were recorded on a Jasco J-1100 spectropolarimeter from 260 to 187 nm with 0.5 nm step size, 50 nm/min scan speed, 1 nm bandwidth and 10 scans per sample. Background correction was performed by subtraction of corresponding buffer spectra.

### ThT assay

Lyophilized peptides were dissolved to a final concentration of 25 μM in buffer (20–25% TFE in 50 mM potassium phosphate, pH 2.8) containing 10 μM ThT. Aggregation assays were performed in black non-binding 96-well plates (Sigma-Aldrich, Germany) at 20°C with a total volume of 100 μl per well. Each reaction was performed fivefold and background corrected by subtraction of the buffer control. Fluorescence was monitored in 10 min steps using a microplate reader (PolarStar Optima, BMG, Offenburg, Germany) with 440 excitation and 492 nm emission filters, respectively, in bottom-read mode. Wells were shaken 30°s prior to measurement.

### TEM microscopy

Lyophilized pEAβ(3–40) was dissolved in aqueous buffer (20% TFE in 50 mM potassium phosphate, pH 2.8) and incubated for five days at 20°C. Fibrils were absorbed on formval/carbon coated copper grids (S162, Plano, Wetzlar, Germany) for 5 min and washed with water. Negative staining was performed by incubation with 1% (w/v) uranylacetate for 1 min. Images were taken with a Libra 120 transmission electron microscope (Zeiss, Oberkochen, Germany) at 120 kV.

### NMR spectroscopy

Lyophilized [$U$-$^{15}$N]-pEAβ(3–40) and [$U$-$^{15}$N]-Aβ(1–40) were directly dissolved in 100% TFE-d2-OH and diluted with 50 mM potassium phosphate, pH 2.8 to a final concentration of 25 μM peptide in 20% TFE. NMR spectra were acquired using a TXI- or QCI-cryoprobe equipped Bruker Avance III HD 600 MHz spectrometer. $^{1}$H,$^{15}$N-HSQC correlation spectra were recorded according to standard Bruker pulse-sequences [31–33]. $^{1}H_{N}$ and $^{15}$N Backbone resonance assignments in 30% TFE were obtained by using BEST-TROSY (BT) HNCA+-optimized pulse sequences [34, 35]. Resonance assignments of spectra recorded at 30% TFE concentration were transferred to the spectrum recorded at 20% TFE through recordings at TFE concentrations of 27% and 23%, respectively. Spectra were processed with NMRPipe [36] and evaluated with CCPNmr Analysis [37]. Analysis of Cα secondary chemical shifts is based on the publication by Zhang *et al.* [38] and sequence corrected according to Schwarzinger [39].

## Results

### Secondary structure analysis by CD spectroscopy

TFE is known to induce α-helical structures by lowering the solvent polarity and promoting intra-molecular hydrogen bonding [40]. Reducing the concentration of this co-solvent prevents this effect e.g. as shown for Aβ(1–40) [41], human carbonic anhydrase II [42], FF domain of URN1 splicing factor [43], transferrin [44], α-synuclein [45] and conalbumin [46]. The α-

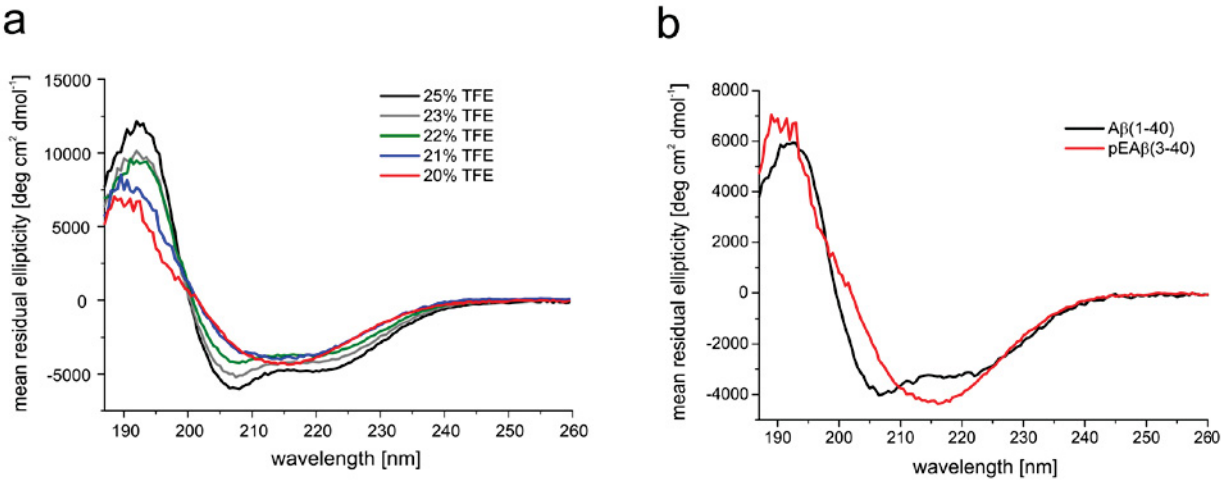


**Fig 1. Far-UV CD spectra of pEAβ(3–40) and Aβ(1–40).** Peptides were dissolved in buffer (20–25% TFE in 50 mM potassium phosphate, pH 2.8). CD spectra were recorded at 20°C from 260 to 187 nm, accumulated 10 times and background corrected. (a) CD spectra of 25 μM pEAβ(3–40) in 25%, 23%, 22%, 21% and 20% TFE showed a shift from α-helical structure towards β-sheets with decreasing TFE concentrations. (b) The CD spectrum of 25 μM Aβ(1–40) indicated α-helices in 20% TFE while the spectrum of 25 μM pEAβ(3–40) in 20% TFE showed mainly β-sheet rich structures.

doi:10.1371/journal.pone.0143647.g001

helices inducing effect of TFE on pEAβ(3–40) and the shift towards β-sheets by lowering the TFE contents was analyzed by recording CD spectra in aqueous buffer in different TFE concentrations. CD spectra in solutions containing varying concentrations of TFE ranging from 25% to 22% at pH 2.8 indicated a mainly α-helical conformation based on minima at 208 nm and 222 nm, a maximum at 193 nm and an x-axis intercept at 200 nm. Marginally loweringthe TFE concentration from 22% to 20% or 21% was sufficient to alter the α-helical protein conformation of pEAβ(3–40) to a β-sheet dominated secondary structure (Fig 1a) as indicated by the evolvement of characteristic β-sheet features in the corresponding CD spectra with a single minimum at 216 nm, a x-axis intercept at 202 nm and a shift of the maximum to a lower wavelength, i.e. 190 nm. CD spectra of Aβ(1–40) recorded under the same condition (20% TFE) differed compared to the spectra of pEAβ(3–40) by indicating α-helices (Fig 1b).

## Aggregation kinetics and fibrillation

Aggregation analysis supported the CD data of pEAβ(3–40) and Aβ(1–40) indicating different secondary structural elements in aqueous solution containing 20% TFE. Fig 2a displays the aggregation kinetics in TFE containing solutions ranging from 20% to 25% TFE at 20°C for pEAβ(3–40) as monitored by ThT assay. pEAβ(3–40) aggregation reaches its maximum at TFE concentrations of 20% and 21%. A distinct lag phase of 9h (20% TFE) or 14 h (21% TFE) is observable following a clear growth phase where aggregation increased indicating that β-sheet formation is not hindered by the presence of TFE. In the presence of 25% TFE no THT fluorescence increase was observed during 72 h, which indicate that pEAβ(3–40) stays monomeric at that condition. However, when the TFE concentration was lowered to 23% or 22% TFE a significant delay as well as decreased maximum was detected within 72 h exploration time. Aggregation of Aβ(1–40) could not be observed at all under the same conditions as no increase in fluorescence intensity was detected within 72 h (Fig 2b). Thus, fibrillation and/or ThT positive β-sheet formation of Aβ(1–40) seemed to be inhibited or at least significantly delayed in the presence of the helix-stabilizing fluoroalcohol TFE.

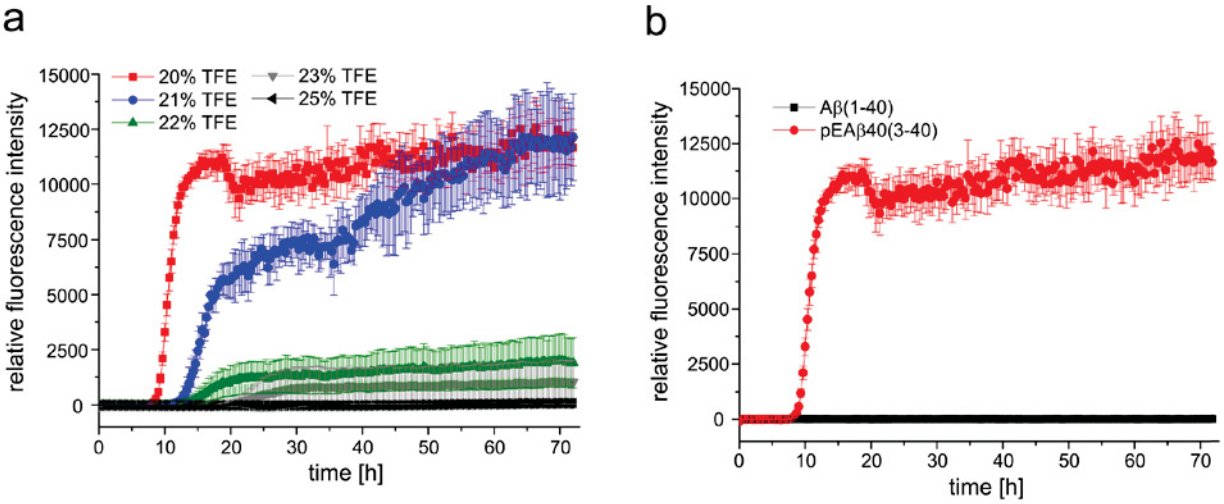


**Fig 2. Aggregation kinetics of pEAβ(3–40) and Aβ(1–40) in TFE.** (a) 25 μM of monomerized pEAβ(3–40) were dissolved in buffer with various TFE contents (25%, 23%, 22%, 21% and 20% TFE in 50 mM potassium phosphate, pH 2.8) including 10 μM ThT. pEAβ(3–40) aggregated in 20% and 21% TFE but was significantly decreased in aqueous solution with higher TFE concentration. (b) 25 μM of monomerized pEAβ(3–40) and Aβ(1–40) were dissolved in buffer (20% TFE in 50 mM potassium phosphate, pH 2.8) including 10 μM ThT. An increase in ThT fluorescence was observed for pEAβ(3–40) but not for Aβ (1–40) within 72 h.

doi:10.1371/journal.pone.0143647.g002

TEM microscopy was performed to analyze the structure of pEAβ(3–40) aggregation products formed after incubation of the monomerized pepide in 20% TFE (Fig 3). pEAβ(3–40) built large fibrils accumulating into aggregates with several μm in diameter. The fibrils were twisted, exhibit a rather homogeneous morphology and accumulate into plaques comparable with fibrils matured in aqueous solution [47].

## NMR spectroscopy

Since pEAβ(3–40) started to aggregate at room temperature and built large fibrils in 20% TFE (pH 2.8), 2D NMR spectroscopy was performed with only 25 μM recombinantly produced [$U$-$^{15}$N]-pEAβ(3–40). Nonetheless, considerably protein aggregation within 2 days even at the low concentration applied impeded the recording of 3D experiments. To overcome this problem, backbone $^{1}H_{N}$ and $^{15}$N resonance assignments of pEAβ(3–40) in 20% TFE were obtained by a time optimized BT-HNCA+ pulse sequence performed with pEAβ(3–40) in 30% TFE (S1 Fig). Transfer of the resonance assignments to the $^{1}$H,$^{15}$N-HSQC spectrum in 20% TFE was performed gradually from 30% through 27% and 23% TFE (S2 Fig). The Cα secondary chemical shifts of pEAβ(3–40) in 30% TFE were neighbor-corrected and plotted as a function of the aa sequence (S3 Fig). There is evidence that aa Y10-A21 and K28-V36 are involved in the α-helix formation as indicated by positive secondary chemical shifts. This is in accordance with the secondary structure of pEAβ(3–40) in 40%TFE obtained from proton chemical shift data [29].

For reference, the spectrum of recombinant [$U$-$^{15}$N]-Aβ(1–40) was acquired under identical conditions and both $^{1}$H,$^{15}$N-HSQC spectra were overlaid for comparison (Fig 4). The absence of the first two amino acid residues D1 and A2 and the substitution of E3 to pE3 is the only difference between pEAβ(3–40) and Aβ(1–40). The main changes in chemical shifts are therefore expected to be primarily observed for the very N-terminal amino acid residues. Interestingly, signals of the N-terminal region up to E11 differed significantly (Fig 5). Cross-peaks further

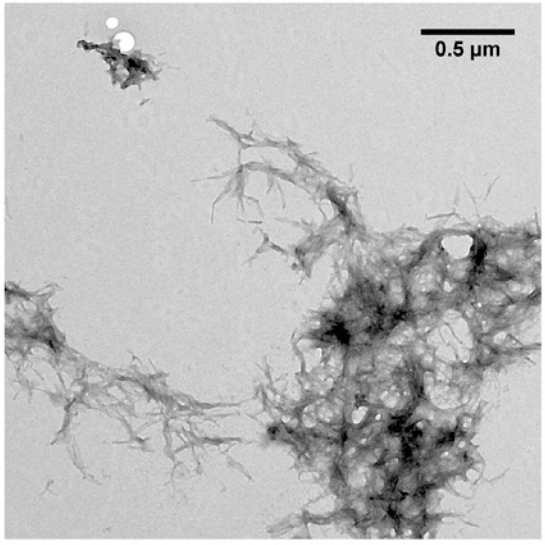


**Fig 3. TEM image of pEAβ(3–40) in 50 mM potassium phosphate pH 2.8 containing 20% TFE.** Monomerized pEAβ(3–40) (25 µM) was incubated for fibrillation at 20°C for five days and grids were prepared by negative staining. pEAβ(3–40) incubated in aqueous TFE solution formed large twisted fibrils up to several hundred nm in size which accumulate into large aggregates ranging from 1–5 µm in diameter.

doi:10.1371/journal.pone.0143647.g003

downstream towards the C-terminus, except of the C-terminal amino acid V40, were not or only marginally changed.

## Discussion

Previous data indicated that pyroglutamate-modified Aβ shows increased tendency to form β-sheets compared to the unstructured Aβ in aqueous buffer at neutral pH [22, 48, 49]. Here, we expand structural knowledge on pEAβ(3–40) by showing that it forms β-sheets even in the presence of considerably amounts of the co-solvent TFE. This is consistent with data indicating that the tendency to build α-helical structures is decreased for pEAβ(3–40) as compared to unstructured Aβ(1–40) as analyzed by proton NMR spectroscopy at higher TFE concentrations, where both peptides stay in monomeric conformation [29]. Our data indicate a change in conformation of pEAβ(3–40) as a result of lowering the TFE concentration. We identified the exact TFE concentration (20% at pH 2.8) where pEAβ(3–40) already is in a β-sheet conformation, whereas Aβ(1–40) exhibits still an overall α-helical conformation. This confirms, that TFE is not simply favoring α-helical secondary structures, but secondary structures in general [50].

The differences in the secondary structure content observed by CD spectroscopy seem to be a result of the modification from Aβ to pEAβ, which modifies the N-terminal region significantly. ThT and TEM data support this evidence by yielding characteristic aggregation kinetics and large matured fibrils for pEAβ(3–40) in 20% TFE but not for Aβ(1–40) under same conditions.

Using NMR spectroscopy, we analyzed pEAβ(3–40) monomers in 20% TFE (pH 2.8). Under these conditions, pEAβ(3–40) slowly forms β-sheet containing aggregates that could not be observed by solution NMR. Although it was shown in a model peptide starting with a N-terminal E1 that conversion to pE1 results in altered chemical shifts only of the following two amino acids [51], pE formation of Aβ peptides obviously affects not only the immediately

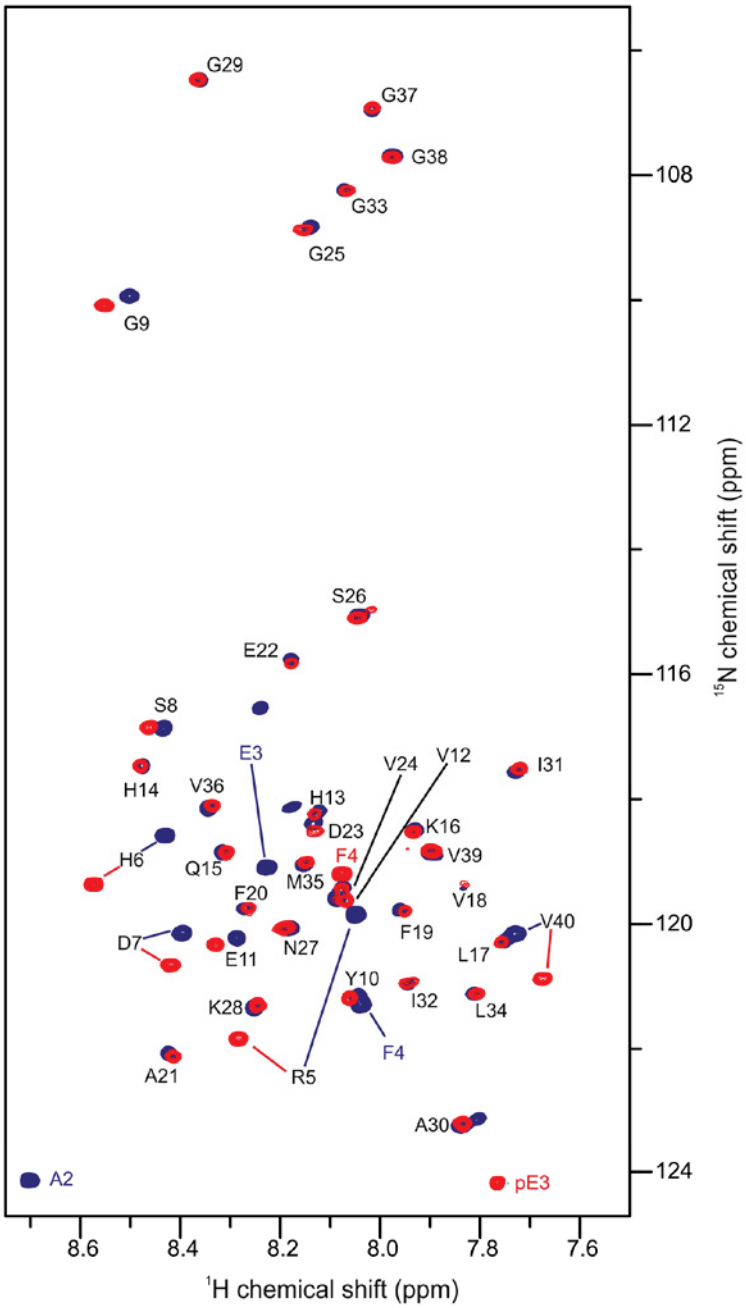


**Fig 4. $^{1}$H,$^{15}$N-HSQC of pEAβ(3–40) and Aβ(1–40).** 25 μM of the monomerized peptides were dissolved in aqueous solution (50 mM potassium phosphate, pH 2.8) containing 20% TFE. Spectra were recorded on a 600 MHz Bruker spectrometer at 5°C. Overlay of the spectrum of pEAβ(3–40) (red) and Aβ(1–40) (blue) indicate that the pyroglutamate modification affects the N-terminal signals significantly towards E11 as well as V40.

doi:10.1371/journal.pone.0143647.g004


**Fig 5. Chemical shift changes $\Delta\delta(^1H,^{15}N) = ((10*\Delta\delta 1H^N)^2 + (\Delta\delta^{15}N)^2)^{1/2}$ between pEAβ(3–40) and Aβ (1–40) plotted as a function of the pEAβ(3–40) sequence.** Pyroglutamate formation affects the N-terminal amino acids with decreasing effect towards the C-terminus and, interestingly, also the C-terminal V40.

doi:10.1371/journal.pone.0143647.g005

adjacent N-terminus. It was previously shown by $H_N$ and $H_\alpha$ proton chemical shift differences between pEAβ(3–40) and Aβ(1–40) in higher TFE concentrations (40%), that mostly protons of the six following amino acids from pE3 to S8 with decreasing influence towards the C-terminus were affected [29]. In the presence of only 20% TFE, we observed many resonance differences of pEAβ(3–40) compared to Aβ(1–40). Chemical shift differences of the N-terminal amino acids towards E11 as well as the C-terminal V40 were mostly affected as shown in Fig 5. Thus, it seems that the modification of Aβ(1–40) to pEAβ(3–40) not only influence the neighboring amino acids, but also change significantly the conformational state of at least 25% of all amino acids. This result suggests that the N-terminal modification to pEAβ has a significant effect on secondary structure elements and thus is the driving force for pEAβ(3–40) to be more likely to build β-sheet structures under exactly the same conditions when compared to Aβ(1–40). The propensity of pEAβ(3–40) to aggregate in aqueous TFE solution seems to be propagated by the modified N-terminus, but V40 obviously play also a central role, maybe due to interactions of both termini. Since C-terminally truncated Aβ peptides are less prone to aggregation, e.g. Aβ(1–38) < Aβ(1–40) < Aβ(1–42) [52, 53], it is likely that their pE modified isoforms would show an increased aggregation propensity as compared to the non-pE-modified isoforms, analogous to the results obtained within this study.

## Supporting Information

**S1 Fig. $^{15}$N-HSQC of pEAβ(3–40) in 30% TFE.**
(TIF)

**S2 Fig. $^{15}$N-HSQC of pEAβ(3–40) in different TFE concentrations.**
(TIF)

**S3 Fig. Cα secondary chemical shifts of pEAβ(3–40) in 30% TFE.**
(TIF)

## Acknowledgments

Matthias Stoldt, Justin Lecher and Maren Thomaier are highly acknowledged for fruitful discussions. We gratefully acknowledge support of CD from the International NRW Research School BioStruct, granted by the Ministry of Innovation, Science and Research of the State North Rhine-Westphalia, the Heinrich Heine University of Düsseldorf, and the Entrepreneur Foundation at the Heinrich Heine University of Düsseldorf. The authors acknowledge access to the Jülich-Düsseldorf Biomolecular NMR Center. DW was supported by grants from the

"Portfolio Technology and Medicine", the "Portfolio Drug Research" and the Helmholtz-Validierungsfonds of the "Impuls und Vernetzungs-Fonds der Helmholtzgemeinschaft".

## Author Contributions

Conceived and designed the experiments: CD MS LG NS HUD DW. Performed the experiments: CD ANK KR. Analyzed the data: CD MS RH PN. Wrote the paper: CD MS LG DW.

## References

1. Walsh DM, Selkoe DJ. Deciphering the molecular basis of memory failure in Alzheimer's disease. Neuron. 2004; 44(1):181–93. doi: 10.1016/j.neuron.2004.09.010 PMID: 15450169.
2. Ballard C, Khan Z, Clack H, Corbett A. Nonpharmacological treatment of Alzheimer disease. Can J Psychiatry. 2011; 56(10):589–95. PMID: 22014691.
3. Haass C, Selkoe DJ. Cellular processing of beta-amyloid precursor protein and the genesis of amyloid beta-peptide. Cell. 1993; 75(6):1039–42. Epub 1993/12/17. PMID: 8261505.
4. Weidemann A, Konig G, Bunke D, Fischer P, Salbaum JM, Masters CL, et al. Identification, biogenesis, and localization of precursors of Alzheimer's disease A4 amyloid protein. Cell. 1989; 57(1):115–26. Epub 1989/04/07. PMID: 2649245.
5. De Strooper B, Vassar R, Golde T. The secretases: enzymes with therapeutic potential in Alzheimer disease. Nature reviews Neurology. 2010; 6(2):99–107. Epub 2010/02/09. doi: 10.1038/nrneurol.2009.218 PMID: 20139999; PubMed Central PMCID: PMC2879045.
6. De Strooper B. Proteases and proteolysis in Alzheimer disease: a multifactorial view on the disease process. Physiological reviews. 2010; 90(2):465–94. Epub 2010/04/16. doi: 10.1152/physrev.00023.2009 PMID: 20393191.
7. Gunn AP, Masters CL, Cherny RA. Pyroglutamate-Abeta: role in the natural history of Alzheimer's disease. The international journal of biochemistry & cell biology. 2010; 42(12):1915–8. Epub 2010/09/14. doi: 10.1016/j.biocel.2010.08.015 PMID: 20833262.
8. Mori H, Takio K, Ogawara M, Selkoe DJ. Mass spectrometry of purified amyloid beta protein in Alzheimer's disease. The Journal of biological chemistry. 1992; 267(24):17082–6. Epub 1992/08/25. PMID: 1512246.
9. Perez-Garmendia R, Gevorkian G. Pyroglutamate-Modified Amyloid Beta Peptides: Emerging Targets for Alzheimer s Disease Immunotherapy. Current neuropharmacology. 2013; 11(5):491–8. Epub 2014/01/10. doi: 10.2174/1570159X11311050004 PMID: 24403873; PubMed Central PMCID: PMC3763757.
10. Sergeant N, Bombois S, Ghestem A, Drobecq H, Kostanjevecki V, Missiaen C, et al. Truncated beta-amyloid peptide species in pre-clinical Alzheimer's disease as new targets for the vaccination approach. Journal of neurochemistry. 2003; 85(6):1581–91. PMID: 12787077.
11. Meissner JN, Bouter Y, Bayer TA. Neuron Loss and Behavioral Deficits in the TBA42 Mouse Model Expressing N-Truncated Pyroglutamate Amyloid-beta3-42. Journal of Alzheimer's disease: JAD. 2015; 45(2):471–82. Epub 2014/12/31. doi: 10.3233/JAD-142868 PMID: 25547635.
12. Wirths O, Breyhan H, Cynis H, Schilling S, Demuth HU, Bayer TA. Intraneuronal pyroglutamate-Abeta 3–42 triggers neurodegeneration and lethal neurological deficits in a transgenic mouse model. Acta neuropathologica. 2009; 118(4):487–96. Epub 2009/06/24. doi: 10.1007/s00401-009-0557-5 PMID: 19547991; PubMed Central PMCID: PMC2737116.
13. Schilling S, Hoffmann T, Manhart S, Hoffmann M, Demuth HU. Glutaminyl cyclases unfold glutamyl cyclase activity under mild acid conditions. FEBS letters. 2004; 563(1–3):191–6. Epub 2004/04/06. doi: 10.1016/S0014-5793(04)00300-X PMID: 15063747.
14. Cynis H, Rahfeld JU, Stephan A, Kehlen A, Koch B, Wermann M, et al. Isolation of an isoenzyme of human glutaminyl cyclase: retention in the Golgi complex suggests involvement in the protein maturation machinery. Journal of molecular biology. 2008; 379(5):966–80. doi: 10.1016/j.jmb.2008.03.078 PMID: 18486145.
15. Harigaya Y, Saido TC, Eckman CB, Prada CM, Shoji M, Younkin SG. Amyloid beta protein starting pyroglutamate at position 3 is a major component of the amyloid deposits in the Alzheimer's disease brain. Biochemical and biophysical research communications. 2000; 276(2):422–7. Epub 2000/10/12. doi: 10.1006/bbrc.2000.3490 PMID: 11027491.
16. Portelius E, Bogdanovic N, Gustavsson MK, Volkmann I, Brinkmalm G, Zetterberg H, et al. Mass spectrometric characterization of brain amyloid beta isoform signatures in familial and sporadic Alzheimer's disease. Acta neuropathologica. 2010; 120(2):185–93. Epub 2010/04/27. doi: 10.1007/s00401-010-0690-1 PMID: 20419305; PubMed Central PMCID: PMC3568930.

17. Wirths O, Erck C, Martens H, Harmeier A, Geumann C, Jawhar S, et al. Identification of low molecular weight pyroglutamate Abeta oligomers in Alzheimer disease: a novel tool for therapy and diagnosis. The Journal of biological chemistry. 2010; 285(53):41517–24. Epub 2010/10/26. doi: 10.1074/jbc.M110.178707 PMID: 20971852; PubMed Central PMCID: PMC3009878.

18. Hosoda R, Saido TC, Otvos L Jr., Arai T, Mann DM, Lee VM, et al. Quantification of modified amyloid beta peptides in Alzheimer disease and Down syndrome brains. J Neuropathol Exp Neurol. 1998; 57(11):1089–95. PMID: 9825946.

19. Jawhar S, Wirths O, Bayer TA. Pyroglutamate amyloid-beta (Abeta): a hatchet man in Alzheimer disease. The Journal of biological chemistry. 2011; 286(45):38825–32. Epub 2011/10/04. doi: 10.1074/jbc.R111.288308 PMID: 21965666; PubMed Central PMCID: PMC3234707.

20. Cummins PM, O'Connor B. Pyroglutamyl peptidase: an overview of the three known enzymatic forms. Biochimica et biophysica acta. 1998; 1429(1):1–17. PMID: 9920379.

21. Saido TC, Yamao-Harigaya W, Iwatsubo T, Kawashima S. Amino- and carboxyl-terminal heterogeneity of beta-amyloid peptides deposited in human brain. Neuroscience letters. 1996; 215(3):173–6. PMID: 8899741.

22. Schilling S, Lauber T, Schaupp M, Manhart S, Scheel E, Bohm G, et al. On the seeding and oligomerization of pGlu-amyloid peptides (in vitro). Biochemistry. 2006; 45(41):12393–9. Epub 2006/10/13. doi: 10.1021/bi0612667 PMID: 17029395.

23. Bayer TA, Wirths O. Focusing the amyloid cascade hypothesis on N-truncated Abeta peptides as drug targets against Alzheimer's disease. Acta neuropathologica. 2014; 127(6):787–801. Epub 2014/05/08. doi: 10.1007/s00401-014-1287-x PMID: 24803226; PubMed Central PMCID: PMC4024135.

24. Russo C, Violani E, Salis S, Venezia V, Dolcini V, Damonte G, et al. Pyroglutamate-modified amyloid beta-peptides—AbetaN3(pE)—strongly affect cultured neuron and astrocyte survival. Journal of neurochemistry. 2002; 82(6):1480–9. PMID: 12354296.

25. Dammers C, Gremer L, Neudecker P, Demuth HU, Schwarten M, Willbold D. Purification and Characterization of Recombinant N-Terminally Pyroglutamate-Modified Amyloid-beta Variants and Structural Analysis by Solution NMR Spectroscopy. PloS one. 2015; 10(10):e0139710. doi: 10.1371/journal.pone.0139710 PMID: 26436664.

26. Shao H, Jao S, Ma K, Zagorski MG. Solution structures of micelle-bound amyloid beta-(1–40) and beta-(1–42) peptides of Alzheimer's disease. Journal of molecular biology. 1999; 285(2):755–73. Epub 1999/01/08. PMID: 9878442.

27. Crescenzi O, Tomaselli S, Guerrini R, Salvadori S, D'Ursi AM, Temussi PA, et al. Solution structure of the Alzheimer amyloid beta-peptide (1–42) in an apolar microenvironment. Similarity with a virus fusion domain. European journal of biochemistry / FEBS. 2002; 269(22):5642–8. Epub 2002/11/09. PMID: 12423364.

28. Sticht H, Bayer P, Willbold D, Dames S, Hilbich C, Beyreuther K, et al. Structure of amyloid A4-(1–40)-peptide of Alzheimer's disease. European journal of biochemistry / FEBS. 1995; 233(1):293–8. Epub 1995/10/01. PMID: 7588758.

29. Sun N, Hartmann R, Lecher J, Stoldt M, Funke SA, Gremer L, et al. Structural analysis of the pyroglutamate-modified isoform of the Alzheimer's disease-related amyloid-beta using NMR spectroscopy. Journal of peptide science: an official publication of the European Peptide Society. 2012; 18(11):691–5. Epub 2012/09/25. doi: 10.1002/psc.2456 PMID: 23001756.

30. Finder VH, Vodopivec I, Nitsch RM, Glockshuber R. The recombinant amyloid-beta peptide Abeta1-42 aggregates faster and is more neurotoxic than synthetic Abeta1-42. Journal of molecular biology. 2010; 396(1):9–18. Epub 2009/12/23. doi: 10.1016/j.jmb.2009.12.016 PMID: 20026079.

31. Kay LE, Keifer P, Saarinen T. Pure absorption gradient enhanced heteronuclear single quantum correlation spectroscopy with improved sensitivity. Journal of the American Chemical Society. 1992; 114(26):10663–5. doi: 10.1021/ja00052a088 WOS:A1992KD71700088.

32. Palmer AG, Cavanagh J, Wright PE, Rance M. Sensitivity improvement in proton-detected two-dimensional heteronuclear correlation NMR spectroscopy. Journal of magnetic resonance. 1991; 93(1):151–70. doi: 10.1016/0022-2364(91)90036-s WOS:A1991FL34200012.

33. Schleucher J, Schwendinger M, Sattler M, Schmidt P, Schedletzky O, Glaser SJ, et al. A general enhancement scheme in heteronuclear multidimensional NMR employing pulsed field gradients. Journal of biomolecular NMR. 1994; 4(2):301–6. WOS:A1994NC39000011. PMID: 8019138

34. Solyom Z, Schwarten M, Geist L, Konrat R, Willbold D, Brutscher B. BEST-TROSY experiments for time-efficient sequential resonance assignment of large disordered proteins. Journal of biomolecular NMR. 2013; 55(4):311–21. Epub 2013/02/26. doi: 10.1007/s10858-013-9715-0 PMID: 23435576.

35. Gil-Caballero S, Favier A, Brutscher B. HNCA+, HNCO+, and HNCACB+ experiments: improved performance by simultaneous detection of orthogonal coherence transfer pathways. Journal of biomolecular NMR. 2014; 60(1):1–9. Epub 2014/07/25. doi: 10.1007/s10858-014-9847-x PMID: 25056271.

36. Delaglio F, Grzesiek S, Vuister GW, Zhu G, Pfeifer J, Bax A. NMRPipe: a multidimensional spectral processing system based on UNIX pipes. Journal of biomolecular NMR. 1995; 6(3):277–93. Epub 1995/11/01. PMID: 8520220.

37. Vranken WF, Boucher W, Stevens TJ, Fogh RH, Pajon A, Llinas M, et al. The CCPN data model for NMR spectroscopy: development of a software pipeline. Proteins. 2005; 59(4):687–96. Epub 2005/04/09. doi: 10.1002/prot.20449 PMID: 15815974.

38. Zhang H, Neal S, Wishart DS. RefDB: a database of uniformly referenced protein chemical shifts. Journal of biomolecular NMR. 2003; 25(3):173–95. Epub 2003/03/26. PMID: 12652131.

39. Schwarzinger S, Kroon GJ, Foss TR, Chung J, Wright PE, Dyson HJ. Sequence-dependent correction of random coil NMR chemical shifts. Journal of the American Chemical Society. 2001; 123(13):2970–8. Epub 2001/07/18. PMID: 11457007.

40. Kumar S, Udgaonkar JB. Structurally distinct amyloid protofibrils form on separate pathways of aggregation of a small protein. Biochemistry. 2009; 48(27):6441–9. Epub 2009/06/10. doi: 10.1021/bi900682w PMID: 19505087.

41. Chen YR, Huang HB, Chyan CL, Shiao MS, Lin TH, Chen YC. The effect of Abeta conformation on the metal affinity and aggregation mechanism studied by circular dichroism spectroscopy. Journal of biochemistry. 2006; 139(4):733–40. Epub 2006/05/05. doi: 10.1093/jb/mvj083 PMID: 16672274.

42. Gupta P, Deep S. Intermediate conformation between native beta-sheet and non-native alpha-helix is a precursor of trifluoroethanol-induced aggregation of human carbonic anhydrase-II. Biochemical and biophysical research communications. 2014; 449(1):126–31. doi: 10.1016/j.bbrc.2014.04.160 PMID: 24813993.

43. Marinelli P, Castillo V, Ventura S. Trifluoroethanol modulates amyloid formation by the all alpha-helical URN1 FF domain. Int J Mol Sci. 2013; 14(9):17830–44. doi: 10.3390/ijms140917830 PMID: 23999589; PubMed Central PMCID: PMC3794755.

44. Amani S, Naeem A. Transition of transferrin from native to fibrillar state: An implication for amyloid-linked diseases. Biochem Eng J. 2014; 91:120–8. doi: 10.1016/j.bej.2014.08.004 WOS:000343950800016.

45. Anderson VL, Ramlall TF, Rospigliosi CC, Webb WW, Eliezer D. Identification of a helical intermediate in trifluoroethanol-induced alpha-synuclein aggregation. Proceedings of the National Academy of Sciences of the United States of America. 2010; 107(44):18850–5. doi: 10.1073/pnas.1012336107 PMID: 20947801; PubMed Central PMCID: PMC2973859.

46. Khan MV, Rabbani G, Ahmad E, Khan RH. Fluoroalcohols-induced modulation and amyloid formation in conalbumin. International journal of biological macromolecules. 2014; 70:606–14. doi: 10.1016/j.ijbiomac.2014.07.027 PMID: 25062993.

47. Schlenzig D, Manhart S, Cinar Y, Kleinschmidt M, Hause G, Willbold D, et al. Pyroglutamate formation influences solubility and amyloidogenicity of amyloid peptides. Biochemistry. 2009; 48(29):7072–8. Epub 2009/06/13. doi: 10.1021/bi900818a PMID: 19518051.

48. He W, Barrow CJ. The A beta 3-pyroglutamyl and 11-pyroglutamyl peptides found in senile plaque have greater beta-sheet forming and aggregation propensities in vitro than full-length A beta. Biochemistry. 1999; 38(33):10871–7. doi: 10.1021/bi990563r PMID: 10451383.

49. Schlenzig D, Ronicke R, Cynis H, Ludwig HH, Scheel E, Reymann K, et al. N-Terminal pyroglutamate formation of Abeta38 and Abeta40 enforces oligomer formation and potency to disrupt hippocampal long-term potentiation. Journal of neurochemistry. 2012; 121(5):774–84. Epub 2012/03/02. doi: 10.1111/j.1471-4159.2012.07707.x PMID: 22375951.

50. Sonnichsen FD, Van Eyk JE, Hodges RS, Sykes BD. Effect of trifluoroethanol on protein secondary structure: an NMR and CD study using a synthetic actin peptide. Biochemistry. 1992; 31(37):8790–8. PMID: 1390666.

51. Mischo A, Ohlenschlager O, Guhrs KH, Gorlach M. Recombinant production of isotope-labeled peptides and spontaneous cyclization of amino-terminal glutamine into pyroglutamic acid. Chembiochem: a European journal of chemical biology. 2012; 13(10):1421–3. Epub 2012/05/24. doi: 10.1002/cbic.201200178 PMID: 22619187.

52. Gravina SA, Ho L, Eckman CB, Long KE, Otvos L Jr., Younkin LH, et al. Amyloid beta protein (A beta) in Alzheimer's disease brain. Biochemical and immunocytochemical analysis with antibodies specific for forms ending at A beta 40 or A beta 42(43). The Journal of biological chemistry. 1995; 270(13):7013–6. PMID: 7706234.

53. Kim J, Onstead L, Randle S, Price R, Smithson L, Zwizinski C, et al. Abeta40 inhibits amyloid deposition in vivo. The Journal of neuroscience: the official journal of the Society for Neuroscience. 2007; 27(3):627–33. doi: 10.1523/JNEUROSCI.4849-06.2007 PMID: 17234594.

## Supporting Information

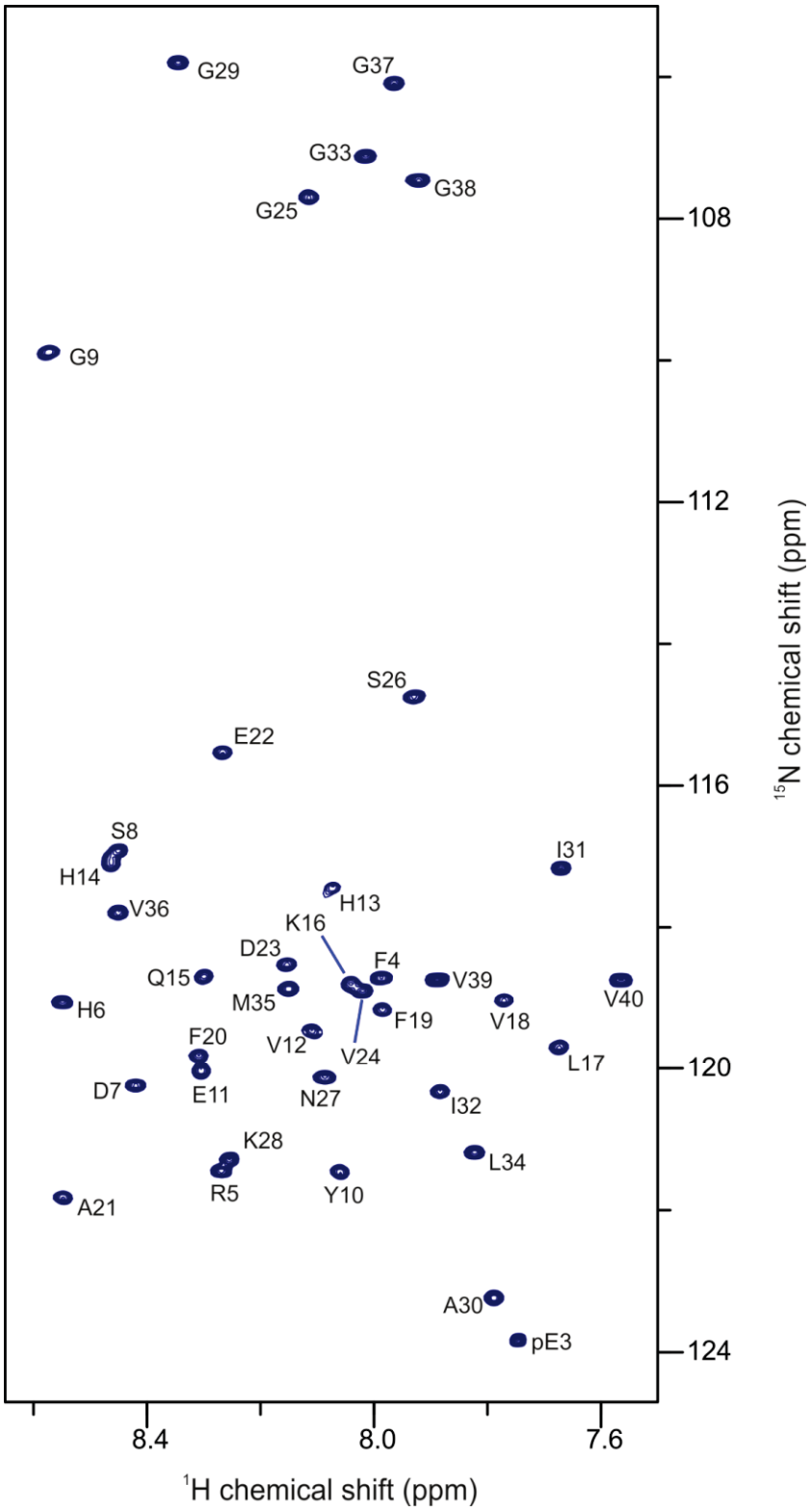


**S1 $^{15}$N-HSQC of pEAβ(3-40) in 30 % TFE.** 25 µM peptide was dissolved in aqueous solution (50 mM potassium phosphate, pH 2.8) containing 30 % TFE. Spectra were recorded on a 600 MHz Bruker spectrometer at 5 °C and assignment was done using HNCA+ pulse sequence.

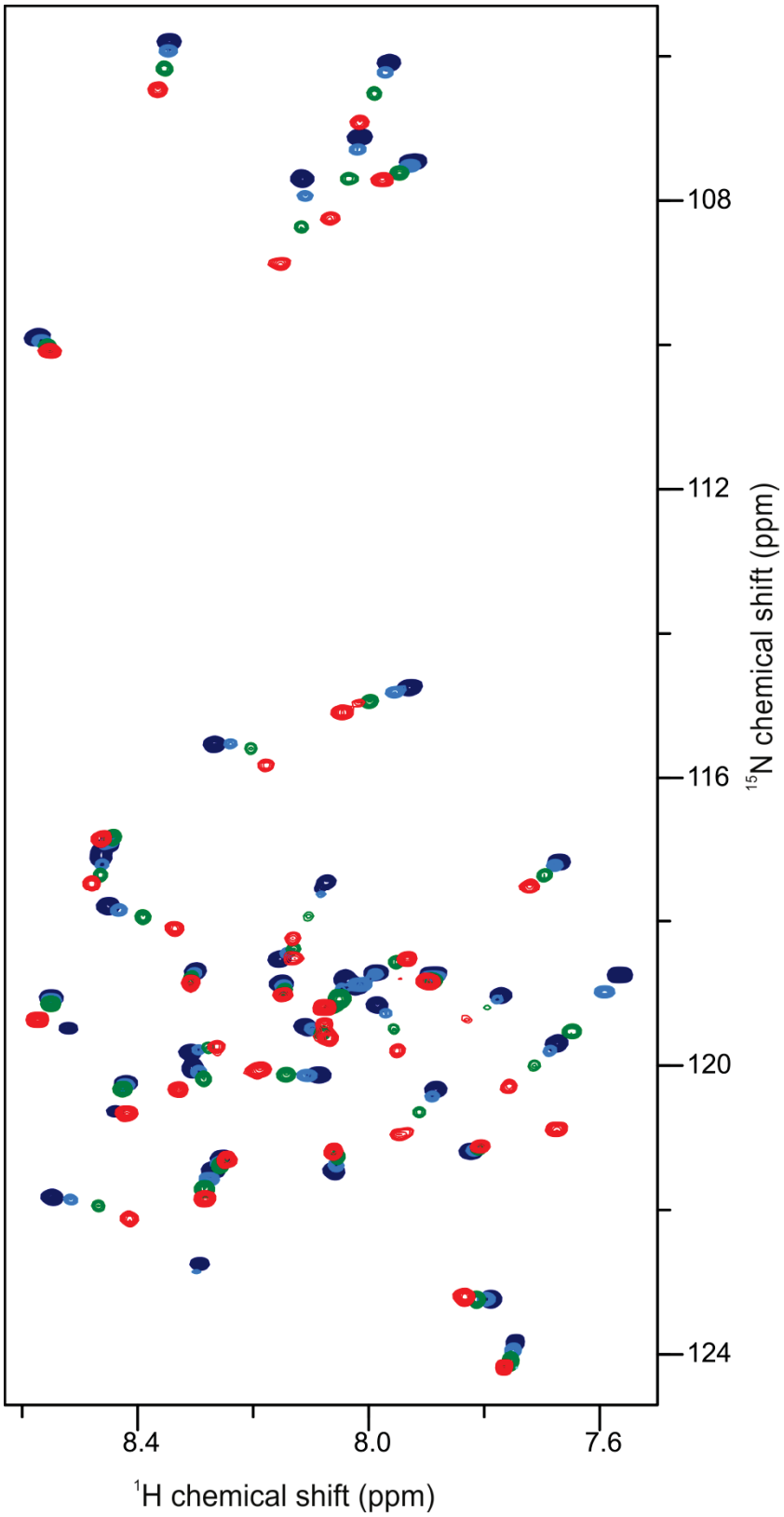


**S2 $^{15}$N-HSQC of pEAβ(3-40) in different TFE concentrations.** 25 µM peptide were dissolved in aqueous solution (50 mM $KH_3PO_4$, pH 2.8) containing 20 % (red), 23 % (green), 27 % (light blue) and 30 % (dark blue) TFE. Spectra were recorded on a 600 MHz Bruker spectrometer at 5 °C.

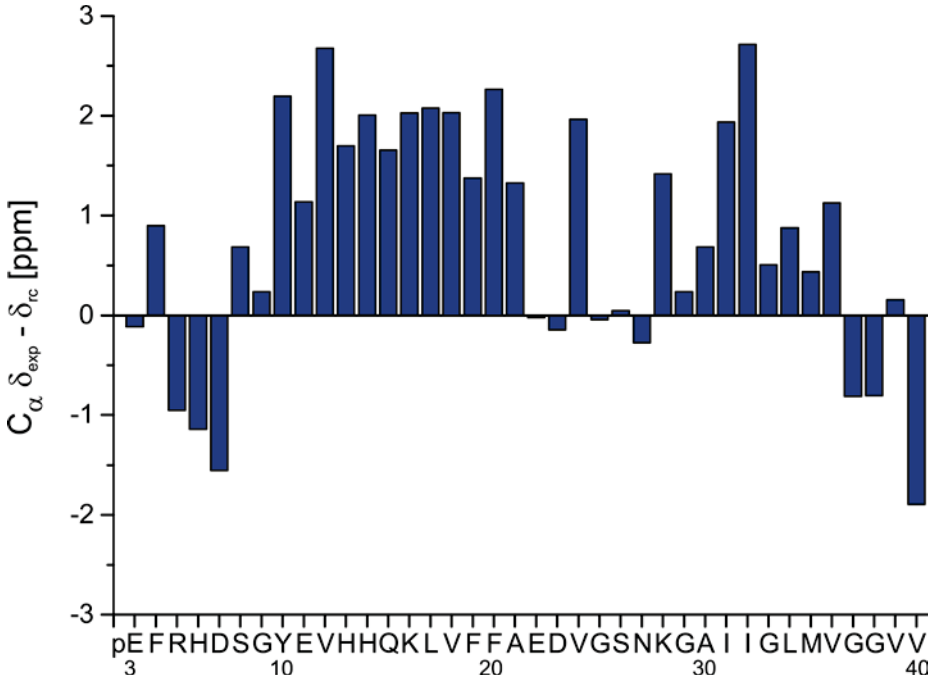


**S3 Fig. Cα secondary chemical shifts of pEAβ(3-40) in 30 % TFE.** Cα secondary chemical shifts calculated as the difference between measured and random coil chemical shifts described by Zhang et al. and sequence corrected for neighbor effects.

## 3.3 pEAβ(3-42) undergoes amyloid formation via an α-helical intermediate as revealed by 3D NMR spectroscopy

Christina Dammers, Kerstin Reiß, Lothar Gremer, Tamar Ziehm, Justin Lecher, Melanie Schwarten and Dieter Willbold

Journal: PNAS (to be submitted)

Impact Factor: 9.67

Contributions: 80 %, protein production, experimental design, performance and data analysis of CD spectroscopy, TEM, ThT assays and NMR spectroscopy, manuscript writing

# pEAβ(3-42) undergoes amyloid formation via an α-helical intermediate as revealed by 3D NMR spectroscopy

**Christina Dammers[1], Kerstin Reiß[1], Lothar Gremer[1,2], Justin Lecher[2], Tamar Ziehm[1], Matthias Stoldt[1], Melanie Schwarten[1] and Dieter Willbold[1,2]**

[1]Institute of Complex Systems (ICS-6) Structural Biochemistry, Forschungszentrum Jülich, 52425 Jülich, Germany
[2]Institut für Physikalische Biologie, Heinrich-Heine-Universität Düsseldorf, 40225 Düsseldorf, Germany

To whom correspondence should be adressed: Dieter Willbold, Forschungszentrum Jülich, ICS-6 / Structural Biochemistry, 52425 Jülich, Germany, Tel.: (0049) 2461-612100; Fax: (0049) 2461-6121023; E-mail: d.willbold@fz-juelich.de

**Keywords:** Alzheimer disease, amyloid-beta (Aβ), pyroglutamate-modified Aβ, aggregation, fibril formation, secondary structure, structural biology, nuclear magnetic resonance (NMR), helical intermediates

## ABSTRACT

Pyroglutamate-modified Aβ (pEAβ) has been described as a major compound in Alzheimer's disease brains with pEAβ(3-42) as a dominant isoform. pEAβ(3-42) was shown to be one of the most toxic and aggregation prone Aβ variants and thus high resolution structural studies are hindered. Circular dichroism spectroscopy data indicate that pEAβ(3-42) has an increased tendency to form β-sheet-rich structures in solution conditions, where Aβ(1-42) forms α-helices. Thioflavin-T assays and transmission electron microscopy show increased aggregation leading to large fibrils of pEAβ(3-42) but not for Aβ(1-42). Three-dimensional nuclear magnetic resonance (NMR) spectroscopy was performed for complete backbone and partial sidechain assignments. The modification to pEAβ(3-42) affects 30 % of the total amino acids when compared to Aβ(1-42). NMR chemical shift analysis indicated that soluble pEAβ(3-42) contains two helical regions connected by a flexible linker. These α-helical monomers are instable due to intermolecular interactions. The N-terminal modification to pEAβ has a significant effect on structural elements resulting in a severe tendency to form β-sheet-rich structures extending to fibrils via α-helices. These transient helical intermediates seem to be on-pathway to the amyloidogenic fibrils.

## INTRODUCTION

Extracellular neuronal deposits belong to the pathology of Alzheimer's disease (AD), a neurodegenerative disorder leading to progressive decline of cognitive functions (1). These extracellular plaques are consisting of insoluble fibrillary structures of amyloid beta peptides (Aβ), which are processed from the amyloid precursor protein (APP) through cleavage by β- and γ-secretases (2,3). Post-translational modifications increase the diversity of Aβ species resulting in an extensive heterogeneity as well as in N-terminal and C-terminal truncations. Pyroglutamate-modified Aβ (pEAβ) was described as a major isoform amongst them; up to 20 % of the total Aβ start with a pyroglutamate (pE) at the N-terminus (4-6). pEAβ(3-x) was reported to be present in equivalent amounts in senile plaques as Aβ(1-x) (7) and to play an important role in plaque formation and neurological deficits (7,8). Aβ(3-x) is generated by the cleavage of the first two amino acids (aa) (D1 and A2) from Aβ(1-x) or by alternative splicing leading to E3 at the N-terminus (5). The enzyme glutaminyl cyclase (QC) catalyzes intra-E lactam ring formation involving the N-terminal amino group of E3 and its γ–carboxyl group by dehydration leading to pEAβ (9,10). The conversion leads to increased aggregation propensity due to the loss of three charges by the formation of the N-terminal pE lactam ring (5,11) and the resulting assemblies have a stronger seeding effect for other Aβ species (12,13). Moreover, the inaccessible N-

terminus is more stable to degradation mediated by amino peptidases (14) and the toxicity compared to non-truncated peptides independent of their C-terminal lengths is dramatically increased (13,15).

Structural analysis of Aβ species by nuclear magnetic resonance (NMR) spectroscopy have proven to be useful to elucidate high structural information on Aβ species under given solution conditions (16,17). Here, we intend to use NMR spectroscopy to structurally characterize pEAβ(3-42) and to compare it with Aβ(1-42). The main problem for these studies is the fast aggregation kinetics and the low solubility impeding such studies drastically. The choice of solvent is important to overcome this problem. It was shown that Aβ builds α-helical structures in solutions containing micelles (18), hexafluoro-2-propanol (19) or 2,2,2-trifluoroethanol (TFE)(17) facilitating structural studies.

Our group performed high resolution NMR spectroscopy and compared pEAβ(3-40) with Aβ(1-40) in varying aqueous TFE solution (20,21). The results indicated that the pyroglutamate-modified peptide had a decreased helix propensity since it has a higher hydrophobicity and faster aggregation kinetics. It was shown, that pEAβ(3-40) forms β-sheet based structures under conditions were the non-modified isoform forms α-helices (21). Here, we expanded the study by investigating pEAβ(3-42), which shows an even higher aggregation tendency, faster aggregation kinetics and is known to be more neurotoxic than pEAβ(3-40) and also than Aβ(1-42). Circular dichroism (CD) spectroscopy combined with thioflavin-T (ThT) assays and size exclusion chromatography (SEC) were performed to investigate the secondary structure and aggregation kinetics of pEAβ(3-42). The data were completed by three dimensional NMR experiments for backbone and side chain assignments. Thus, chemical shift data analysis allowed secondary structure determination of the pEAβ(3-42) monomer on a residue specific level prior before aggregation starts. The comparison between Aβ(1-42) and pEAβ(3-42) regarding fibril formation and morphology thereof extends the insights into structural differences of the N-terminal pyroglutamate modified variant as one of the most toxic Aβ species. There is evidence that pEAβ(3-42) builds β-sheet-rich structures and fibrils via instable transient α-helical intermediates under the assayed conditions.

## EXPERIMENTAL PROCEDURE

*Peptides*—Expression and purification of recombinant natural isotope abundant, [U-$^{13}$C,$^{15}$N]-pEAβ(3-42) and [U-$^{15}$N]-Aβ(1-42) were performed as described recently (22,23). Recombinant [U-$^{13}$C,$^{15}$N]-Aβ(1-42) was manufactured by Isoloid GmbH (Düsseldorf, Germany). Aβ(1-42) in natural isotope abundancy was chemically synthesized and purchased from Bachem (Heidelberg, Germany).

*Sample preparation*—All preparations were performed in Protein LowBinding tubes (Eppendorf AG, Hamburg, Germany). The Aβ peptides were pre-dissolved in 1,1,1,3,3,3-hexafluoro-2-propanol (HFIP; Sigma-Aldrich, Germany) and incubated for 3 days at room temperature to assure monomers. HFIP was removed by lyophilization and samples were stored at -20 °C.

*CD spectroscopy*—Far-UV CD spectra were recorded on a Jasco J-1100 spectropolarimeter from 260 to 190 nm with 0.5 nm stepsize, 50 nm/min scan speed and 1 nm bandwidth. 25 µM peptide was dissolved in buffer (30, 40 or 50 % TFE in 50 mM potassium phosphate, pH 2.8) and measured in 1 mm path-length cuvettes at 20 °C. Signal to noise ratio was increased by accumulation of 10 scans per sample. Spectra for the buffer were subtracted for background correction.

*Aggregation assay by ThT fluorescence (ThT assay)*—Aggregation assays were performed in black non-binding 96-well plates (Sigma-Aldrich, Germany) at 20 °C. Wells were prepared to a total volume of 100 µL and comprised 25 µM of initially monomeric pEAβ(3-42) and 10 µM ThT in buffer (30, 40 or 50 % TFE in 50 mM potassium phosphate, pH 2.8). Each reaction was performed fivefold and background corrected. Fluorescence was monitored using a microplate reader (PolarStar Optima, BMG, Offenburg, Germany) with 440 and 492 nm excitation and emission filters, respectively. Wells were scanned by bottom-read every 15 min with 30 s shaking prior to use.

*Transmission electron microscopy (TEM)*—Monomeric pEAβ(3-42) and Aβ(1-42) were dissolved in aqueous solutions of 40 % TFE in 50 mM potassium phosphate, pH 2.8 and incubated for five days at 20 °C without agitation. Matured fibrils were absorbed on formvar/carbon coated copper grids (S162, Plano, Wetzlar, Germany) for 5 min. The grids were washed twice with water, then the samples were negative stained using 1 % (w/v) uranyl acetate for 1 min and finally washed twice with

water. Images were recorded with a Libra 120 transmission electron microscope (Zeiss, Oberkochen, Germany) at 120 kV.

*NMR spectroscopy*—NMR measurements were performed on Agilent 800 MHz or Bruker 600 MHz spectrometers equipped with cryogenically-cooled triple resonance probes and pulsed z-field gradients. Lyophilized [U-$^{13}$C,$^{15}$N]-pEAβ(3-42) and [U-$^{13}$C,$^{15}$N]-Aβ(1-42) were directly dissolved in 100 % TFE-d2-OH and diluted with 50 mM potassium phosphate, pH 2.8 to a final TFE concentration of 30, 40 or 50 %. Each experiment was performed with a 100 µM freshly prepared sample in Shigemi tubes (Sigma-Aldrich, Germany) at 20 °C unless otherwise specified. 2D-(1H-15N)-HSQC and (1H-13C)-HSQC correlation spectra were recorded according to the standard Bruker sequences. Backbone 1HN, 15N, 13Co 13Cα and sidechain 13Cβ, 1Hα and 1Hβ resonance assignments were obtained by using BEST-TROSY (BT) optimized pulse sequences (24,25) or standard Bruker/Varian pulse sequences. Seven triple-resonance 3D correlation spectra were recorded: BT-HNCA+, BT-HNcoCA, BT-HNCO+, BT-HNcaCO, BT-HNcoCACB, HCCH-COSY (26,27) and standard Varian (1H-1H-15N)-NOESY-HSQC pulse sequences. Proton and carbon shifts were referenced to an internal standard of 4,4-dimethyl-4-silapentane-1-sulfonic acid (DSS) and nitrogen was referenced indirectly according to its gyromagnetic ratio (28). Spectra were processed by NMRPipe (29) and evaluated with CCPNmr Analysis(30). Assignments were deposited at the BMRB with corresponding numbers 26678, 26679 and 26680.

*Secondary chemical shift calculation and secondary structure prediction*—Analysis of secondary chemical shifts is based on the publication by Zhang et al.(31) and sequence corrected according to Schwarzinger (32). Secondary structure prediction was performed using the software TALOS-N (33). Structural propensities were calculated with the program SSP (34).

## RESULTS

*pEAβ(3-42) is more prone to form β-sheets and forms high molecular weight fibrils*—CD spectra of pEAβ(3-42) were recorded in aqueous buffer containing different TFE concentrations. The CD spectra in 50 % TFE indicated an α-helical conformation based upon characteristic minima at 208 and 222 nm, an x-axis intercept at 201 nm and a maximum at 195 nm. At lower TFE concentrations, however, the conformation of pEAβ(3-42) was changed towards β-sheet dominated structure (Fig. 1a). The spectrum in 40 % TFE showed a mixture of α-helical and β-sheet containing secondary structural elements with a reduced proportion of α-helices, as indicated by the loss of the two distinct CD absorbance minima at at 208 and 222 nm typical for α-helical structures. The analysis of the CD spectrum of pEAβ(3-42) in 30 % TFE indicate, that the conformation is now mainly β-sheet based on the minimum at 218 nm, an x-axis intercept at 212 nm and a maximum shift to higher wavelength, i.e. 200 nm. In contrast, the CD spectrum of Aβ(1-42) in buffer containing 40 % TFE evidenced only an α-helical dominated structure whereas the spectrum of Aβ(1-42) in 30 % TFE looks exactly the same as pEAβ(3-42) in 40 % TFE, indicating a mixed α-helical/β-sheet structure (Fig. 1b). In general, Aβ(1-42) showed increased tendency to build α-helical structures when compared to pEAβ(3-42).

Aβ aggregation kinetics observed by ThT assay supported a β-sheet conformation of pEAβ(3-42) in aqueous TFE solutions when compared to Aβ(1-42) under the same conditions. Figure 1c displays the kinetics in 30, 40 and 50 % TFE at 20 °C, respectively. The fluorescence intensity of pEAβ(3-42) in 50 % TFE did not increase significantly within 60 h. The aggregation kinetics in 40 % TFE showed a distinct lag phase of about 11 h following an growth phase and the characteristic stationary phase upon approximately 20 h. Fibril formation in 30 % TFE occurred faster; the lag phase lasted 6 h and fluorescence reached its maximum after 11 h. Moreover, the total fluorescence intensity of pEAβ(3-42) incubated in 30 % TFE was higher than in 40 % TFE indicating higher contents of β-sheeted fibrils. In contrast, an aggregation of Aβ(1-42) was not observable under the same conditions, as no increase in fluorescence intensity was observed either in 40 % TFE or in 30 % TFE within 60 h (Fig. 1d). Thus, fibril formation of Aβ(1-42) seems to be hindered or drastically delayed in the presence of TFE.

SEC was performed to analyze the distribution of monomers and oligomers of pEAβ(3-42) and Aβ(1-42) in 40 % TFE directly after dissolving (Supplemental Fig. 1). The monomeric percentage of the pyroglutamate-modified variant pEAβ(3-42) was reduced to a minimum, while approximately 10 % monomers

remained for Aβ(1-42) indicating, that pEAβ(3-42) shows increased tendency to aggregate.

The morphology of matured aggregates in the presence of TFE was analyzed with negative-stained electron microscopy. For that, monomeric pEAβ(3-42) and Aβ(1-42) were incubated in 40 % TFE for aggregation and visualized by TEM. As seen in figure 2 (upper panels) pEAβ(3-42) built large fibrils in µm scale. The fibrils were twisted, exhibit a rather homogeneous morphology and accumulate into plaques. In contrast, Aβ(1-42) showed a completely different conformation (Fig. 2, lower panels). The structure was amorphous without any characteristic fibril morphology and branched into networks of non-fibrillary particles.

*Characteristic differences in 2D correlation NMR spectra of pEAβ(3-42) compared to Aβ(1-42)*—($^{1}$H-$^{15}$N)-HSQC spectra of pEAβ(3-42) in different TFE concentrations ranging from 30 to 50 % are shown in figure 3a. Resonance assignments were performed using various 3D experiments as described in the Methods section. The spectra of pEAβ(3-42) recorded in buffer containing 50 % TFE exhibits all amide cross peak signals in a single conformation and similar intensities. The results of pEAβ(3-42) in 40 % TFE are similar, minor peak shifts are likely due to the change in TFE concentration. Nonetheless, some peak intensities were decreased, for example H13, E22 M35 and G37. This effect was dramatically increased in 30 % TFE. There, only the N-terminal cross peaks of aa residues pE3, F4 and R5 were detectable while all other resonances were missing.

($^{1}$H-$^{15}$N)-HSQC spectra of pEAβ(3-42) and Aβ(1-42) recorded in 40 % TFE are compared in figure 3b. Chemical shifts of the N-terminal aa towards H14 differ significantly due to the pyroglutamate modification. The cleavage of the first two aa and pE formation affects the N-terminal aa residues through H14 indicated by altered chemical shifts with decreasing influence towards the C-terminus. Chemical shift changes were plotted as a function of the primary sequence of pEAβ(3-42) (Fig. 4). Chemical shifts changes decreased almost exponentially from the N-terminus toward the C-terminus affecting significantly almost 30 % of the total aa residues.

*Chemical shift based secondary structure prediction*—Secondary chemical shifts are the deviation of the measured resonance frequencies from known random-coil values and are used to predict secondary structure elements. Secondary chemical shifts for Cα and C' are shown in figure 5a. Values above 1.5 ppm indicate segments of α-helical structures while negative scores are indicative for β-strands or extended conformations. Thus, C' secondary chemical shifts of Y10 to D23 and A30 to V36 and almost all Cα secondary chemical shifts despite the N- and C-terminus indicated α-helical structures. This is in accordance to the results for Cβ and Hα secondary chemical shifts, where positive values indicate β-sheets and negative values α-helices (Fig 5a). There is no indication for the evidence of β-sheet structure in the observable Aβ moiety.

Secondary structural propensities were calculated via the SSP program (34) using Hα, Cα, Cβ, C' chemical shifts as input data (Fig 5b). Positive score values are indicative for α-helices and negative scores for β-strands or extended conformation.

Secondary structure prediction was calculated with TALOS-N using all available chemical shifts (HN, Hα, Hβ, N, Cα, Cβ, C') (33) and the result is shown in figure 5c. No β-sheet structures but two α-helical regions at Y10 to D23 and A30 to V36 were predicted with a certainty above 80 %. The results are in agreement with both previously performed methods indicating strong α-helices in the regions Y10 to D23 and A30 to V36 with decreased helical propensity in between. Both termini showed negative score values.

NMR chemical shifts analysis by three methods did not provide any evidence for β-sheet structures of pEAβ(3-42) in 40 % TFE. Interestingly, Aβ(1-42) in 40 % TFE and pEAβ(3-42) in 50 % TFE showed the same secondary structure prediction by secondary chemical shift calculation and TALOS-N: Two helices connected by a flexible linker in accordance to the CD data indicating α-helices and no increase in ThT fluorescence due to fibril formation (Supplemental Fig. 2 and 3).

*Aggregation dependent cross peak attenuation in 3D spectra*—Cross peak intensity changes of Aβ(1-42) compared to pEAβ(3-42) in aqueous 40 % TFE containing buffer as well as between pEAβ(3-42) in 40 % and 50 % TFE containing buffer were analyzed by plotting the peak height gained by 3D BT-HNCA+ and BT-HNCO as a function of aa sequence (Fig. 6a,b). The Cα intensities of pEAβ(3-42) were decreased by an average of 15 to 20 % when compared to Aβ(1-42) under the same

conditions. Especially weak cross peak intensities, for example E22 or M35, were almost doubled in the spectra of the non-modified variant (Fig. 6a). For pEAβ(3-42) in 40 % TFE compared to 50 % TFE, Cα intensities between V12 and E22 as well as between I31 and G37 were approximately reduced by 50 %. M35, for example, was affected even stronger (Fig. 6a). The N-terminus and residues G25 to A30 were less affected. Changes in C' intensities were nearly identical, peak height of pEAβ(3-42) was 15 -20 % decreased compared to Aβ(1-42) under the same conditions. Comparison of the peak intensity of pEAβ(3-42) in 40 % TFE and 50 % TFE indicated drastically signal reduction. All aa residues, except of the very N-terminal residues pE3 and F4 are reduced to at least the half (Fig. 6b).

*Decrease in monomer population over time*—The cross peak intensities of pEAβ(3-42) and Aβ(1-42) were plotted against the incubation time and represent the monomer population (Fig. 6c). The cross peak heights of ($^{1}$H-$^{15}$N)-HSQC were averaged over all residues in each peptide and normalized to its initial value at the first measurement. The monomer population of pEAβ(3-42) decreased drastically and more rapidly when compared with Aβ(1-42). The cross peak intensities for pEAβ(3-42) after 50 h were reduced to approximately 10 % relative to its initial value, whereas still 50 % monomer derived cross peak intensities were left for Aβ(1-42).

This result was supported by analyzing the stability of pEAβ(3-42) in 40 % TFE by a time-dependent series of several ($^{1}$H-$^{15}$N)-HSQC within 3 days and evaluating all residue-specific cross peak intensities individually. The amide cross peak intensities were plotted against the time and residue sequence position (Supplemental Fig. 4). The loss of cross peak intensities most probably results from the conversion of peptide monomers to assemblies whose peaks are broadened beyond detection because of their large size or conformational exchange.

To elucidate whether the chemical exchange results from intra- or intermolecular conformational change of the peptide, ($^{1}$H-$^{15}$N)-HSQC spectra of [U-$^{15}$N]-pEAβ(3-42) were measured in the presence and absence of an excess amount of [NA]-pEAβ(3-42). The 10-fold molar excess of the peptide in natural abundancy reduced the peak intensity to approximately 20 %. The reduction in peak intensity indicates that the observed chemical exchange over time cannot be (exclusively) caused by intramolecular interactions but rather by intermolecular association, which are concentration dependent (Fig. 7).

## DISCUSSION

TFE is often used as a co-solvent, to induce and stabilize secondary structure elements (35). It disrupts tertiary interactions due to lowered solvent polarity and induced intra-molecular hydrogen bonding, which supports secondary structure formation in proteins and peptides (36). MD simulation by Roccatano and co-workers confirmed that the α-helix inducing effect of TFE is based on the displacement of water and a decreased dielectric constant favoring intra-molecular interactions (37).

*β-sheet formation and amyloid fibrillation*—pEAβ is more likely to aggregate and has a higher β-sheet stabilization in aqueous solutions compared to its non-modified variant (5,13). The conversion from α-helices to β-sheets by lowering the TFE concentration was described so far for Aβ(1-40) (38). Chen and coworkers showed that Aβ(1-40) undergoes a TFE-induced three-state transition from an α-helical conformational state to β-sheets in TFE concentrations ≤ 25 %. Amyloid formation by a TFE-induced pathway was also described for other unstructured peptides. Khan et al. demonstrated that conalbumin shows the fastest aggregation at a TFE concentration of 15 % although TFE stabilizes α-helices in conalbumin at concentrations above 50 % (39). For IAPP, it was investigated that low concentrations of TFE in combination with heparin induce aggregation and also in the presence of TFE alone when its concentration is at least 15 %(40). The formation of amyloids in the presence of TFE was also shown for e.g. human carbonic anhydrase II (41), the FF domain of URN1 splicing factor (42), transferrin (43) and α-synuclein (44). Here, our data show that this effect is also observable for pEAβ(3-42).

Secondary structure analysis by CD data suggests an increase in β-sheet-rich structures for pEAβ(3-42) in aqueous solutions with decreasing TFE concentrations. The data indicate a high amount of α-helices in 50 % TFE but this changed to a less helical and more β-sheet-rich structure with TFE concentrations ≤ 40 %. These data were confirmed by analyzing the aggregation kinetics by ThT assay. No increase in fluorescence intensity, and thus no β-sheet formation, was detected under conditions where the CD spectra indicated only α-helices. pEAβ(3-

42) started to form ThT positive structures in concentrations where the first β-sheets were observed by CD spectroscopy. Fibril formation was accelerated in reduced TFE concentrations. As TFE stabilizes intramolecular hydrogen bonds, it supports the formation of α-helices and β-hairpins (45). Here, high concentrations of TFE seem to stabilize helical pEAβ(3-42) by destabilizing hydrophobic interactions and thus preventing fibril formation (46). However, low TFE concentrations drive secondary structure elements towards β-sheets and pEAβ(3-42) aggregation occurs.

CD data of Aβ(1-42) showed α-helical conformation in 40 % TFE, according to a previously described simulation study (47), and β-sheet structures in 30 % TFE. Interestingly, Aβ(1-42) aggregation kinetics could not be detected, neither in 40 % nor in 30 % TFE as shown by ThT assay. Conversion of secondary structure elements from helices to β-strands started at lower TFE concentrations leads to the conclusion that helical Aβ(1-42) is more stabilized by TFE than pEAβ(3-42) as already shown for the shortened isoforms pEAβ(3-40) and Aβ(1-40) (21). This was further verified by SEC, where pEAβ(3-42) shows very low monomer abundance compared to Aβ(1-42).

Incubation of pEAβ(3-42) and Aβ(1-42) under identical conditions leads to aggregates differing in size and morphology, as observed by TEM data. Aggregates of pEAβ(3-42) in the presence of TFE are β-sheet-rich and thus represent a type of amyloid fibrils while aggregates of Aβ(1-42) incubated in TFE have an irregular amorphous ultrastructure.

*Fibrillation via an α-helical intermediate*—While our CD and ThT data show that pEAβ(3-42) builds β-sheets in 40 % TFE where Aβ(1-42) mainly forms α-helices, the NMR results apparently differ. Structural analysis of pEAβ(3-42) by NMR under identical solvent conditions as used for CD indicated an α-helical state. Two helical regions from Y10 to D23 and A30 to V36 connected with a linker were determined using different tools based on the secondary chemical shifts (31,32,34). Additionally, lowering the TFE concentration did not change the observed chemical shifts towards β-sheet structures but the cross peak intensities were drastically decreased. The β-sheet-rich structures detected via CD, ThT and TEM are thus not observable by solution state NMR, maybe due to exchange processes or due to the high molecular weight of the β-sheet-rich assembly state. As the cross peak intensity should not depend on the peptide concentration if chemical exchange occurs within a molecule, we added a 10-fold molar excess of pEAβ(3-42) in natural abundancy to [U-$^{15}$N]- pEAβ(3-42). This led to decreased cross peak intensity to 20 % indicating intermolecular interactions. Thus, the concentration of α-helical monomers was reduced due to peptide-peptide interactions resulting in non-observable assemblies.

There is also evidence to the assumption, that pEAβ(3-42) undergoes amyloid fibril formation based on an α-helical intermediate. Teplow and co-workers gave the first hint that helical intermediates could play a central role in aggregation processes. They showed by the use of a model peptide, that partially folded intermediates containing no observable β-sheet structures can mediate the initial stages of amyloid fibril formation via helix-rich oligomeric intermediates (48). They also investigated that 18 different Aβ species, amongst others pEAβ(3-42), incubated in glycine buffer showed a transient increase in helicity before the appearance of β-sheet structures (49). The same group showed, that TFE stabilizes this partially folded helical conformer, which potentially is an intermediate in Aβ fibril assembly (46). Helical intermediates of amyloidogenic peptides were also observed by Anderson *et al.* (44) by showing that α-synuclein builds fibrils which are strongly correlated with the TFE-mediated formation of a monomeric, partly helical intermediate. This intermediate exists in equilibrium with the natively disordered state at low TFE concentrations, whereas high TFE concentrations shift the equilibrium to the α-helical conformation (44). These helical intermediates are prone to fibrillation and has been reported for a number of amyloidogenic peptides by Abedini and Raleigh (50). They hypothesized that transiently populated helical structures associate leading to a high local concentration of an aggregation prone sequence which promotes intermolecular β-sheet formation (50,51). Nevertheless, it is not necessary that helical intermediates have to lead to an increase in the rate of amyloid formation. Stable helical intermediates can decrease or actually prevent the rate of amyloid formation (50,51). This is the case for TFE concentrations ≥ 50 % where fibril formation of both, Aβ(1-42) and pEAβ(3-42) is inhibited due to the destabilization of hydrophobic interactions (45).

*Aβ modification to pEAβ affects fibrillation kinetics*—By comparing ($^{1}$H-$^{15}$N)-HSQC spectra of pEAβ(3-42) with Aβ(1-42), the

secondary structure prediction based on measured chemical shifts indicates only α-helical monomers, this conformation is unstable and accumulates into fibrils. There is evidence to the conclusion that pEAβ(3-42) builds transient intermediates with α-helical secondary structure as a precursor to β-sheet formation and fibrillation.

**Acknowledgments:** Rudolf Hartmann and Maren Thomaier are highly acknowledged for scientific advices. We gratefully acknowledge support of CD from the International NRW Research School BioStruct, granted by the Ministry of Innovation, Science and Research of the State North Rhine-Westphalia, the Heinrich Heine University Düsseldorf, and the Entrepreneur Foundation at the Heinrich Heine University Düsseldorf. The authors acknowledge access to the Jülich-Düsseldorf Biomolecular NMR Center. DW was supported by grants from the "Portfolio Technology and Medicine", the "Portfolio Drug Research" and the Helmholtz-Validierungsfonds of the Impuls und Vernetzungs-Fonds der Helmholtzgemeinschaft.

**Conflict of interest:** The authors declare that they have no conflicts of interest with the contents of this article.

**Author contributions:** MSc, CD, LG and DW conceived and designed the experiments. CD, MSc, KR, MSt and TZ performed the experiments. CD, MSc and JL analyzed the data. CD wrote the paper and MSc, LG and DW revised the manuscript.

REFERENCES


1. Palop, J. J., and Mucke, L. (2009) Epilepsy and cognitive impairments in Alzheimer disease. *Archives of neurology* **66**, 435-440
2. Huang, Y., and Mucke, L. (2012) Alzheimer mechanisms and therapeutic strategies. *Cell* **148**, 1204-1222
3. De Strooper, B., Vassar, R., and Golde, T. (2010) The secretases: enzymes with therapeutic potential in Alzheimer disease. *Nature reviews. Neurology* **6**, 99-107
4. Gunn, A. P., Masters, C. L., and Cherny, R. A. (2010) Pyroglutamate-Abeta: role in the natural history of Alzheimer's disease. *The international journal of biochemistry & cell biology* **42**, 1915-1918
5. Jawhar, S., Wirths, O., and Bayer, T. A. (2011) Pyroglutamate amyloid-beta (Abeta): a hatchet man in Alzheimer disease. *The Journal of biological chemistry* **286**, 38825-38832
6. Perez-Garmendia, R., and Gevorkian, G. (2013) Pyroglutamate-Modified Amyloid Beta Peptides: Emerging Targets for Alzheimer s Disease Immunotherapy. *Current neuropharmacology* **11**, 491-498
7. Saido, T. C., Iwatsubo, T., Mann, D. M., Shimada, H., Ihara, Y., and Kawashima, S. (1995) Dominant and differential deposition of distinct beta-amyloid peptide species, A beta N3(pE), in senile plaques. *Neuron* **14**, 457-466
8. Wirths, O., Bethge, T., Marcello, A., Harmeier, A., Jawhar, S., Lucassen, P. J., Multhaup, G., Brody, D. L., Esparza, T., Ingelsson, M., Kalimo, H., Lannfelt, L., and Bayer, T. A. (2010) Pyroglutamate Abeta pathology in APP/PS1KI mice, sporadic and familial Alzheimer's disease cases. *Journal of neural transmission* **117**, 85-96
9. Schilling, S., Manhart, S., Hoffmann, T., Ludwig, H. H., Wasternack, C., and Demuth, H. U. (2003) Substrate specificity of glutaminyl cyclases from plants and animals. *Biological chemistry* **384**, 1583-1592
10. Schilling, S., Hoffmann, T., Manhart, S., Hoffmann, M., and Demuth, H. U. (2004) Glutaminyl cyclases unfold glutamyl cyclase activity under mild acid conditions. *FEBS letters* **563**, 191-196
11. D'Arrigo, C., Tabaton, M., and Perico, A. (2009) N-terminal truncated pyroglutamyl beta amyloid peptide Abetapy3-42 shows a faster aggregation kinetics than the full-length Abeta1-42. *Biopolymers* **91**, 861-873
12. Schlenzig, D., Manhart, S., Cinar, Y., Kleinschmidt, M., Hause, G., Willbold, D., Funke, S. A., Schilling, S., and Demuth, H. U. (2009) Pyroglutamate formation influences solubility and amyloidogenicity of amyloid peptides. *Biochemistry* **48**, 7072-7078
13. Schilling, S., Lauber, T., Schaupp, M., Manhart, S., Scheel, E., Bohm, G., and Demuth, H. U. (2006) On the seeding and oligomerization of pGlu-amyloid peptides (in vitro). *Biochemistry* **45**, 12393-12399
14. Bayer, T. A., and Wirths, O. (2014) Focusing the amyloid cascade hypothesis on N-truncated Abeta peptides as drug targets against Alzheimer's disease. *Acta neuropathologica* **127**, 787-801
15. Meissner, J. N., Bouter, Y., and Bayer, T. A. (2015) Neuron Loss and Behavioral Deficits in the TBA42 Mouse Model Expressing N-Truncated Pyroglutamate Amyloid-beta3-42. *Journal of Alzheimer's disease : JAD* **45**, 471-482
16. Zagorski, M. G., and Barrow, C. J. (1992) NMR studies of amyloid beta-peptides: proton assignments, secondary structure, and mechanism of an alpha-helix----beta-sheet conversion for a homologous, 28-residue, N-terminal fragment. *Biochemistry* **31**, 5621-5631
17. Sticht, H., Bayer, P., Willbold, D., Dames, S., Hilbich, C., Beyreuther, K., Frank, R. W., and Rosch, P. (1995) Structure of amyloid A4-(1-40)-peptide of Alzheimer's disease. *European journal of biochemistry / FEBS* **233**, 293-298
18. Shao, H., Jao, S., Ma, K., and Zagorski, M. G. (1999) Solution structures of micelle-bound amyloid beta-(1-40) and beta-(1-42) peptides of Alzheimer's disease. *Journal of molecular biology* **285**, 755-773
19. Crescenzi, O., Tomaselli, S., Guerrini, R., Salvadori, S., D'Ursi, A. M., Temussi, P. A., and Picone, D. (2002) Solution structure of the Alzheimer amyloid beta-peptide (1-42) in an apolar microenvironment. Similarity with a virus fusion domain. *European journal of biochemistry / FEBS* **269**, 5642-5648

38. Chen, Y. R., Huang, H. B., Chyan, C. L., Shiao, M. S., Lin, T. H., and Chen, Y. C. (2006) The effect of Abeta conformation on the metal affinity and aggregation mechanism studied by circular dichroism spectroscopy. *Journal of biochemistry* **139**, 733-740
39. Khan, M. V., Rabbani, G., Ahmad, E., and Khan, R. H. (2014) Fluoroalcohols-induced modulation and amyloid formation in conalbumin. *International journal of biological macromolecules* **70**, 606-614
40. Konno, T., Oiki, S., and Morii, T. (2007) Synergistic action of polyanionic and non-polar cofactors in fibrillation of human islet amyloid polypeptide. *FEBS letters* **581**, 1635-1638
41. Gupta, P., and Deep, S. (2014) Intermediate conformation between native beta-sheet and non-native alpha-helix is a precursor of trifluoroethanol-induced aggregation of human carbonic anhydrase-II. *Biochemical and biophysical research communications* **449**, 126-131
42. Marinelli, P., Castillo, V., and Ventura, S. (2013) Trifluoroethanol modulates amyloid formation by the all alpha-helical URN1 FF domain. *Int J Mol Sci* **14**, 17830-17844
43. Amani, S., and Naeem, A. (2014) Transition of transferrin from native to fibrillar state: An implication for amyloid-linked diseases. *Biochem Eng J* **91**, 120-128
44. Anderson, V. L., Ramlall, T. F., Rospigliosi, C. C., Webb, W. W., and Eliezer, D. (2010) Identification of a helical intermediate in trifluoroethanol-induced alpha-synuclein aggregation. *Proceedings of the National Academy of Sciences of the United States of America* **107**, 18850-18855
45. Buck, M. (1998) Trifluoroethanol and colleagues: cosolvents come of age. Recent studies with peptides and proteins. *Q Rev Biophys* **31**, 297-355
46. Fezoui, Y., and Teplow, D. B. (2002) Kinetic studies of amyloid beta-protein fibril assembly. Differential effects of alpha-helix stabilization. *The Journal of biological chemistry* **277**, 36948-36954
47. Jalili, S., and Akhavan, M. (2009) A molecular dynamics simulation of conformational changes and solvation of Aβ peptide in trifluoroethanol and water. *Journal of Theoretical and Computational Chemistry* **08**, 215-231
48. Fezoui, Y., Hartley, D. M., Walsh, D. M., Selkoe, D. J., Osterhout, J. J., and Teplow, D. B. (2000) A de novo designed helix-turn-helix peptide forms nontoxic amyloid fibrils. *Nat Struct Biol* **7**, 1095-1099
49. Kirkitadze, M. D., Condron, M. M., and Teplow, D. B. (2001) Identification and characterization of key kinetic intermediates in amyloid beta-protein fibrillogenesis. *Journal of molecular biology* **312**, 1103-1119
50. Abedini, A., and Raleigh, D. P. (2009) A role for helical intermediates in amyloid formation by natively unfolded polypeptides? *Physical biology* **6**, 015005
51. Abedini, A., and Raleigh, D. P. (2009) A critical assessment of the role of helical intermediates in amyloid formation by natively unfolded proteins and polypeptides. *Protein engineering, design & selection : PEDS* **22**, 453-459
52. Mischo, A., Ohlenschlager, O., Guhrs, K. H., and Gorlach, M. (2012) Recombinant production of isotope-labeled peptides and spontaneous cyclization of amino-terminal glutamine into pyroglutamic acid. *Chembiochem : a European journal of chemical biology* **13**, 1421-1423
53. Mihara, H., and Takahashi, Y. (1997) Engineering peptides and proteins that undergo alpha-to-beta transitions. *Curr Opin Struct Biol* **7**, 501-508
54. Liu, G., Prabhakar, A., Aucoin, D., Simon, M., Sparks, S., Robbins, K. J., Sheen, A., Petty, S. A., and Lazo, N. D. (2010) Mechanistic studies of peptide self-assembly: transient alpha-helices to stable beta-sheets. *Journal of the American Chemical Society* **132**, 18223-18232
55. van Beek, J. D., Beaulieu, L., Schafer, H., Demura, M., Asakura, T., and Meier, B. H. (2000) Solid-state NMR determination of the secondary structure of Samia cynthia ricini silk. *Nature* **405**, 1077-1079
56. Garai, K., Sahoo, B., Sengupta, P., and Maiti, S. (2008) Quasihomogeneous nucleation of amyloid beta yields numerical bounds for the critical radius, the surface tension, and the free energy barrier for nucleus formation. *The Journal of chemical physics* **128**, 045102
57. Nag, S., Sarkar, B., Bandyopadhyay, A., Sahoo, B., Sreenivasan, V. K., Kombrabail, M., Muralidharan, C., and Maiti, S. (2011) Nature of the amyloid-beta monomer and the monomer-oligomer equilibrium. *The Journal of biological chemistry* **286**, 13827-13833

58. Bjerke, M., Portelius, E., Minthon, L., Wallin, A., Anckarsater, H., Anckarsater, R., Andreasen, N., Zetterberg, H., Andreasson, U., and Blennow, K. (2010) Confounding factors influencing amyloid Beta concentration in cerebrospinal fluid. *International journal of Alzheimer's disease* **2010**
59. De Meyer, G., Shapiro, F., Vanderstichele, H., Vanmechelen, E., Engelborghs, S., De Deyn, P. P., Coart, E., Hansson, O., Minthon, L., Zetterberg, H., Blennow, K., Shaw, L., Trojanowski, J. Q., and Alzheimer's Disease Neuroimaging, I. (2010) Diagnosis-independent Alzheimer disease biomarker signature in cognitively normal elderly people. *Archives of neurology* **67**, 949-956
60. Serpell, L. C. (2000) Alzheimer's amyloid fibrils: structure and assembly. *Biochimica et biophysica acta* **1502**, 16-30

## FIGURE LEGENDS

**FIGURE 1.** CD spectra and aggregation kinetics of pEAβ(3-42) and Aβ(1-42). Far-UV CD spectra were recorded on a Jasco J-1100 spectropolarimeter at 20 °C from 260 to 190 nm, accumulated 12 times and corrected for the buffer. (a) CD spectra of 25 μM pEAβ(3-42) in 50 mM potassium phosphate, pH 2.8 containing 30, 40 or 50 % TFE, respectively (black, red, blue). With decreasing TFE concentration the content of α-helices was reduced and β-sheet-rich structures appeared. (b) CD spectra of 25 μM Aβ(1-42) in 50 mM potassium phosphate, pH 2.8 containing 30 or 40 % TFE (green, purple), respectively. While the spectrum of pEAβ(3-42) showed β-sheet structural elements in 40 % TFE, Aβ(1-42) is primarily α-helix-rich but builds β-sheet structures in 30 % TFE comparable to that of pEAβ(3-42) at higher TFE concentrations, i.e. 40 %. (c) Aggregation kinetics measured by ThT assay. 25 μM pEAβ(3-42) were dissolved in 50 mM potassium phosphate, pH 2.8 containing 30, 40 or 50 % TFE (black, red, blue) including 10 μM ThT, respectively. (d) Kinetics of 25 μM Aβ(1-42) were measured in 50 mM potassium phosphate, pH 2.8 containing 30 and 40 % TFE (green, purple) including 10 μM ThT (pH 2.8). The fluorescence emission at 492 nm was monitored on a fluorescence spectrometer (excitation at 440 nm), recorded every 15 min for 62 h. The measurement was performed in five-fold, averaged and the buffer was subtracted for background correction. An increase of ThT fluorescence and faster aggregation kinetics of pEAβ(3-42) were observed with decreasing TFE concentration. No fibril formation of Aβ(1-42) could be detected within 62 h.

**FIGURE 2.** TEM images of pEAβ(3-42) (top) and Aβ(1-42) (bottom). Peptides were dissolved in 50 mM potassium phosphate, pH 2.8 containing 40 % TFE and incubated at 20 °C for five days. Grids were prepared by negative staining. Aggregated pEAβ(3-42) formed large twisted fibrils while Aβ(1-42) formed non-fibrillary branched networks.

**FIGURE 3.** ($^1$H-$^{15}$N)-HSQC of pEAβ(3-42) and Aβ(1-42). (a) 100 μM pEAβ(3-42)m were dissolved in aqueous solution containing 30, 40 or 50 % TFE in 50 mM potassium phosphate pH 2.8 (black, red, blue), respectively. Spectra were recorded on a 600 MHz Bruker spectrometer at 20 °C. The spectra of pEAβ(3-42) in 50 % differs slightly from that in 40 % TFE due to the change of the TFE concentration. Notably, some peak intensities are drastically decreased like H13, E22, M35 and G37. The spectrum of pEAβ(3-42) in 30 % TFE revealed that only the cross peaks of the very N-terminal aa residues pE3, F4 and R5 were left. (b) Overlay of 100 μM pEAβ(3-42) (red) and Aβ(1-42) (purple) in aqueous solution (50 mM potassium phosphate, pH 2.8) containing 40 % TFE. Peaks with prominent changes in chemicall shifts are marked with assignments. Spectra were recorded on a 600 MHz Bruker spectrometer at 20 °C. Pyroglutamate modification affects the N-terminal cross peaks towards H14 (assigned in black). Cross peaks exclusively for Aβ(1-42) were labelled in purple and in red for pEAβ(3-42).

**FIGURE 4.** Structural characterization of pEAβ(3-42). Structural analysis was based on NMR chemical shift data of 100 μM pEAβ(3-42) in buffer (40 % TFE in 50 mM potassium phosphate, pH 2.8) at 20 °C. (a) C', $C^{\alpha}$, $C^{\beta}$ and $H^{\alpha}$ chemical shifts calculated as the difference between measured and random coil chemical shifts described by Zhang *et al.* **(31)** and sequence corrected for neighbor effects **(32)**. (b) SSP score. (c) Secondary structure prediction by TALOS-N **(33)**. The probability for an α-helical conformation is plotted for each aa residue.

**FIGURE 5.** Chemical shift changes. Changes in chemical shifts of pEAβ(3-42) compared to Aβ(1-42) were obtained from ($^1$H-$^{15}$N)-HSQC of pEAβ(3-42) and Aβ(1-42) in 40 % TFE and calculated according to the formula $\Delta\delta(^1H,^{15}N) = ((10*\Delta\delta 1H^N)^2 + (\Delta\delta^{15}N)^2)^{1/2}$. Chemical shift changes are plotted as a function of the primary sequence of pEAβ(3-42). Pyroglutamate formation affects the N-terminal aa residues towards H14 with decreasing effect towards the C-terminus.

**FIGURE 6.** Normalized cross peak intensities of pEAβ(3-42) compared to Aβ(1-42). Cross peak intensities of pEAβ(3-42) and Aβ(1-42) obtained from BT-HNCA+ (a) and BT-HNCO (b) spectra. Peak intensity of pEAβ(3-42) in 40 % TFE was normalized to pEAβ(3-42) in 50 % TFE (red) and to Aβ(1-42) in 40 % TFE (black). The normalized cross peak intensity is plotted against the primary aa sequence of pEAβ(3-42). Stars indicate overlapping cross peaks and therefore no analysis in peak

height. Cα and C' intensities of pEAβ(3-42) are decreased by an average of 15-20 % when compared with Aβ(1-42). Cα and C' intensities of pEAβ(3-42) in 40 % TFE were only half of the intensities of pEAβ(3-42) in 50 % TFE but had less effect on the N-terminus and residues G25 to A30. (c) The ($^{1}$H-$^{15}$N)-HSQC cross peak intensities were averaged over all residues in Aβ(1-42) (black) and pEAβ(3-42) (red) and reported relatively to its initial value at the first measurement. The monomer abundance in pEAβ(3-42) decreased more rapidly than in Aβ(1-42).

**FIGURE 7**. Normalized cross peak intensities in the presence of a molar excess of non-isotopically enriched peptide. ($^{1}$H-$^{15}$N)-HSQC peak height of 25 µM [*U*-$^{15}$N]- with an excess of 250 µM [*U*-$^{14}$N]-pEAβ(3-42) was normalized to 25 µM [*U*-$^{15}$N]-pEAβ(3-42) in 40 % TFE. The decrease in cross peak intensity is plotted against the primary aa sequence of pEAβ(3-42). Peak intensities are decreased by an average to approximately 20 %.

**FIGURE 8**. Schematic diagram of the transition of an α-helical intermediate to β-sheets. α-helices are depicted as cylinders and β-strands as zigzagged lines. Unstructured pEAβ(3-42) monomers build TFE induced α-helices. These helices bundle together and generate a high local concentration of an aggregation prone sequence which is likely to build β-strands. The formation of β-strands disrupts the α-helices and leads to the formation of β-sheet-rich assemblies.

**Figure 1**

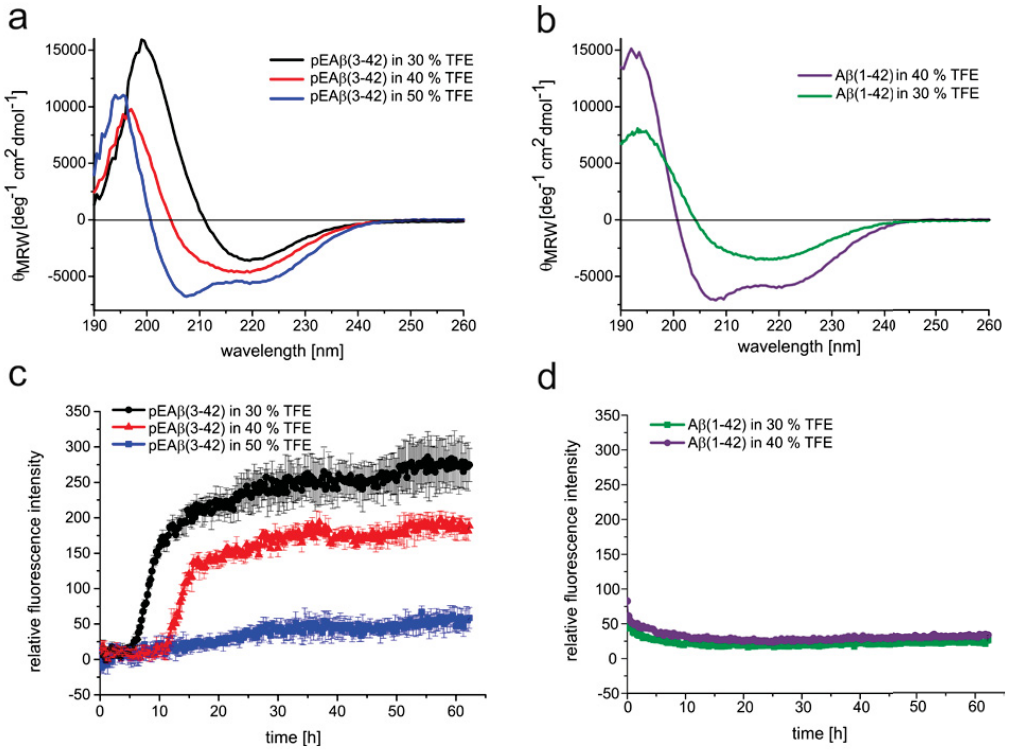
a
pEAβ(3-42) in 30 % TFE
pEAβ(3-42) in 40 % TFE
pEAβ(3-42) in 50 % TFE
θMRW [deg-1 cm2 dmol-1]
wavelength [nm]
b
Aβ(1-42) in 40 % TFE
Aβ(1-42) in 30 % TFE
θMRW [deg-1 cm2 dmol-1]
wavelength [nm]
c
pEAβ(3-42) in 30 % TFE
pEAβ(3-42) in 40 % TFE
pEAβ(3-42) in 50 % TFE
relative fluorescence intensity
time [h]
d
Aβ(1-42) in 30 % TFE
Aβ(1-42) in 40 % TFE
relative fluorescence intensity
time [h]

**Figure 2**

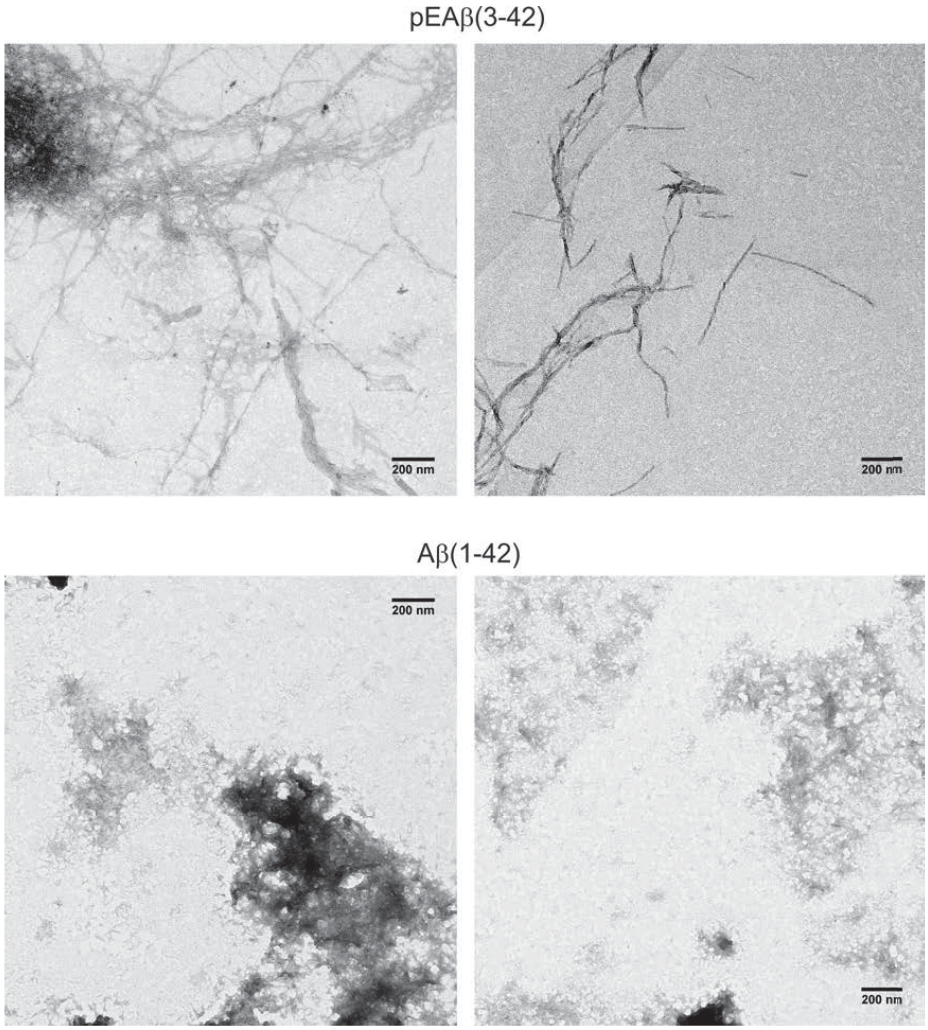

**Figure 3**

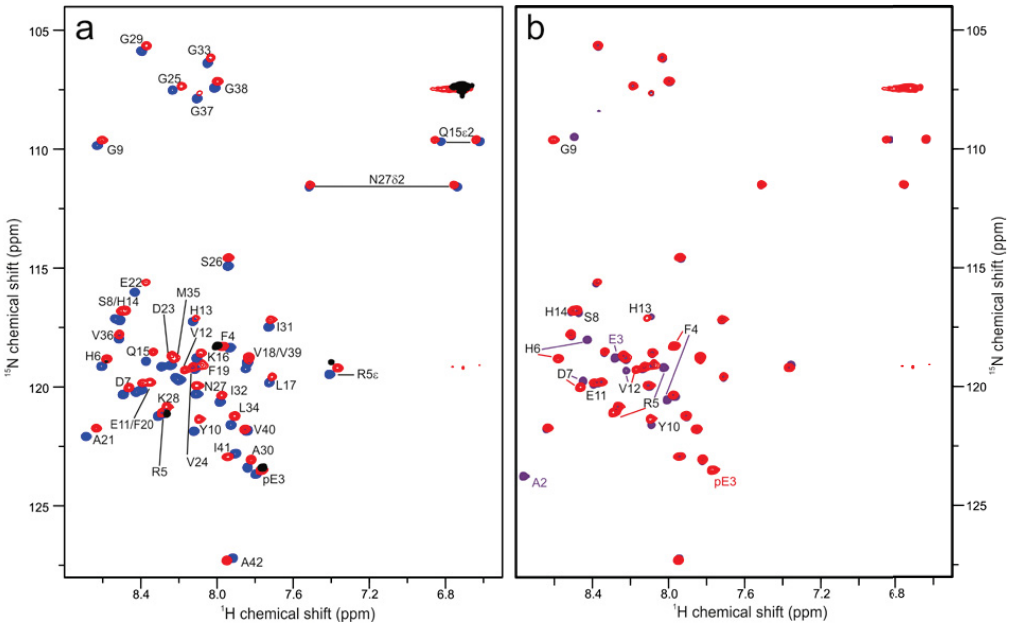
a
b
G29
G33
G25
G38
G37
G9
Q15ε2
N27δ2
S26
E22
M35
S8/H14
D23
H13
V36
V12
F4
I31
H6
Q15
K16
V18/V39
F19
R5ε
D7
N27
I32
L17
K28
L34
E11/F20
Y10
V40
A21
I41
A30
V24
R5
pE3
A42
H14
S8
H13
E3
F4
H6
D7
E11
V12
R5
Y10
A2
pE3
105
110
115
120
125
8.4
8.0
7.6
7.2
6.8
$^{15}$N chemical shift (ppm)
$^{1}$H chemical shift (ppm)

**Figure 4**

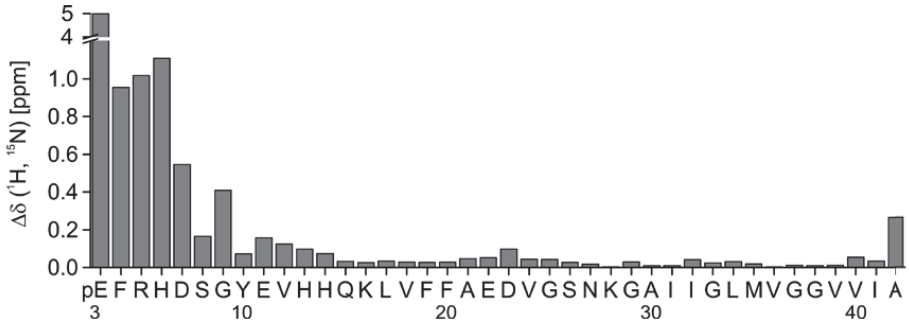
5
4
1.0
0.8
0.6
0.4
0.2
0.0
Δδ (¹H, ¹⁵N) [ppm]
pE F R H D S G Y E V H H Q K L V F F A E D V G S N K G A I I G L M V G G V V I A
3
10
20
30
40

**Figure 5**

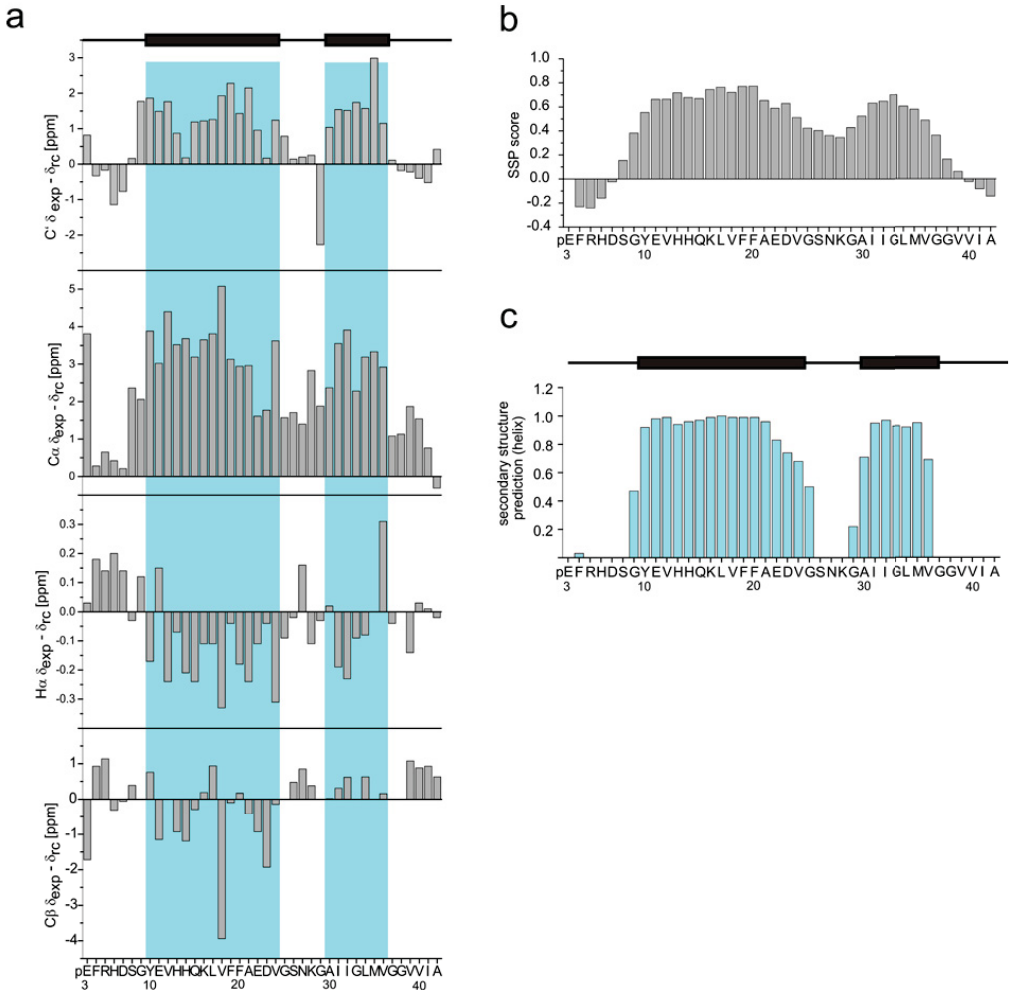
a
C' δ exp - δrc [ppm]
Cα δexp - δrc [ppm]
Hα δexp - δrc [ppm]
Cβ δexp - δrc [ppm]
pEFRHDSGYEVHHQKLVFFAEDVGSNKGAIIGLMVGGVVIA
3
10
20
30
40
b
SSP score
pEFRHDSGYEVHHQKLVFFAEDVGSNKGAIIGLMVGGVVIA
c
secondary structure prediction (helix)
pEFRHDSGYEVHHQKLVFFAEDVGSNKGAIIGLMVGGVVIA

**Figure 6**

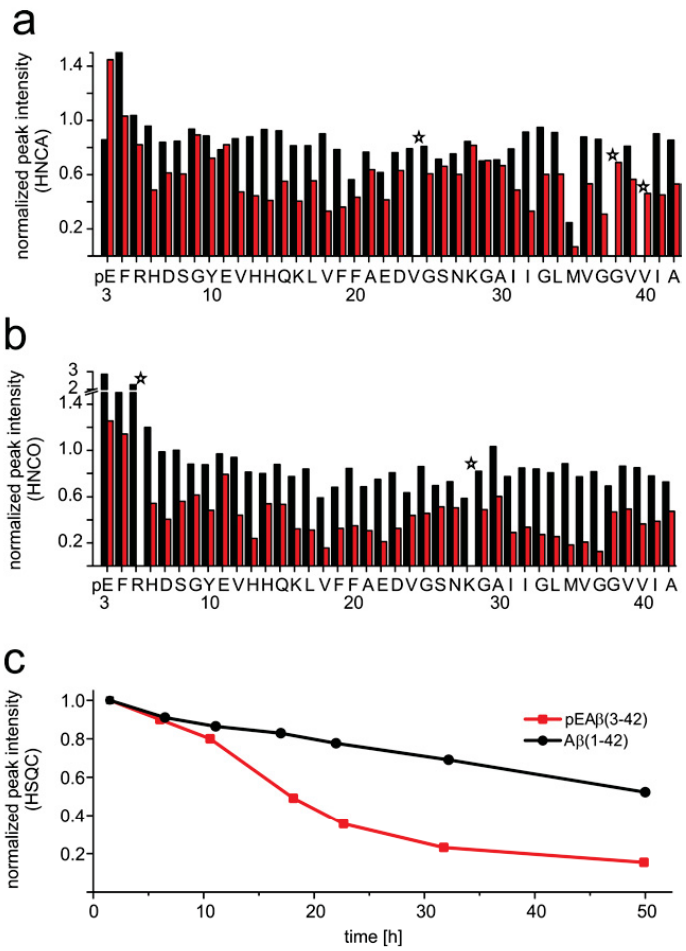
a
normalized peak intensity (HNCA)
1.4
1.0
0.6
0.2
pE F R H D S G Y E V H H Q K L V F F A E D V G S N K G A I I G L M V G G V V I A
3
10
20
30
40
b
normalized peak intensity (HNCO)
3
2
1.4
1.0
0.6
0.2
pE F R H D S G Y E V H H Q K L V F F A E D V G S N K G A I I G L M V G G V V I A
3
10
20
30
40
c
normalized peak intensity (HSQC)
1.0
0.8
0.6
0.4
0.2
pEAβ(3-42)
Aβ(1-42)
0
10
20
30
40
50
time [h]

**Figure 7**

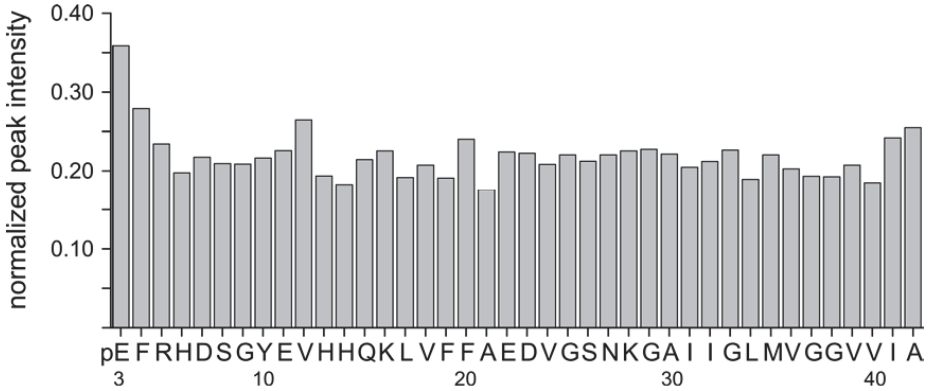
normalized peak intensity
0.40
0.30
0.20
0.10
pE F R H D S G Y E V H H Q K L V F F A E D V G S N K G A I I G L M V G G V V I A
3
10
20
30
40

**Figure 8**

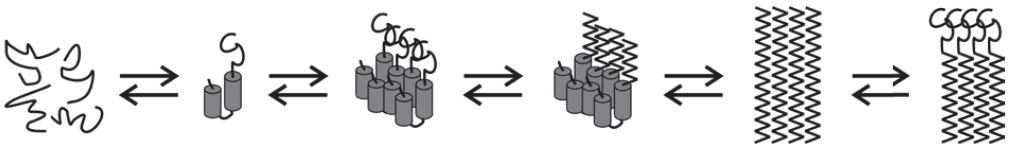

pEAβ(3-42) undergoes amyloid formation via an α-helical intermediate as revealed by 3D NMR spectroscopy

**Christina Dammers[1], Kerstin Reiß[1], Lothar Gremer[1,2], Justin Lecher[2], Tamar Ziehm[1], Matthias Stoldt[1], Melanie Schwarten[1] and Dieter Willbold[1,2]**

1Institute of Complex Systems (ICS-6) Structural Biochemistry, Forschungszentrum Jülich, 52425 Jülich, Germany

2Institut für Physikalische Biologie, Heinrich-Heine-Universität Düsseldorf, 40225 Düsseldorf, Germany

## SUPPLEMENTARY FIGURE LEGENDS

**Supplementary Figure 1** SEC of pEAβ(3-42) and Aβ(1-42) under identical conditions was performed on an ÄKTAexplorer 100 system (GE Healthcare, Freiburg, Germany) using a Superdex 75 PC 3.2/30 column (GE Healthcare, Freiburg, Germany). The system was equilibrated with 40 % TFE in 50 mM potassium phosphate, pH 2.8 and the run was performed with a flow-rate of 0.5 µl/min at room temperature. Absorbance at 214 nm was recorded. SEC was performed to analyze the distribution of monomers and oligomers of pEAβ(3-42) and Aβ(1-42) in 40 % TFE. Aβ monomers have a retention volume of 2 ml while larger species elute earlier. The monomeric percentage of pEAβ(3-42) is reduced to a minimum while approximately 10 % monomers are left for Aβ(1-42).

**Supplementary Figure 2** Structural characterization of Aβ(1-42) in 40 % TFE, 50 mM potassium phosphate, pH 2.8 at 20 °C from NMR chemical shift data. (a) C' and $C^{\alpha}$ chemical shifts calculated as the difference between measured and random coil chemical shifts described by Zhang *et al.*[1] and sequence corrected for neighbor effects[2]. (b) Secondary structure prediction by TALOS-N[3]. The probability for an α-helical conformation is plotted for each aa residue.

**Supplementary Figure 3** Structural characterization of pEAβ(3-42) in 50 % TFE, 50 mM potassium phosphate, pH 2.8 at 20 °C from NMR chemical shift data. (a) C' and $C^{\alpha}$ chemical shifts calculated as the difference between measured and random coil chemical shifts described by Zhang *et al.*[1] and sequence corrected for neighbor effects[2]. (b) Secondary structure prediction by TALOS-N[3]. The probability for an α-helical conformation is plotted for each aa residue.

**Supplementary Figure 4** Cross peak intensities over time of 100 µM pEAβ(3-42) (40 % TFE in 50 mM potassium phosphate, pH 2.8) at 20 °C. A time series of 48 ($^{1}H$-$^{15}N$)-HSQCs (each 90 min) was recorded on a 600 MHz Bruker spectrometer. Total acquisition time was approximately 72 h. Amide cross peak intensity for each aa residue is plotted against the time. Within 15 h, most of the cross peaks were near the background but the N-terminal aa residues pE3, F4 and R5 were more stabl

**Supplementary figure 1**

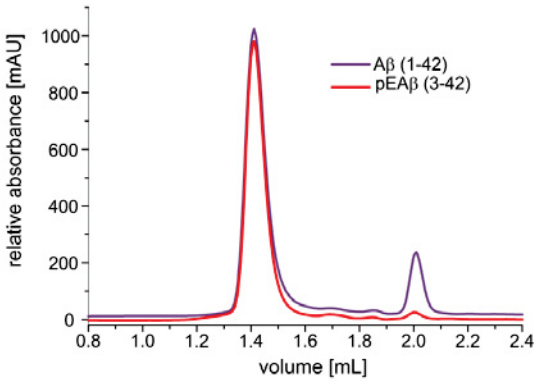

**Supplementary figure 2**

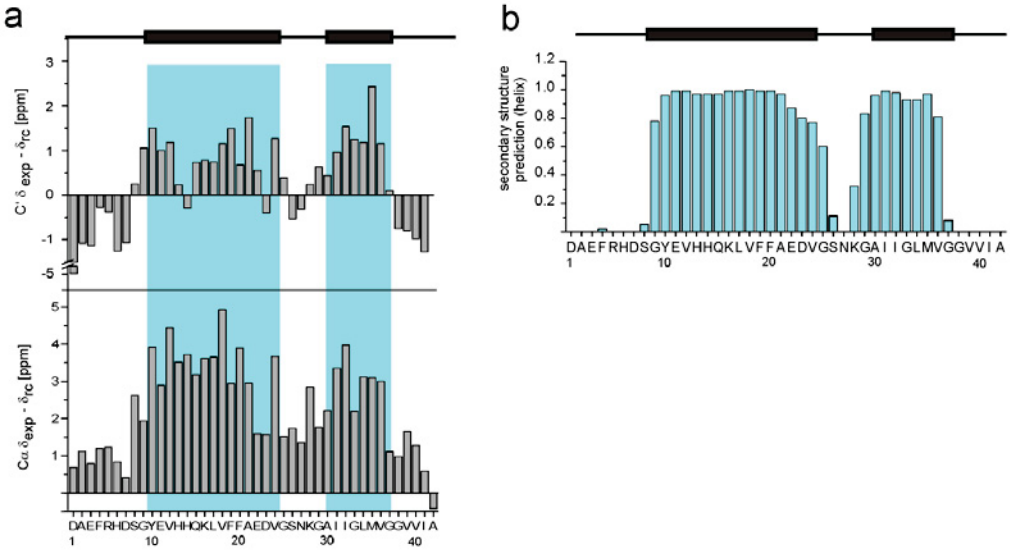

**Supplementary figure 3**

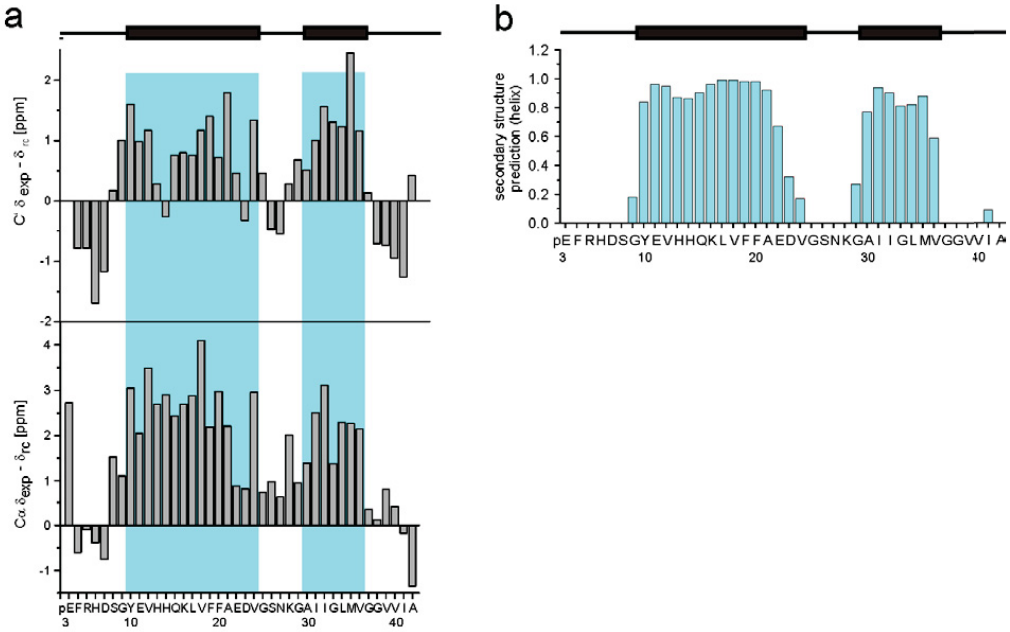

**Supplementary figure 4**

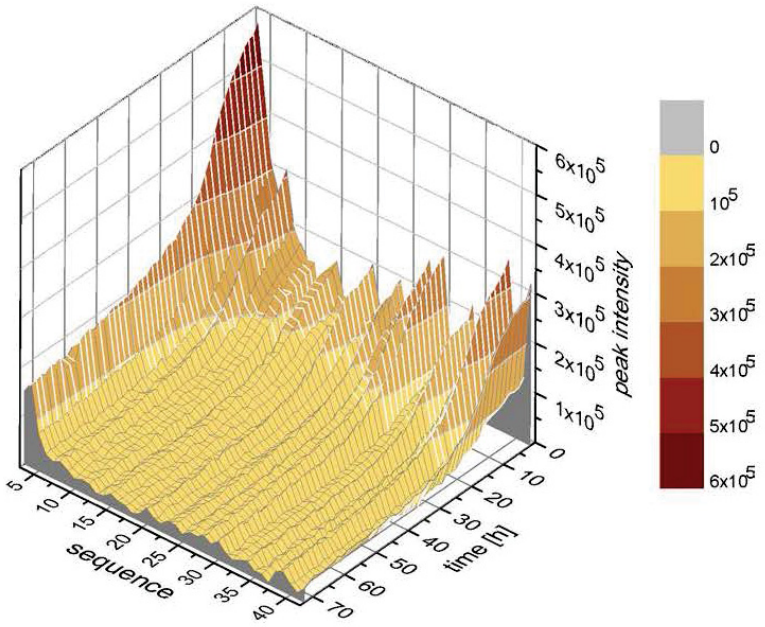

## SUPPLEMENTARY INFORMATION REFERENCES


1. Zhang, H., Neal, S. & Wishart, D.S. RefDB: a database of uniformly referenced protein chemical shifts. *J Biomol NMR* **25**, 173-95 (2003).
2. Schwarzinger, S. et al. Sequence-dependent correction of random coil NMR chemical shifts. *J Am Chem Soc* **123**, 2970-8 (2001).
3. Shen, Y. & Bax, A. Protein backbone and sidechain torsion angles predicted from NMR chemical shifts using artificial neural networks. *J Biomol NMR* **56**, 227-41 (2013).

## 3.4 Aβ-directed therapy interferes successfully with pEAβ(3-42) induced degenerative phenotype in transgenic mice

*Tina Dunkelmann[1], Kerstin Teichmann[1], Markus Tusche[1], Christina Dammers[1], Dagmar Jürgens[1], Karl-Josef Langen[2,3], Hans-Ulrich Demuth[4,5], Nadim Jon Shah[2], Janine Kutzsche[1], Antje Willuweit[2], Dieter Willbold[1,6]*

*[1]Institute of Complex Systems, Structural Biochemistry (ICS-6), Forschungszentrum Jülich GmbH, 52425 Jülich, Germany*

*[2]Institute of Neuroscience and Medicine (INM-4), Medical Imaging Physics, Forschungszentrum Jülich GmbH, 52425 Jülich, Germany*

*[3]Department of Nuclear Medicine, Universitätsklinikum der RWTH Aachen, 52074 Aachen, Germany*

*[4]Fraunhofer-Institute of Cell Therapy and Immunology (IZI), 04103 Leipzig, Germany*

*[5]Department of Drug Design and Target Validation (MWT), Biozentrum, 06120 Halle, Germany*

*[6]Institut für Physikalische Biologie, Heinrich Heine Universität Düsseldorf, 40225 Düsseldorf, Germany*

**Corresponding authors**

Dieter Willbold

Institute of Complex Systems

Structural Biochemistry (ICS-6)

Forschungszentrum Jülich GmbH

d.willbold@fz-juelich.de

Antje Willuweit

Institute of Neuroscience and Medicine (INM-4)

Medical Imaging Physics

Forschungszentrum Jülich GmbH

a.willuweit@fz-juelich.de

## Acknowledgements

Financial support of D.W. was provided by “Portfolio Technology and Medicine”, the Helmholtz-Validierungsfonds of the Impuls and Vernetzungs-Fonds der Helmholtzgemeinschaft. D.W. and K.-J.L. were supported by the “Portfolio Drug Research” of the Impuls and Vernetzungs-Fonds der Helmholtzgemeinschaft. The first breeding pairs of TBA2.1 mice were a generous gift by Probiodrug AG. We thank Elke Butzküven and Verena Graf for excellent technical assistance.

## Significant statement

pEAβ(3-42) is discussed to initiate the amyloid cascade in the progression of Alzheimer’s disease . In the TBA2.1 mouse model a progressive motor neurodegenerative phenotype is caused by pEAβ(3-42), which can be set back by therapeutic treatment with the D-enantiomeric peptides D3 and D3D3.

## Abstract

Today, no causative or disease modifying treatment is available for Alzheimer's disease (AD). Previously, it has been shown that D3, a small, fully D-enantiomeric peptide is able to eliminate low molecular weight Aβ oligomers *in vitro*, enhance cognition and reduce plaque load in AD transgenic mice. To further characterise the therapeutic potential of D3 towards N-terminally truncated and pyroglutamated Aβ (pEAβ(3-42)) we tested D3 and its head-to-tail tandem derivative D3D3 in the new mouse model TBA2.1. TBA2.1 express human pEAβ(3-42) leading very early to a strong motor neurodegenerative phenotype. In the present study, we were 1) able to show higher binding affinity of both D3 and D3D3 to pEAβ(3-42) and 2) could confirm increased affinity of the tandem derivative D3D3 in comparison to D3. Subsequently we tested the therapeutic potential of both peptides in the TBA2.1 model. Truly therapeutic, non-preventive treatment with D3 and D3D3 clearly slowed down the progression of the neurodegenerative TBA2.1 phenotype indicating therapeutic action of both peptides towards pEAβ(3-42) induced neurodegeneration.


## Visual abstract

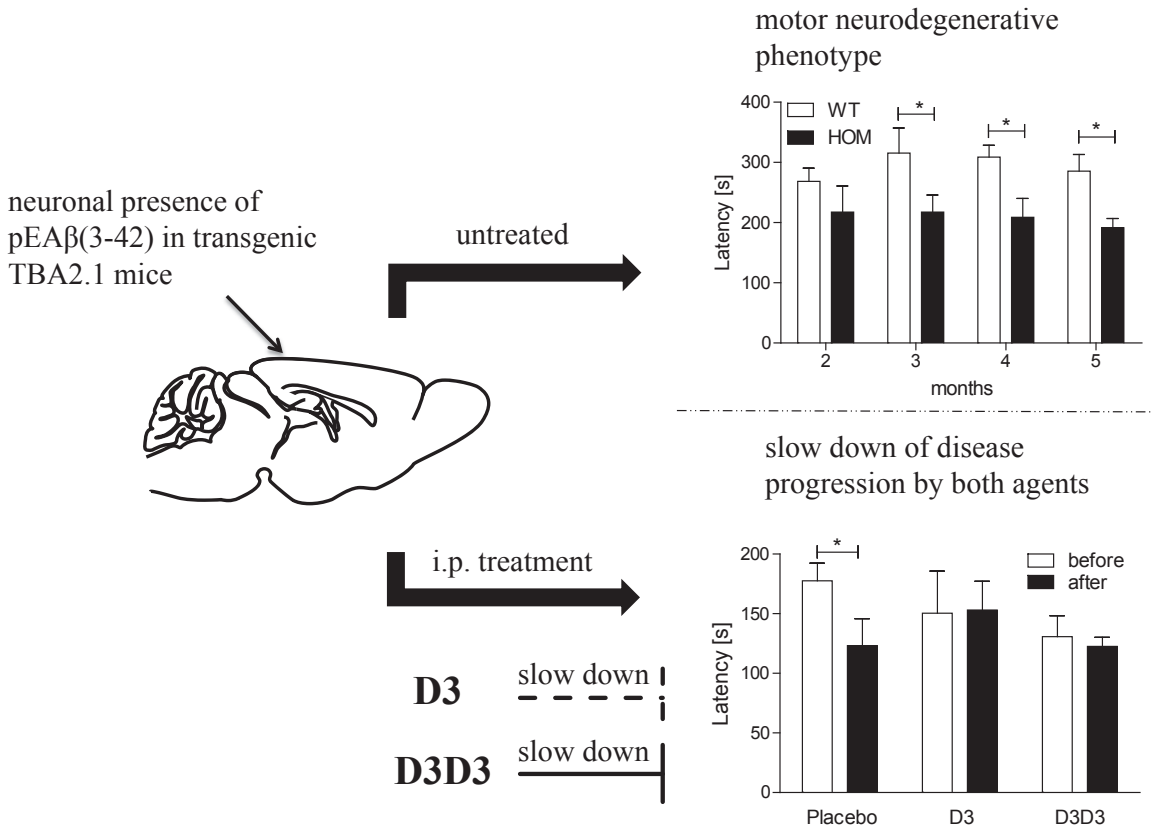

## Introduction

The number of patients suffering from Alzheimer's disease (AD) is expected to increase dramatically if no causal therapy becomes available[1]. Major hallmarks of AD are progressive neurodegeneration, and the deposition of tau protein containing neurofibrillary tangles and amyloid β peptide (Aβ) containing extracellular plaques[2]. Aβ is produced by the cleavage of the amyloid precursor protein (APP) through β- and γ-secretases. The resulting Aβ monomers assemble in a series of different Aβ aggregates, e.g. the Aβ oligomers, which are thought to play an important role in the development and progression of the disease. Currently, there is no causal treatment available to cure or slow down AD progression[3]. Previously, the potent D-enantiomeric peptide D3 has been identified by mirror image phage display[4] for binding to Aβ[5,6]. The two advantages of peptides consisting solely of D-enantiomeric amino acids are the lower immunogenic potential and the higher resistance to proteases[7-9]. It was shown that D3 reduces Aβ(1-42) mediated cell toxicity, prevents further aggregation of Aβ[10] and converts toxic oligomers into large, non-toxic amorphous aggregates *in vitro*[11]. In preceding *in vivo* studies, oral administration of D3 improves the spatial learning behaviour in the Morris water maze, reduces Aβ load and the inflammatory situation in transgenic APP/PS1 mice[10-12].

So far, most compounds that could prove suitable for AD therapy in humans were previously tested in animal models that did not show any neurodegenerative phenotype. Here, we used homozygous TBA2.1 mice for treatment studies exhibiting hippocampal neuron loss and a progressive motor neurodegenerative phenotype induced by pyroglutamate modified Aβ (pEAβ(3-42)). Transgenic TBA2.1 express Aβ starting at the N-terminal with glutamine followed by the residue of 4 to 42 of human Aβ, Aβ(Q3-42), in neuronal tissue. Aβ(Q3-42) is posttranslationally modified by endogenous glutaminyl cyclase to pEAβ(3-42)[13]. Owing to its very fast aggregation and formation of toxic oligomers, pEAβ(3-42) is thought to be involved in the initiation of the amyloid cascade.

Due to the promising properties of D3 and its derivative D3D3 against Aβ(1-42) , we here wanted to evaluate whether these compounds are also capable of binding and neutralising pEAβ(3-42) and are able to prevent or slow down pEAβ(3-42) induced neurodegeneration in the newly available mouse model TBA2.1

## Material and Methods

### Experimental design

To prove our hypothesis *in vitro*, we first determined the binding affinities of D3 and D3D3 to Aβ(1-42) and pEAβ(3-42) via SPR spectroscopy and tested their influence on the cytotoxicity of pEAβ(3-42) using MTT analysis. For these experiments, recombinant Aβ(1-42) was purchased from Isoloid (Germany) and recombinant pEAβ(3-42) was purified as described recently[14]. Both Aβ variants were dissolved in HFIP overnight prior usage to destroy any existing aggregates and lyophilised to remove HFIP.

After the positive evaluation of both compounds, it was planned to determine their properties in the TBA2.1 mouse models. Therefore, we initially characterised the phenotype of the transgenic, male mice. The phenotype assessment and the motor balance were determined longitudinally by testing ten wild type and eleven homozygous mice every four weeks starting at two months of age. For the treatment studies, four-month-old female mice were stratified into groups according to their SHIRPA score. Additionally, the mice were tested before and after treatment in the accelerating Rotarod. Due to a possible heterogeneity of the phenotype, we used only male mice for characterisation and female mice for the treatment studies. All experimenters were blind to genotype or treatment and all tests were carried out at the same time of day.

### SPR spectroscopy

SPR measurements were performed using a Biacore T200 instrument (GE Healthcare, Sweden) at 25 °C with 20 mM sodium phosphate, 50 mM sodium chloride, pH 7.4 as running buffer. For preparation of the flow cells, a CM5 sensor chip (GE Healthcare, Sweden) was activated with EDC / NHS (0.2 M / 0.05 M) and Aβ(1-42) (300 µg/ml) and pEAβ(3-42) (100 µg/ml), diluted in 10 mM sodium acetate pH 4.0, were immobilized to final levels of 8000 RU (pEAβ(3-42)) and 1000 RU (Aβ(1-42)). Ligand and reference flow cells were deactivated with 1 M ethanolamine-HCl. D3 and D3D3 affinity determinations were performed in single cycle kinetics at 30 µl/min flow rate. The analytes were diluted in running buffer to the final concentrations of 100, 33.33, 11.11, 3.70, 1.23 and 0.41 µM for D3 and 10, 3.33, 1.11, 0.37, 0.12 and 0.04 µM for D3D3. Association of the peptides was recorded for 120 s, followed by a dissociation of 240 s. After each cycle, a conditional regeneration step with 2 M guanidine hydrochloride was implemented. After measurement, the sensorgrams were double referenced using the reference flow cell and a buffer cycle. Evaluation was performed by plotting the respective response levels

against the applied peptide concentrations. The curves were fitted using Langmuir´s 1:1 binding model (Hill function with n = 1, OriginPro 8.5G, OriginLab, Northampton, USA).

**MTT-Assay**

Lyophilized pEAβ(3-42) was dissolved in 10 mM sodium phosphate buffer, pH 7.4 to a total concentration of 51 µM and the D-peptides D3 and D3D3 (molar ratio of 1:0, 1:0.1, 1:1, 1:10 for pEAβ(3-42):D3 and 1:0, 1:0.2, 1:1, 1:5 for pEAβ(3-42):D3D3) were added, respectively, and incubated at 37 °C for 5 days without shaking. The highest concentration of D-peptides, i.e. 510 µM for D3 and 255 µM for D3D3, were treated the same without co-incubation of pEAβ(3-42).

PC-12 cells (Leibniz-Institut DSMZ-Deutsche Sammlung von Mikroorganismen und Zellkulturen GmbH, Braunschweig, Germany) were cultured in Dulbecco's modified Eagle's medium (DMEM) (Sigma-Aldrich Chemie GmbH, Taufkirchen, Germany) supplemented with 10 % fetal bovine serum (FCS) (Sigma-Aldrich Chemie GmbH, Taufkirchen, Germany) and 5 % horse serum (HS) (Sigma-Aldrich Chemie GmbH, Taufkirchen, Germany) at 37 ˚C and 5 % $CO_2$. Cells were harvested and seeded onto 96-well plates (Gibco, Life Technologies, Carlsbad, California) at $1x10^3$ cells/well and incubated at 37 °C and 5 % $CO_2$ for 24 h. The cells were treated with 1 µM incubated pEAβ(3-42) and 1 µM pEAβ(3-42) co-incubated with D3 (in molar ratios of 1:0.1, 1:1 and 1:1) or D3D3 (in molar ratios of 1:0.2, 1:1 and 1:5), respectively, as well as 10 µM D3, 10 µM D3D3 and the buffer alone (10 mM sodium phosphate, pH 7.4). The buffer containing 0.125 % Triton X-100 (AppliChem, Darmstadt, Germany) was used as negativ control. All samples were added five-fold in a three-fold-determination. The treated cells were incubated at 37 °C and 5 % $CO_2$ for 24 h. MTT-assay was performed using the “Cell Proliferation Kit 1” (Roche, Mannheim, Germany) according to the manufacturer’s instructions. The 96-well plate was analysed using a MicroPlate Reader (PolarStar Optima, BMG Labtech, Offenburg, Deutschland) by measuring the absorbance at 570 nm and 660 nm and background corrected.

**Animals**

Experiments were conducted using homozygous TBA2.1 mice and wild type littermates as control mice. Transgenic TBA2.1 mice exhibited neuronal expression of Aβ(Q3-42) on a C57BL/6 x DBA1 background. Aβ(Q3-42) was modified by glutaminyl cyclase to pEAβ(3-42) within the secretory pathway in TBA2.1 mice[13]. All animal procedures were performed in accordance with the [Author University] animal care committee's regulations. The

animals were kept in a controlled environment on a 12/12-hours light/dark cycle (lights on from 7 a.m.-7 p.m.), with 54 % humidity and a temperature of 22 °C. Up to four mice per cage were housed with food and water available *ad libitum*. Only heterozygous TBA2.1 mice were used for breeding and homozygous mice were sacrificed at five months of age to prevent suffering due to the severity of the phenotype.

**Peptides**

The D-enantiomeric peptides D3 (rprtrlhthrnr, all amino acids are D-enantiomers) and D3D3 (rprtrlhthrnrrprtrlhthrnr, all amino acids are D-enantiomers) with ≥ 95 % purity were purchased C-terminally amidated from JPT Peptide Technologies GmbH, Germany.

**Phenotype assessment**

For phenotype assessment the primary screen of the SHIRPA test battery was used[15]. This includes the following subtests: abnormal body carriage, alertness, abnormal gait, startle response, loss of righting reflex, touch response, pinna reflex, cornea reflex, forelimb placing reflex, hanging behaviour and pain response. Additionally, the body weight was measured. For individual observation and analysis an arena of 42.5 cm x 18 cm x 26.5 cm (L x H x W) was used. The observations were scored from 0 (similar to wild type) to 3 (extremely abnormal from wild type). The sum of all subtests per animal was used for analysis.

**Accelerating Rotarod**

To analyse motor coordination and motor balance TBA2.1 mice were placed on a Rotarod apparatus (Ugo Basile Srl, Italy). Testing was performed according to the previously published protocol[13]. In the morning of the first day mice were trained to stay on the rod for at least 60 sec at a constant 10 rpm. The test sessions were performed in the afternoon as well as the following morning and afternoon. Before starting the test session the mice were habituated for 30 minutes in single cages. In one test session the mice had to run in three trials on the beam accelerating from 4 to 40 rpm. The escape latency of running was measured. Maximum time was 10 minutes. For analysis the mean value of all nine trials was used.

**Treatment with D3 and D3D3**

Wild type and homozygous four months old TBA2.1 mice were treated intraperitoneally for four weeks with a daily dosage of 5 mg per kg peptide in PBS (pH 7.4) or vehicle (PBS,

pH 7.4) using Alzet mini-osmotic pumps (model 1004, DURECT Corporation, USA). The body weight and conditions of the mice were controlled twice a week. A loss of 15 % body weight and severe conspicuities were defined as exclusion criteria. No animal was affected by these exclusion criteria.

**Tissue preparation**

The mice were sacrificed and the brain was harvested. The right hemisphere was used for immunohistochemical analysis and the left was used for enzyme-linked immunosorbent assay (ELISA) measurements. Both hemispheres were stored at -80 °C until further processing.

**Immunofluorescence**

Immunofluorescence analysis was assessed to determine the Aβ load. The right hemisphere was cryosectioned sagittally into 10 µm thin sections. Six sections per animal were fixed with 4 % paraformaldehyde and treated with 70 % formic acid for antigen retrieval. After washing and blocking with Mouse Ig Blocking Reagent (Vector Laboratories, Inc., USA) slides were treated with primary antibody (6E10, Covance Inc., USA) overnight. After washing the secondary antibody (mouse anti goat 488, Life Technologies GmbH, Germany) was incubated for two hours. Images were taken with a LMD6000 microscope (Leica Camera, Germany) with a DFC310 FX camera (Leica Camera, Germany). The stained area of Aβ (Aβ load) per brain hemisphere was quantified using ImageJ (National Institute of Health, USA).

**ELISA**

In brief, an Aβ ELISA (N3pE-42, IBL International GmbH, Germany) was used to quantify the pEAβ(3-42) levels. Therefore, left hemispheres were homogenised with Tris buffer (20 mM Tris pH 8.3, 250 mM NaCl, Roche EDTA free Complete Protease Inhibitor) using the PreCellys24 homogeniser (2x20 sec at 6,500 rpm, Bertin Technologies, France). After vortexing, a 15 min sonification and additional vortexing the homogenate was then centrifuged (175,000 g, 4 °C, 30 min). The resulting pellet was incubated and resuspended with diethanolamine (DEA) on ice and again centrifuged. The supernatant represents the DEA soluble fraction which was used for analysis. The pellet was incubated and resuspended with formic acid on ice. After the final centrifugation step the interphase was taken and neutralised with 1 M Tris pH 11.3 representing the insoluble Aβ fraction. DEA soluble and insoluble Aβ fractions were subjected to the ELISA to determine

the pEAβ(3-42) concentrations according to the manufacturer's protocol. The samples were normalised to their protein concentration. For the DEA-soluble fraction, the Micro BCA Protein Assay Kit (Pierce Biotechnology, USA) was used and for the insoluble fraction, the Bio-Rad Protein Assay (Bio-Rad, Germany).

**Statistical analysis**

To assess Gaussian distribution, all data was tested using the Shapiro-Wilk-Test or in a normality probability plot. In the case of normally distributed data the Repeated-Measures Parametric Analyses, Two- or One-Way-ANOVA with Bonferroni *post hoc* analysis or (paired) t-test were used, respectively. For the non-parametric analysis, the Friedman-test or Kruskal-Wallis test were used. Multiple Comparison Tests by Dunn was used for appropriate non-parametric *post hoc* analysis. All data was expressed as mean with SEM. Results are considered as significantly different to $p \leq 0.05$. All statistical analyses were performed using GraphPad PRISM 5 (GraphPad Software, Inc., USA) and InVivoStat 2.5 (InVivoStat by Simon Bate and Robin Clark, United Kingdom[16])

## Results

### In vitro binding activity of D3 and D3D3 for Aβ(1-42) and pEAβ(3-42)

In order to enhance the intensity of D3 in its binding properties, we chose a head-to-tail tandem version of it, D3D3, which was expected to interact stronger with the target Aβ due to increased avidity. Thus, we wanted to validate the increased therapeutic potential of D3D3 *in vitro* and we compared the binding affinities of both peptides towards Aβ(1-42) and pEAβ(3-42). Interestingly, a higher binding affinity of both D3 and D3D3 for pEAβ(3-42) could be observed as indicated by lower $K_D$ values (Fig. 1).

### Inhibition of pEAβ(3-42) mediated toxicity by D3 and D3D3

Encouraged by the binding experiments to pEAβ(3-42) we then compared the potential of D3 and D3D3 to neutralize the cytotoxicity of recombinant pEAβ(3-42) in PC-12 cells (Fig. 2). Already a concentration of 1 µM recombinant pEAβ(3-42) reduced the cell viability to more than 30 % (15 measurements per treatment in 3 tests; Kruskal-Wallis test, $p \leq 0.0001^{a}$, post hoc Buffer vs. 1 µM pEAβ(3-42)). Treatment with D3 had no significant influence on this effect (post hoc 1 µM pEAβ(3-42) vs. D3 at any concentration, not significant (ns)). But the addition of 0.05 µM or higher concentration of D3D3 to 1 µM pEAβ(3-42) was able to enhance the cell viability significantly (post hoc 1 µM pEAβ(3-42) vs. addition of 5 µM D3D3 $p \leq 0.001$, 1 µM pEAβ(3-42) vs. addition of 0.5 µM D3D3 $p \leq 0.01$, 1 µM pEAβ(3-42) vs. addition of 0.05 µM D3D3 $p \leq 0.05$). Thus, as expected, the increased avidity of D3D3 as compared to D3 led to superior efficacy of D3D3 *in vitro*[17].

### Characterisation of the motor phenotype of TBA2.1 mice

Based on the results of the SPR and cytotoxicity measurements, it was our aim to prove our hypothesis *in vivo* by treatment of homozygous TBA2.1 mice with D3 and D3D3 against Placebo. For that aim, we validated the behaviour of transgenic TBA2.1 mice referring to their motor performance and their overall phenotype. Afterwards, we treated homozygous mice intraperitoneally with D3 or its head-to-tail tandem derivative D3D3 for four weeks.

We characterised the motor neurodegenerative phenotype of this mouse model longitudinally using wild type (WT) and homozygous (HOM) TBA2.1 mice up to five months of age. Phenotype assessment revealed HOM TBA2.1 mice to have a significant phenotype already at two months of age (Fig. 3). Scored observations showed

a severely restricted sensorimotor function of HOM TBA2.1 mice, which among other deficits, resulted rapidly in a hunched, wobbly and rigid gait. At two months of age they achieved four times the WT score which increased further up to five months of age with ten times the WT score (number of animals: 10 WT and 11 HOM; Repeated-Measures-Parametric Analyses, genotype ($F_{(2,25)} = 59.01$, $p \leq 0.001^{b}$), interaction genotype with age ($F_{(6,75)} = 20.30$, $p \leq 0.001^{c}$), pairwise tests WT vs. HOM $p \leq 0.001$ at all ages, Fig. 3A). In addition, the weight gain from two to five months of age differed significantly between the groups (number of animals: 10 WT and 11 HOM; Repeated-Measures-Parametric Analyses, weight ($F_{(3,75)} = 136.19$, $p \leq 0.001^{d}$), interaction genotype with age ($F_{(6,75)} = 4.88$, $p \leq 0.001^{e}$)). More precisely, the body weight of WT TBA2.1 mice increased successively up to five months of age (pairwise tests $p \leq 0.01$), whereas a weight gain in HOM TBA2.1 mice was observed until four months of age (pairwise tests of two to four months old HOM $p \leq 0.05$ and pairwise test four to five months HOM ns) (Fig. 3C).

Analysis of the motor coordination performance of HOM TBA2.1 mice showed a decrease starting already at the age of three months and the deficit remained for all later time points (number of animals: 10 WT and 11 HOM; Repeated-Measures-Parametric Analyses, genotype ($F_{(2,25)} = 3.59$ and $p = 0.043^{f}$), pairwise WT vs. HOM at two months ns and at three to five months $p \leq 0.05$) (Fig. 3B). Overall, these results indicated the rapid progression of the phenotype in HOM TBA2.1 mice from two to five months of age.

**Treatment with D3 and D3D3**

Since the motor neurodegenerative phenotype of HOM TBA2.1 mice was highly prominent at five months of age we decided to start the treatment at four months of age over four weeks to test the truly therapeutic rather than preventive power of D3 and D3D3 in this neurodegenerative mouse model. When comparing the outcome of the motor performance before and after treatment of HOM TBA2.1 mice, the motor balance of placebo treated mice decreased (number of treated animals: placebo 7, D3 8, D3D3 8; Repeated-Measures-Parametric Analyses, before vs. after ($F_{(1,20)} = 2.76$, $p = 0.1122^{g}$, pairwise tests before vs. after treatment $p \leq 0.05$). In contrast, treatment with D3 or D3D3 was able to inhibit the worsening of the Rotarod performance of HOM TBA2.1 mice (Fig. 4A, pairwise tests before vs. after treatment ns). Additionally, WT TBA2.1 mice were treated with D3 or D3D3 to exclude unrelated effects of the peptides. No differences within these three groups could be observed in the Rotarod test indicating the specificity of D3 and D3D3 in HOM TBA2.1 mice (Fig. 4B, number of treated animals: placebo 6, D3 7, D3D3 7; Friedman test $p = 0.1667^{h}$, post hoc analysis ns). Analysis of the pEAβ(3-42)

concentration in the brain of HOM TBA2.1 mice showed an increase in DEA-soluble pEAβ(3-42) after the administration of D3D3 in contrast to the placebo and D3 treated groups (Fig. 4C, number of analysed samples: placebo 7, D3 8; D3D3 8; One-Way-ANOVA $p = 0.0055$[j], post hoc analysis placebo vs. D3 ns, placebo vs. D3D3 $p \leq 0.05$), while no significant differences were detectable between the insoluble fractions of the three groups (Fig. 4D; number of analysed samples: placebo 7, D3 8; D3D3 8; Kruskal-Wallis test $p = 0.9253$[j]; post hoc analysis ns). The latter was confirmed by the quantification of the stained area of Aβ in brain hemispheres (Fig. 5; 6 slices per animal, number of analysed animals: placebo 4, D3 4, D5 5; One-Way-ANOVA, $p = 0.6184$[k], post hoc placebo vs. D3 or D3D3 ns). Overall, both D3 and D3D3 were able to inhibit the deterioration of the motor neuronal degenerative phenotype in HOM TBA2.1, and D3D3 was able to induce a concentration shift towards the DEA-soluble pEAβ(3-42) pool.

## Discussion

It was previously shown that the D-enantiomeric peptide D3 is a promising compound for the treatment of AD. D3 was originally developed as an Aβ(1-42) monomer stabilizing ligand in order to destabilize and eliminate Aβ oligomers, which is the most toxic Aβ species and thought to be decisive for development and progression of Alzheimer's disease. *In vitro* tests with D3 showed an elimination of toxic Aβ(1-42) oligomers[11]. The potential of D3 was further proven by inhibition of Aβ(1-42) toxicity in cell culture, the improvement of spatial learning behaviour and the reduction of the Aβ plaque load in APP/PS1 double transgenic mice[10,11]. D3D3 was rationally designed to yield a multivalent version of D3 with increased affinity to Aβ. In the present study, we have for the first time validated the higher binding affinity of the derivative D3D3 to Aβ(1-42) in comparison to D3. Furthermore, we were able to show that both peptides, and especially D3D3, display increased binding affinity to pEAβ(3-42) compared to Aβ(1-42). We evaluated the inhibition potential of both compounds against pEAβ(3-42) mediated toxicity to neuronal cells. pEAβ(3-42) itself reduced the cell viability already at a very low concentration and minute amounts of D3D3 were able to prevent the neurotoxic effect of pEAβ(3-42), whereas D3 was not able to in the applied concentrations.

To validate the potential of D3 and D3D3 *in vivo*, we analysed the therapeutic efficacies in the new TBA2.1 mouse model which exhibits a motor neurodegenerative phenotype induced by the expression of human pEAβ(3-42).

From ages two to five months the progressing phenotype of the mice influencing posture, gait and motor function of the HOM TBA2.1 mice was severe. Additionally, these mice demonstrated impaired motor coordination starting from three months of age. In contrast, WT TBA2.1 mice did not show any abnormalities until five months of age. These results are in agreement with previously published observations[13] and confirm the motor neurodegenerative phenotype of HOM TBA2.1 mice.

Treatment studies with D3 or D3D3 in HOM TBA2.1 over four weeks with a daily dosage of 5 mg per kg body weight suggested both D3 and D3D3 as potential therapeutic compounds. Both agents were able to stabilise the motor coordination of the transgenic mice. Both compounds were able to reduce phenotype progression to non-significant levels during the treatment period, whereas placebo-treated mice showed significant progression of their phenotype. WT mice demonstrated no adverse effects caused by the treatment, which confirmed the specificities of D3 and D3D3 in HOM mice.

The development of a disease-modifying or even curative treatment is one the most desirable challenges of the 21st century, but most of the potential compounds that are chosen for clinical research failed. One critical aspect could be that most of the animal models used for preclinical research do not show neurodegeneration. Here, we used the TBA2.1 mouse model exhibiting a dramatically increasing motor neurodegenerative phenotype for our study. It was the aim to demonstrate the truly therapeutic potential of the fully D-enantiomeric peptides D3 and its derivative D3D3 in this neurodegenerative model. In the hereby presented work, we could prove the therapeutic power of D3 and demonstrate enhanced properties of D3D3 also *in vivo*, exactly as we had expected from the enhanced *in vitro* properties. In particular, for the first time, we show that the pEAβ(3-42) induced neurodegenerative phenotype of TBA2.1 mice can be arrested by a truly therapeutic treatment with D3 and D3D3 most probably by direct action against pEAβ(3-42).. Thus, D3 and D3D3 represent a potentially interesting class of compounds with a promising mechanism of action to cope with the challenge of treating Alzheimer's disease.

## References


1 Brookmeyer, R., Johnson, E., Ziegler-Graham, K. & Arrighi, H. M. Forecasting the global burden of Alzheimer's disease. *Alzheimer's & dementia : the journal of the Alzheimer's Association* **3**, 186-191, doi:10.1016/j.jalz.2007.04.381 (2007).

2 Parihar, M. S. & Hemnani, T. Alzheimer's disease pathogenesis and therapeutic interventions. *Journal of clinical neuroscience : official journal of the Neurosurgical Society of Australasia* **11**, 456-467, doi:10.1016/j.jocn.2003.12.007 (2004).

3 Bateman, R. Alzheimer's disease and other dementias: advances in 2014. *The Lancet. Neurology* **14**, 4-6, doi:10.1016/s1474-4422(14)70301-1 (2015).

4 Schumacher, T. N. *et al.* Identification of D-peptide ligands through mirror-image phage display. *Science (New York, N.Y.)* **271**, 1854-1857 (1996).

5 Wiesehan, K. & Willbold, D. Mirror-image phage display: aiming at the mirror. *Chembiochem : a European journal of chemical biology* **4**, 811-815, doi:10.1002/cbic.200300570 (2003).

6 Funke, S. A. & Willbold, D. Mirror image phage display--a method to generate D-peptide ligands for use in diagnostic or therapeutical applications. *Molecular bioSystems* **5**, 783-786, doi:10.1039/b904138a (2009).

7 Dintzis, H. M., Symer, D. E., Dintzis, R. Z., Zawadzke, L. E. & Berg, J. M. A comparison of the immunogenicity of a pair of enantiomeric proteins. *Proteins* **16**, 306-308, doi:10.1002/prot.340160309 (1993).

8 Funke, S. A. & Willbold, D. Peptides for therapy and diagnosis of Alzheimer's disease. *Current pharmaceutical design* **18**, 755-767 (2012).

9 Soto, C., Kindy, M. S., Baumann, M. & Frangione, B. Inhibition of Alzheimer's amyloidosis by peptides that prevent beta-sheet conformation. *Biochem Biophys Res Commun* **226**, 672-680, doi:10.1006/bbrc.1996.1413 (1996).

10 van Groen, T. *et al.* Reduction of Alzheimer's disease amyloid plaque load in transgenic mice by D3, A D-enantiomeric peptide identified by mirror image phage display. *ChemMedChem* **3**, 1848-1852, doi:10.1002/cmdc.200800273 (2008).

11 Funke, S. *et al.* Oral treatment with the d-enantiomeric peptide D3 improves the pathology and behavior of Alzheimer's Disease transgenic mice. *ACS chemical neuroscience* **1**, 639-648, doi:10.1021/cn100057j (2010).

12 van Groen, T., Kadish, I., Funke, S. A., Bartnik, D. & Willbold, D. Treatment with D3 removes amyloid deposits, reduces inflammation, and improves cognition in aged AbetaPP/PS1 double transgenic mice. *Journal of Alzheimer's disease : JAD* **34**, 609-620, doi:10.3233/JAD-121792 (2013).

13 Alexandru, A. *et al.* Selective hippocampal neurodegeneration in transgenic mice expressing small amounts of truncated Aβ is induced by pyroglutamate-Aβ formation. *The Journal of neuroscience : the official journal of the Society for Neuroscience* **31**, 12790-12801, doi:10.1523/jneurosci.1794-11.2011 (2011).

14 Dammers, C. *et al.* Purification and Characterization of Recombinant N-Terminally Pyroglutamate-Modified Amyloid-beta Variants and Structural Analysis by Solution NMR Spectroscopy. *PloS one* **10**, e0139710, doi:10.1371/journal.pone.0139710 (2015).

15 Rogers, D. C. *et al.* Behavioral and functional analysis of mouse phenotype: SHIRPA, a proposed protocol for comprehensive phenotype assessment. *Mammalian genome : official journal of the International Mammalian Genome Society* **8**, 711-713 (1997).

16 Clark, R. A., Shoaib, M., Hewitt, K. N., Stanford, S. C. & Bate, S. T. A comparison of InVivoStat with other statistical software packages for analysis of data generated from animal experiments. *Journal of psychopharmacology (Oxford, England)* **26**, 1136-1142, doi:10.1177/0269881111420313 (2012).

17 Brener, C. *et al.* QIAD assay for quantitating a compound's efficacy in elimination of toxic Aβ oligomers. *Sci. Rep. - Nature, in press* (2015).

## Figures

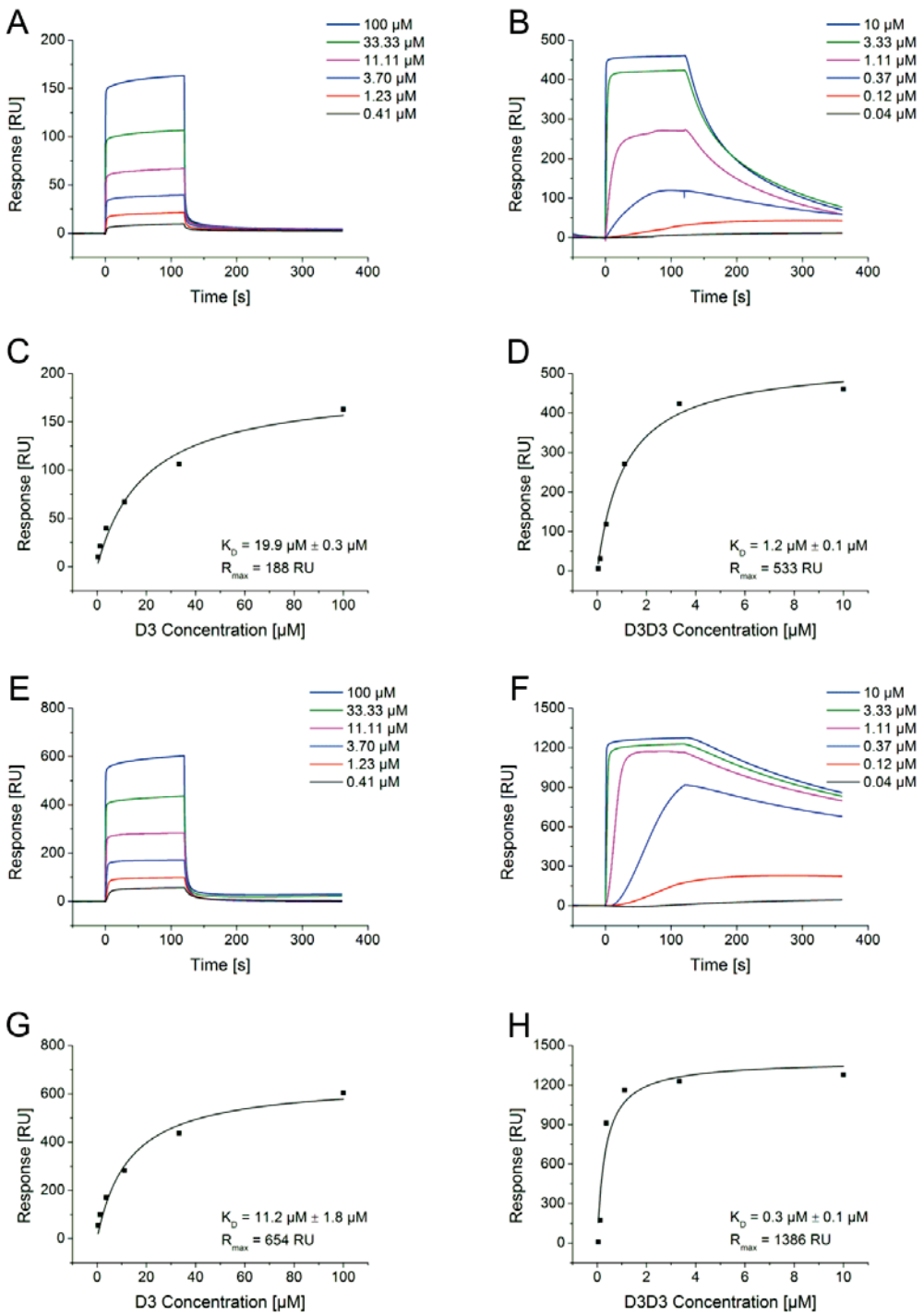


**Figure 1: Affinity determination of D3 and D3D3 to Aβ(1-42) and pEAβ(3-42) by SPR spectroscopy.** Sensorgrams of D3 (A) and D3D3 (B) interaction with Aβ(1-42). The data were fitted by plotting the response levels (RU) against applied peptide concentrations using a steady-state 1:1 binding model (C, D). Sensorgrams of D3 (E) and D3D3 (F) interaction with pEAβ(1-42) and corresponding fit results (G, H). KD values are represented as mean with SD of two independent measurements. Sensorgrams and fit results are representative shown for both measurements.

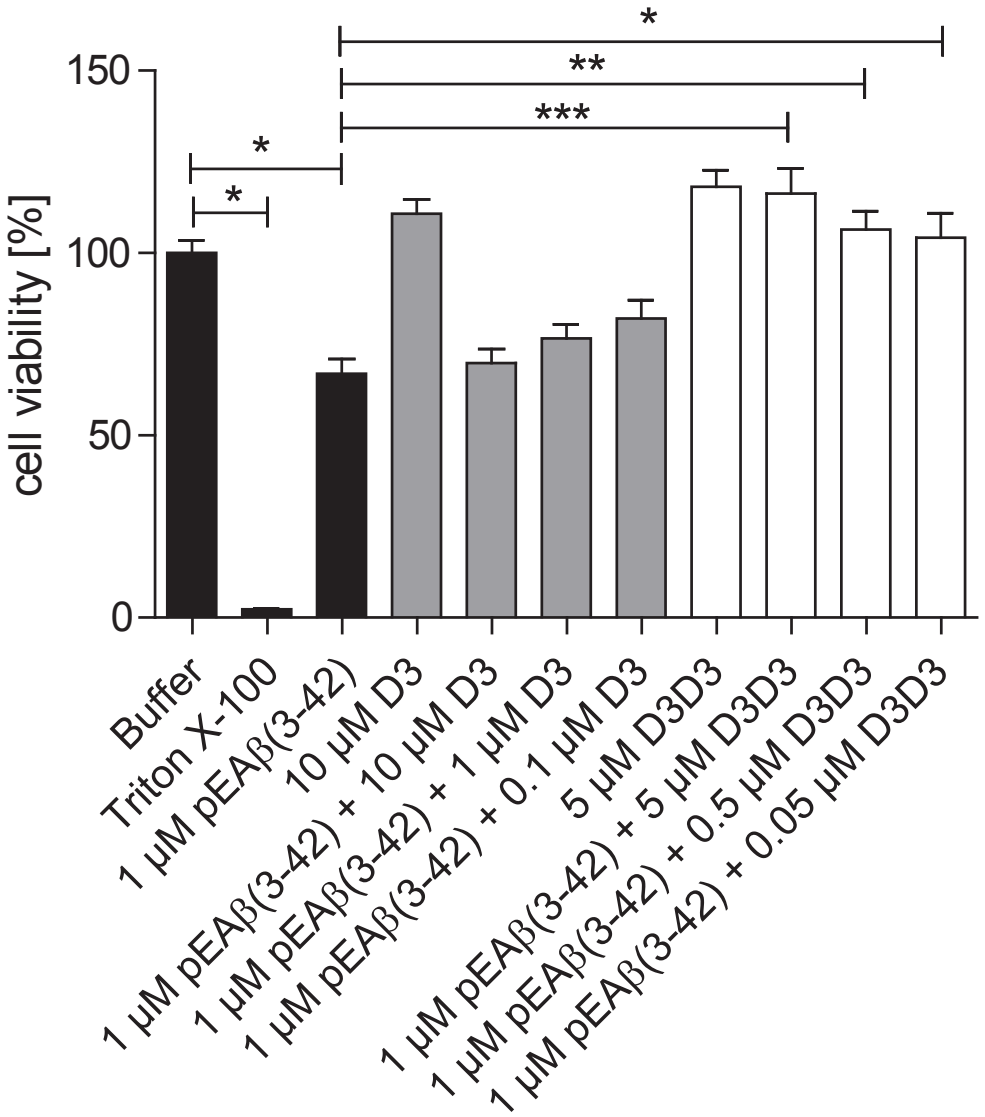


**Figure 2: MTT analysis of the interactions between D3 and D3D3 with pEAβ(3-42).** MTT analysis revealed a reduced cell viability by addition of 1µM pEAβ(3-42), which could be prevented by treatment with D3D3. Data is presented as mean with SEM; *$p \leq 0.05$, **$p \leq 0.01$ and ***$p \leq 0.001$.

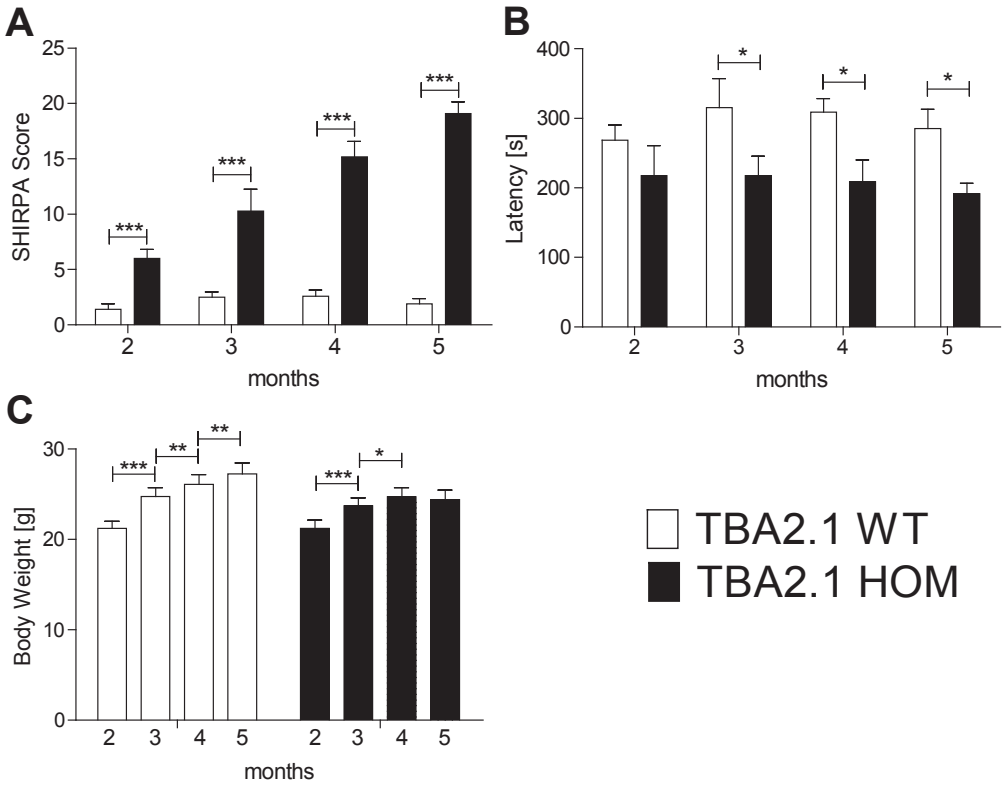


**Figure 3: Longitudinal determination of the sensorimotor phenotype of wild type (WT) and homozygous (HOM) TBA2.1 mice at 2, 3, 4 and 5 months of age.** Assessment using the SHIRPA test battery revealed a continuously increasing phenotype of HOM TBA2.1 mice (A). Motor performance of HOM on the Rotarod is reduced from 3 to 5 months of age compared to WT (B). Body weight of WT mice increased from 2 to 5 months of age, but weight gain of HOM was reduced from 4 to 5 months of age (C). Data is presented as mean with SEM; *$p \leq 0.05$, **$p \leq 0.01$ and ***$p \leq 0.001$.

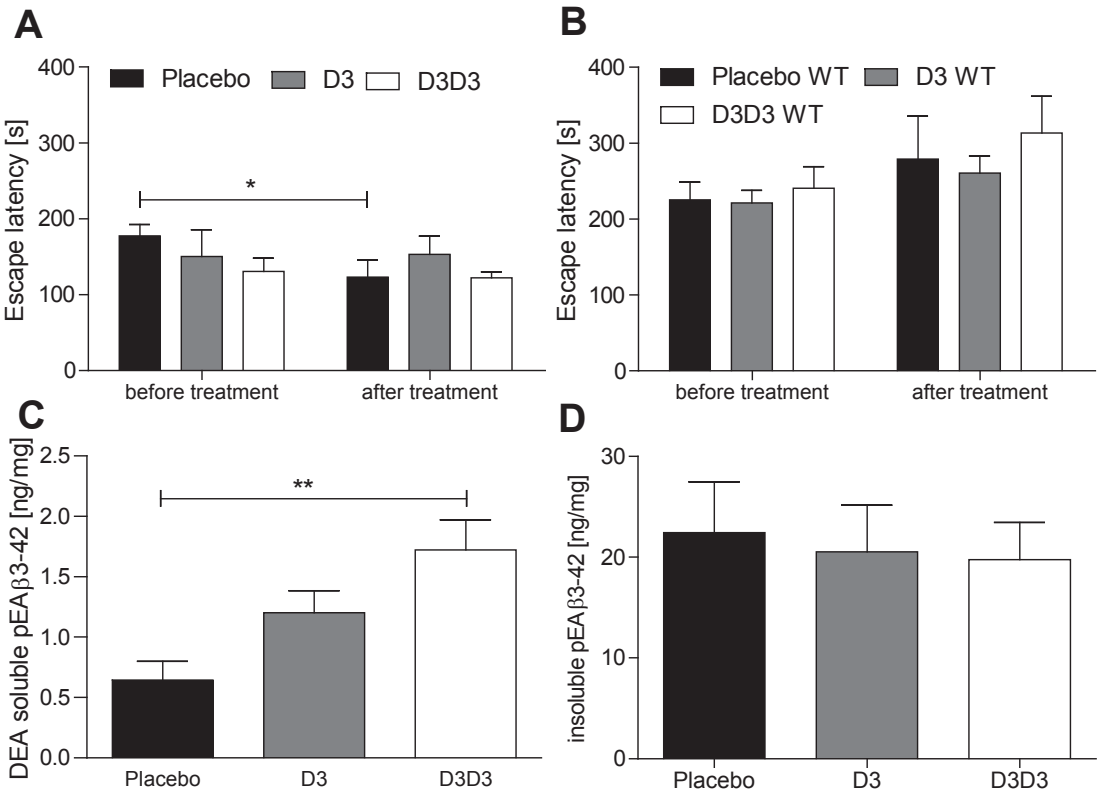


**Figure 4: Treatment of TBA2.1 mice with the D-enantiomeric peptides D3 and D3D3.** Homozygous (HOM) and wild type (WT) TBA2.1 mice were treated intraperitoneally over 4 weeks with vehicle (placebo) or with 5 mg per kg body weight D3 or D3D3 per day. Rotarod analysis of HOM demonstrates a worsening of the motor phenotype in placebo treated mice whereas D3 and D3D3 administration inhibited this process (A). Performance on the Rotarod of wild type mice treated with D3 and D3D3 did not show any significant differences (B). Biochemical quantification of DEA-soluble pEAβ(3-42) in the brain of HOM revealed a significantly higher concentration in D3D3 treated mice compared to placebo treated mice (C). Quantification of the Aβ load on brain sections from HOM animals stained by immunofluorescence is unchanged between treatment groups (D). Data is presented as mean with SEM; *$p \leq 0.05$, **$p \leq 0.01$ and ***$p \leq 0.001$.

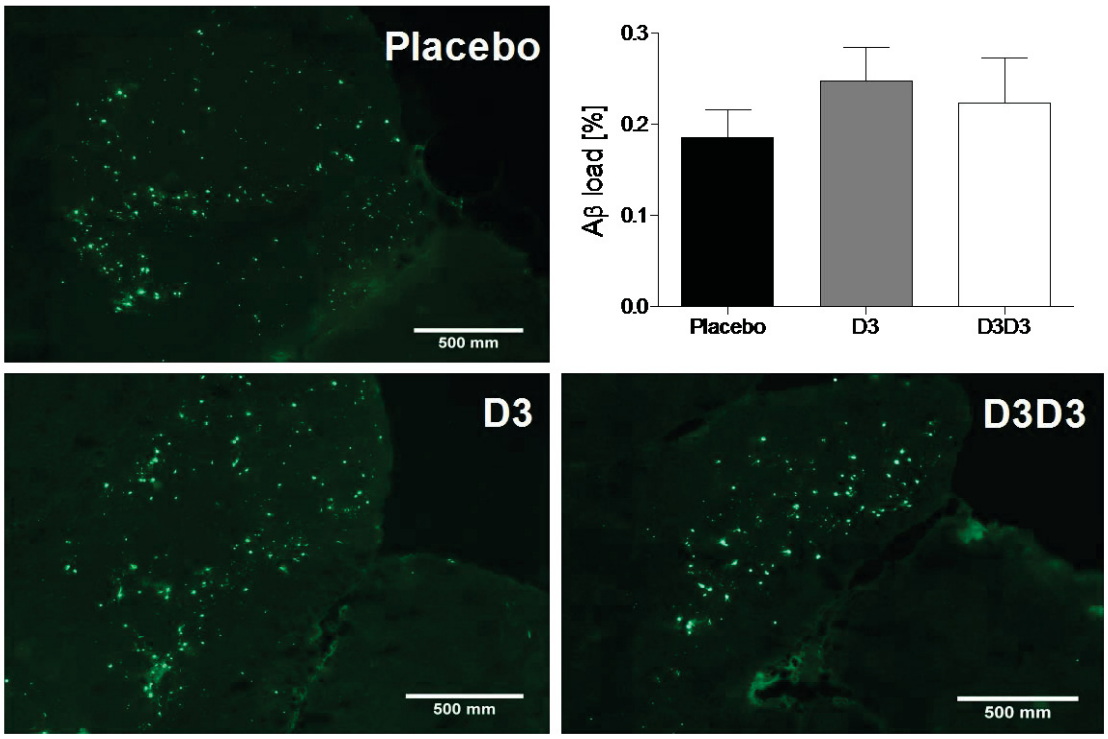


**Figure 5: Immunfluorescence of homozygous mice treated with D3 or D3D3.** After treatment hemispheres of D3 or D3D3 and Placebo treated homozygous TBA2.1 mice were harvested. Brain slices of each group were stained against Aβ (antibody 6E10) (A). Quantification of the percental Aβ load and particle count revealed no significant differences between these groups. Data is presented as mean with SEM (B, C).

## Tables

Table 1: Statistics

| | Data structure | Type of test | Power |
|---|---|---|---|
| a | Non-normal distribution | Kruskal-Wallis test | $p \leq 0.0001$ |
| b | Non-normal distribution | Kruskal-Wallis test | $p \leq 0.001$ |
| c | Normal distribution | Repeated-Measures-Parametric Analyses | $p \leq 0.001$ |
| d | Normal distribution | Repeated-Measures-Parametric Analyses | $p \leq 0.001$ |
| e | Normal distribution | Repeated-Measures-Parametric Analyses | $p \leq 0.001$ |
| f | Normal distribution | Repeated-Measures-Parametric Analyses | $p = 0.043$ |
| g | Normal distribution | Repeated-Measures-Parametric Analyses | $p = 0.1122$ |
| h | Non-Normal distribution | Friedman test | $p = 0.1667$ |
| i | Normal distribution | One-Way-ANOVA | $p = 0.0055$ |
| j | Non-normal distribution | Kruskal-Wallis test | $p = 0.9253$ |
| k | Normal distribution | One-Way-ANOVA | $p = 0.6184$ |

# 4 Discussion and Outlook

Alzheimer's disease (AD) is a neurodegenerative disease characterized by a progressive decline of cognitive functions and has become the main cause for dementia in the elderly (Alzheimer's Association 2015). The number of individuals suffering from AD is expected to increase up to 100 Million by the year 2050 (Ferri et al., 2005). Pathological hallmarks of AD are intracellular neurofibrillary tangles consisting of hyperphosphorylated tau and extracellular plaques containing aggregated amyloid β (Aβ) (Alzheimer's Association 2015). Aβ is generated by the cleavage of the amyloid precursor protein leading to various heterogeneous Aβ isoforms (De Strooper *et al.* 2010). A significant amount of N-terminal modified Aβ variants is deposited in the brains of AD patients whereby pyroglutamate-modified Aβ (pEAβ) was described to be the major isoform (Jawhar *et al.* 2011, Perez-Garmendia *et al.* 2013). pEAβ is present up to equivalently amounts compared to full-length Aβ and plays a central role in triggering neurodegeneration and lethal neurological deficits (Wirths *et al.* 2009). Thus, N-terminally modified Aβ isoforms represent highly desirable therapeutic targets and became more important in the recent years (Venkataramani *et al.* 2012, Perez-Garmendia *et al.* 2013). Although the full-length Aβ is well characterized, knowledge of the structural difference of pEAβ is limited.

In the present study, a method for reproducible production of pEAβ for biophysical characterization was established. To obtain first insights into its secondary structure, pEAβ was analyzed by circular dichroism (CD) spectroscopy. Aggregation kinetics were monitored by Thioflavin-T (ThT) assays and transmission electron microscopy (TEM) was used to visualize matured fibrils. Nuclear magnetic resonance (NMR) spectroscopy is the method of choice when it comes to structural studies. While solid state NMR spectroscopy focusses on large aggregated fibrils, liquid NMR spectroscopy is useful to investigate monomeric peptides and to detect transient species (Kumar *et al.* 2014). Structural analysis of pEAβ was performed in aqueous TFE solution and the data was compared to the non-modified Aβ.

The D-peptide D3 was previously selected to specifically bind Aβ(1-42). It was shown to inhibit the formation of toxic aggregates *in vitro* as well as *in vivo* and to improve pathology and behavior in mice (van Groen *et al.* 2013). The effect of D3 targeting pEAβ was analyzed *in vitro* (using recombinant pEAβ(3-42)) and *in vivo* in pEAβ expressing transgenic mice models by oral administration and the analysis of behavioral phenotyping tests.

## 4.1 Production and characterization of recombinant pyroglutamate amyloid-β peptides

The protocol for the expression and purification of N-terminal truncated pEAβ is based on a previous publication by the Glockshuber group describing the production of recombinant Aβ(1-42) and Aβ(1-40) (Finder *et al.* 2010). The construct contains a $His_6$-tag, a solubilizing fusion partner $(NANP)_{19}$ (Luhrs *et al.* 2005) and a modified TEV protease recognition and cleavage site following the Aβ sequence 3-40/42.

As described by Demuth and coworkers, both enzymatic and non-enzymatic pE formation with an N-terminal Q instead of E is much faster (Schilling *et al.* 2008). Therefore, residue E3 was replaced by Q in order to improve the non-enzymatic reaction to pE. The preceding protease recognition site was modified from typical ENLYFQ↓G/S to ENLYFQ↓Q with the arrow indicating the cleavage site. Changing the C-terminal protease recognition site to Q remains in still approximately 90 % cleavage efficiency (Kapust *et al.* 2002). Thus, Q becomes the first aa of the cleavage product and could be directly used for time and cost efficient non-enzymatically pE conversion. The intra-molecular lactam ring formation was performed under acidic and increased temperature conditions by the release of ammonia (Chelius *et al.* 2006). The pE-modified peptides can easily be separated from non-converted remaining peptide since they are more hydrophobic due to the loss the positively charged hydrophilic amino group. The pEAβ peptides were verified by mass spectrometry. Final yields of pEAβ(3-40) and pEAβ(3-42) were up to 15 mg/l culture broth.

The quality of the recombinant peptides was examined by monitoring their aggregation kinetics. Both recombinant pEAβ peptides showed typical properties of a sigmoidal Aβ aggregation including a distinct lag phase following an elongation phase and, finally, a stationary phase where fibrillation is maximized. The increased C-terminal length in pEAβ(3-42) but also, in comparison to Aβ(1-40/42), N-terminal deletions enhance aggregation (Pike *et al.* 1995, Schilling *et al.* 2006). In accordance, our data showed that pEAβ(3-42) aggregates much faster than the C-terminal shortened variant pEAβ(3-40). Heteronuclear multidimensional NMR spectroscopy in solution state was performed to sequence specifically assign resonances of pEAβ(3-40) and pEAβ(3-42). The $^{1}H,^{15}N$-HSQC NMR spectra differ slightly from that of Aβ(1-40) and Aβ(1-42) under identical conditions published previously (Hou *et al.* 2004, Rezaei-Ghaleh *et al.* 2011, Weber *et al.* 2014). Signals of the N-terminal aa pE3 and F4 are visible but R5 and H6 are missing. An explanation could be the histidine-water proton exchange of H6 at neutral pH that could

also affect the neighboring aa R5. In comparison to non-modified Aβ, pE formation alters the N-terminal chemical shifts through residue S8 with decreasing influence downstream to the C-terminus.

## 4.2 Aggregation of pyroglutamate amyloid-β peptides in aqueous trifluoroethanol

TFE as a co-solvent lowers solvent polarity and thus induces intramolecular hydrogen bonding (Kumar *et al.* 2009). It is therefore used to stabilize the secondary structure in proteins and peptides and to increase solubility. Aβ builds stable α-helical structures in aqueous TFE solution – in sufficient concentrations (Sticht *et al.* 1995, Sun *et al.* 2012). There is evidence, that lowering the TFE concentration decreases the stabilization of helical structures and thus favors β-sheets resulting in fibrillation of Aβ.

Teplow and co-workers were the first who have analyzed the kinetics of soluble Aβ in TFE from monomeric α-helices to β-sheets (Fezoui *et al.* 2002). A TFE-induced three-state transition from α-helical monomers to β-sheets for Aβ(1-40) in TFE, visualized by CD spectroscopy, was then described (Chen *et al.* 2006). Our CD data indicate that this transition is also observable for pEAβ. Interestingly, conversion from α-helices to β-strands starts at higher TFE concentrations for pEAβ than for non-modified Aβ indicating that it is less stable than the non-modified Aβ. This effect was observed by comparing pEAβ(3-40) with Aβ(1-40) as well as pEAβ(3-42) and Aβ(1-42), respectively under the same conditions, using CD spectroscopy, ThT assays and TEM. TFE-induced aggregates of pEAβ are β-sheet rich and thus represent a type of amyloid fibrils. In contrast, TFE-induced aggregates of full-length Aβ have an amorphous non-fibrillar ultrastructure. Previously published data suggested a higher β-sheet stabilization of pEAβ due to the altered N-terminus (Schilling *et al.* 2006, Jawhar *et al.* 2011). pEAβ is more prone to aggregation not only in aqueous solutions but also in the presence of an α-helix stabilizing co-solvent.

The modulation of amyloid formation by a TFE-induced pathway was also described for other unstructured peptides. TFE induces the formation of aggregates significantly for Islet Amyloid Polypeptide (Konno *et al.* 2007), α-synuclein aggregates by a TFE-induced helical intermediate (Anderson *et al.* 2010) and conalbumin build amyloid aggregates at low TFE concentrations although it is stabilized at high concentrations of the co-solvent (Khan *et al.* 2014).

## 4.3 Structural analysis of pyroglutamate amyloid-β by NMR spectroscopy

Although pEAβ shows β-sheets and large fibrils under conditions where non-modified Aβ shows α-helices and non-fibrillar aggregation as indicated by CD, ThT and TEM, NMR spectroscopy monitored helical monomers.

Structural analysis of pEAβ(3-42) and Aβ(1-42) under identical conditions indicated α-helical monomers for both peptides. Secondary structure prediction of pEAβ(3-42) in 40 % TFE is shown in figure 6. The propensity for α-helices is plotted against the aa sequence. Two helical regions from Y10 to D23 and A30 to V36 which are connected by a linker were predicted using different tools (Schwarzinger *et al.* 2001, Zhang *et al.* 2003, Marsh *et al.* 2006, Shen *et al.* 2009). This is in accordance to the results comparing pEAβ(3-40) with Aβ(1-40) obtained earlier by our group (Sun *et al.* 2012). Decreased TFE concentration did not change the $^{1}H_{N}$, $^{15}N$, $^{13}C'$ and $^{13}C\alpha$ chemical shifts of pEAβ(3-42) towards β-sheet rich structures. However, the signal intensities are drastically decreased indicating a loss of monomers. This effect was consistent for both peptides, pEAβ(3-42) and pEAβ(3-40), and led to the conclusion that the β-sheet rich structures detected via CD spectroscopy, THT and TEM are not observable by solution state NMR spectroscopy due to exchange processes and the formation of large aggregates.

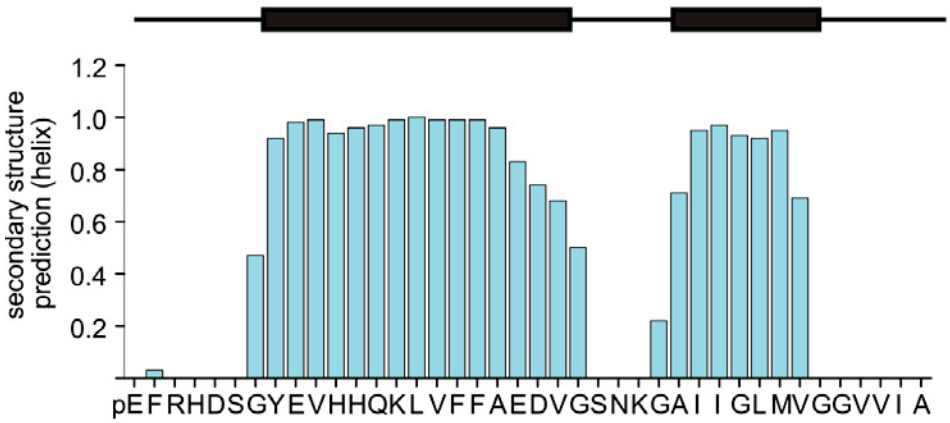


**Figure 6 Secondary structure prediction of pEAβ(3-42).** Structural characterization of pEAβ(3-42) in aqueous TFE solution (40 % TFE in 50 mM $KH_3PO_4$ pH 2.8) at 20 °C from NMR chemical shift data prediction by TALOS+ (Shen *et al.* 2009). The percentage of α-helical structures is plotted against the aa sequence. Helices are indicated from Y10 to D23 and A30 to V36 with a flexible linker in between.

Comparing $^{1}H,^{15}N$-HSQC spectra of monomeric pEAβ(3-42) with Aβ(1-42) as well as pEAβ(3-40) with Aβ(1-40) shows that the pE formation has a significant effect on the N-terminal chemical shifts towards H14, which is in fact almost 30 %. Mischu and coworkers performed a study regarding the effect of pE formation on unstructured model peptides starting with E1 (Mischo *et al.* 2012). Formation of N-terminal pE lead to altered chemical shifts of only the following two neighboring residues without affecting adjacent aa. In contrast, formation to pEAβ changes the following 12 aa resulting in an altered conformational state of the unstructured N-terminus and in a decreased stability compared to the non-modified isoform. Aβ is almost twice as stable as pEAβ, as shown by NMR spectroscopy.

## 4.4 Trifluoroethanol stabilizes an α-helical intermediate

There is evidence that under identical conditions pEAβ but not non-modified Aβ undergoes amyloid fibril formation based on an α-helical intermediate in the presence of TFE. Helical intermediates have been reported to prone fibrillation of a number of amyloidogenic peptides (Abedini *et al.* 2009). The phenomenon of TFE induced aggregation was also observed by Anderson and coworker*s* by showing that α-synuclein fibrillation is strongly correlated with the TFE-induced formation of a monomeric, partly helical intermediate. This intermediate exists in equilibrium with the natively disordered state at low TFE concentrations and with strong α-helical conformation at high TFE concentrations (Anderson *et al.* 2010). Abedini and Raleigh hypothesized that transiently populated helical structures may associate and thus lead to a high local concentration of an aggregation prone sequence, which could promote intermolecular β-sheet formation (Abedini *et al.* 2009, Abedini *et al.* 2009). The first evidence of helical intermediates playing a central role in Aβ aggregation process as a precursor of fibril formation was hypothesized by Teplow and collaborators. They observed a transient increase in helicity immediately before the appearance of β-sheet structures (Fezoui *et al.* 2000, Kirkitadze *et al.* 2001). The transient helices, which bundle together, could be stabilized by intermolecular peptide-peptide interactions and this effect is increased in the presence of TFE.

The conversion of NMR visible helical assemblies of pEAβ to β-sheet rich structures could end in amyloid fibril formation as the transient α-helices are not stabilized. Since the secondary structure prediction for Aβ is nearly identical with that for pEAβ, the unstructured N-terminus towards V12 seems to be responsible for the preferred β-sheet formation. Thus, accumulation of this region could be the high local concentration of an

aggregation prone sequence, which promotes β-sheet formation as described by Abedini and Raleigh (Abedini *et al.* 2009, Abedini *et al.* 2009).

The pathway of pEAβ fibril formation in the presence of TFE could be consisting of four steps: (1) the conversion of unstructured pEAβ(3-42) monomers to transient α-helices; (2) the formation of α-helical assemblies resulting in a high local concentration of an aggregation prone sequence; (3) conversion of these sequence to β-strands and (4) the formation of amyloid fibrils (figure 7). Self-assembly due to a transient α-helical intermediate was demonstrated previously for model peptides (Mihara *et al.* 1997, Fezoui *et al.* 2000) as well as for IAPP (Liu *et al.* 2010), α-synuclein (Anderson *et al.* 2010) and also *in vivo* for silk (van Beek *et al.* 2000).

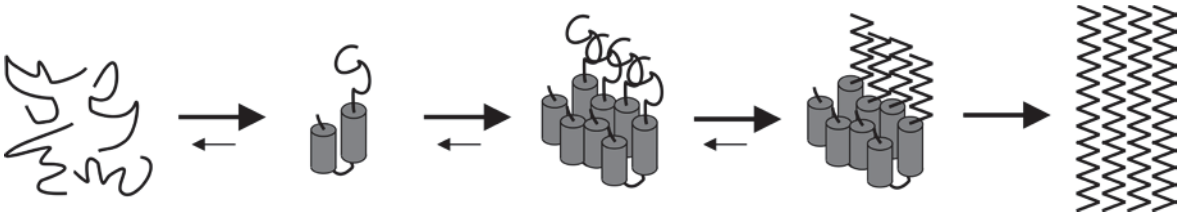

**Figure 7 Schematic diagram of the transition of an α-helical intermediate to β-sheets.** α-helices are depicted as cylinders and β-strands as zigzagged lines. Unstructured monomers build TFE-induced α-helices. These helices bundle together and generate a high local concentration of an aggregation prone sequence which is likely to build β-strands. The formation of β-strands disrupts the α-helices and leads to the formation of β-sheet-rich assemblies. Figure modified according to (Abedini *et al.* 2009).

The formation of Aβ oligomers is kinetically favored, since they are unstable those oligomers precipitate at high concentrations and form thermodynamically preferred large aggregates and amyloid fibrils (Garai *et al.* 2008). Nag and coworkers have shown, that Aβ is in an monomer-oligomer equilibrium in concentrations above 3 μM (Nag *et al.* 2011). Interestingly, this concentration is much higher than the estimated concentration in the CSF of AD patients (Bjerke *et al.* 2010, De Meyer *et al.* 2010). This demonstrated that nucleation has a high energy level to pass and that a significant proportion of Aβ *in vivo* might be monomeric.

Based on the aa sequence, the C-terminal domain of Aβ is likely to adopt β-strand conformation and the N-terminal domain is in equilibrium between an α-helix and β-strand (Serpell 2000). pEAβ might adopt largely helical secondary structure elements *in vivo,* since it is mainly composed of the APP transmembrane region. Then, transition from α-helices to β-sheets precedes amyloid fibrillation (Fezoui *et al.* 2000). If the peptide instead is mainly unstructured, as it is *in vitro*, then the formation of a partially folded intermediate

is needed to promote amyloid formation (Fezoui *et al.* 2000). However, TFE can be used as co-solvent to stabilize this helical conformation as shown in the present study.

Nonetheless, stable helical intermediates do not necessarily have to induce aggregation they can also decrease or actually inhibit amyloid formation (Abedini *et al.* 2009, Abedini *et al.* 2009). This effect seems to be present for non-pyroglutamate modified Aβ peptides as there is no evidence for amyloidogenic aggregation under exactly the same conditions where pEAβ peptides undergo fibrillation. Inhibition of pEAβ fibril formation is also present at higher TFE concentrations and might be due to the destabilization of hydrophobic interactions (Buck 1998).

## 4.5 Inhibition of pyroglutamate amyloid-β(3-42) induced neuropathology

The therapeutic potential of the Aβ-targeting D-enantiomeric peptide D3 (Wiesehan *et al.* 2008, van Groen *et al.* 2013) and its head-to-tail derivative D3D3 (ref qiad) were further tested in the pEAβ(3-42) expressing mouse model TBA2.1 inducing a motor degenerative phenotype. Homozygous mice are marked by a rapid decline of sensorimotor abilities. Treatment with D3 and its tandem derivative D3D3 could successfully decrease pEAβ(3-42)-related progression of the neurodegenerative phenotype in transgenic mice without showing side effects. D3D3 showed an increase in DEA-soluble pEAβ(3-42) which might be a result of the conversion of fibrils to amorphous aggregates. This phenomenon was previously described for D3 and Aβ(1-42) oligomers leading to an increase in Aβ plaque load in transgenic mice (Funke *et al.* 2010, van Groen *et al.* 2013). D3 did not show an effect on DEA-soluble pEAβ(3-42) leading to the conclusion that D3D3 demonstrated higher *in vivo* efficacy to pEAβ(3-42) than D3 which might be due to the higher binding-affinity as characterized before *in vitro*. Nonetheless, both peptides were shown to significantly inhibit pEAβ(3-42) induced degenerative phenotype by increasing motor coordination of transgenic mice while treatment. Thus, D3 and D3D3 are therapeutic options for the treatment of AD.

## 4.6 General Conclusion

Within this study, it was possible to establish a reproducible method for recombinant production of pE-modified Aβ peptides for biophysical and biochemical studies. pEAβ peptides have a higher aggregation propensity and β-sheet stabilization in aqueous TFE solution than the non-modified Aβ as monitored by ThT assay and CD spectroscopy. TEM images of pEAβ in TFE showed large fibrils which accumulate into plaques. High resolution NMR spectroscopy in solution state was performed for complete backbone and partially sidechain chemical shift assignment of pEAβ(3-42). Analysis of secondary structure in the presence of the co-solvent TFE, which is known to favor intra-molecular hydrogen bonding, indicated that Aβ(1-42) as well as pEAβ(3-42) form dominantly α-helical structures in two regions connected by a flexible and disordered linker. However, the pyroglutamate formation affects 30 % of the overall aa and some peak intensities of pEAβ(3-42) are decreased compared to its non-modified isoform. This result suggests that the N-terminal modification to pEAβ has a significant effect on secondary structure elements. However, the observed α-helical monomers are unstable and accumulate into fibrils. pEAβ(3-42) builds TFE-induced transient α-helices as a precursor to β-sheet formation and fibrillation. The difference of TFE-induced aggregation between pEAβ and Aβ raises evidence to the conclusion that physiological amyloid formation in AD brains is also distinguished.

Nonetheless, despite structural differences between pE-modified and non-modified Aβ, *in vivo* studies in transgenic mice interfere with pEAβ pathology. Treatment with the Aβ-targeting D-enantiomeric peptide D3 and its tandem derivative D3D3 successfully inhibit pEAβ(3-42)-driven progression of the neurodegenerative phenotype and are therefore promising candidates for treatment of AD.

## References


Abedini, A. and D. P. Raleigh (2009). "A critical assessment of the role of helical intermediates in amyloid formation by natively unfolded proteins and polypeptides." Protein Eng Des Sel **22**(8): 453-459.

Abedini, A. and D. P. Raleigh (2009). "A role for helical intermediates in amyloid formation by natively unfolded polypeptides?" Phys Biol **6**(1): 015005.

Alexandru, A., W. Jagla, S. Graubner, A. Becker, C. Bauscher, S. Kohlmann, R. Sedlmeier, K. A. Raber, H. Cynis, R. Ronicke, K. G. Reymann, E. Petrasch-Parwez, M. Hartlage-Rubsamen, A. Waniek, S. Rossner, S. Schilling, A. P. Osmand, H. U. Demuth and S. von Horsten (2011). "Selective hippocampal neurodegeneration in transgenic mice expressing small amounts of truncated Abeta is induced by pyroglutamate-Abeta formation." J Neurosci **31**(36): 12790-12801.

Alzheimer's Association (2015). 2015 Alzheimer's Disease Facts and Figures.

Alzheimer's Disease International (2013). World Alzheimer Report 2013 - Journey of Caring: An analysis of long-termn care for dementia.

Alzheimer's Disease International (2014). "World Alzheimer Report 2014 - Dementia and Risk Reduction: An analysis of protective and modifiable factors."

Alzheimer's Disease International. (2015). "Dementia statistics." Retrieved 27 Jul, 2015, from http://www.alz.co.uk/research/statistics.

Alzheimer, A. (1907). "Uber eine eigenartige Erkrankung der Hirnrinde." Allgemeine Zeitschrift Psychiatrie **64**: 146-148.

Anand, R., K. D. Gill and A. A. Mahdi (2014). "Therapeutics of Alzheimer's disease: Past, present and future." Neuropharmacology **76 Pt A**: 27-50.

Anand, R., A. Kaushal, W. Y. Wani and K. D. Gill (2012). "Road to Alzheimer's disease: the pathomechanism underlying." Pathobiology **79**(2): 55-71.

Anderson, V. L., T. F. Ramlall, C. C. Rospigliosi, W. W. Webb and D. Eliezer (2010). "Identification of a helical intermediate in trifluoroethanol-induced alpha-synuclein aggregation." Proc Natl Acad Sci U S A **107**(44): 18850-18855.

Avila, J., J. J. Lucas, M. Perez and F. Hernandez (2004). "Role of tau protein in both physiological and pathological conditions." Physiol Rev **84**(2): 361-384.

Bayer, T. A. and O. Wirths (2011). "Intraneuronal Abeta as a trigger for neuron loss: can this be translated into human pathology?" Biochem Soc Trans **39**(4): 857-861.

Beach, T. G., S. E. Monsell, L. E. Phillips and W. Kukull (2012). "Accuracy of the clinical diagnosis of Alzheimer disease at National Institute on Aging Alzheimer Disease Centers, 2005-2010." J Neuropathol Exp Neurol **71**(4): 266-273.

Bellingham, S. A., G. D. Ciccotosto, B. E. Needham, L. R. Fodero, A. R. White, C. L. Masters, R. Cappai and J. Camakaris (2004). "Gene knockout of amyloid precursor

protein and amyloid precursor-like protein-2 increases cellular copper levels in primary mouse cortical neurons and embryonic fibroblasts." J Neurochem **91**(2): 423-428.

Benilova, I., E. Karran and B. De Strooper (2012). "The toxic Abeta oligomer and Alzheimer's disease: an emperor in need of clothes." Nat Neurosci **15**(3): 349-357.

Bertram, L., C. M. Lill and R. E. Tanzi (2010). "The genetics of Alzheimer disease: back to the future." Neuron **68**(2): 270-281.

Beyreuther, K., P. Pollwein, G. Multhaup, U. Monning, G. Konig, T. Dyrks, W. Schubert and C. L. Masters (1993). "Regulation and expression of the Alzheimer's beta/A4 amyloid protein precursor in health, disease, and Down's syndrome." Ann N Y Acad Sci **695**: 91-102.

Bird, T. D. (1993, last revision 2014). Alzheimer Disease Overview. GeneReviews(R). R. A. Pagon, M. P. Adam, H. H. Ardinger et al. Seattle (WA).

Bird, T. D. (2008). "Genetic aspects of Alzheimer disease." Genet Med **10**(4): 231-239.

Bjerke, M., E. Portelius, L. Minthon, A. Wallin, H. Anckarsater, R. Anckarsater, N. Andreasen, H. Zetterberg, U. Andreasson and K. Blennow (2010). "Confounding factors influencing amyloid Beta concentration in cerebrospinal fluid." Int J Alzheimers Dis **2010**.

Blurton-Jones, M., B. Spencer, S. Michael, N. A. Castello, A. A. Agazaryan, J. L. Davis, F. J. Muller, J. F. Loring, E. Masliah and F. M. LaFerla (2014). "Neural stem cells genetically-modified to express neprilysin reduce pathology in Alzheimer transgenic models." Stem Cell Res Ther **5**(2): 46.

Bouter, Y., K. Dietrich, J. L. Wittnam, N. Rezaei-Ghaleh, T. Pillot, S. Papot-Couturier, T. Lefebvre, F. Sprenger, O. Wirths, M. Zweckstetter and T. A. Bayer (2013). "N-truncated amyloid beta (Abeta) 4-42 forms stable aggregates and induces acute and long-lasting behavioral deficits." Acta Neuropathol.

Buck, M. (1998). "Trifluoroethanol and colleagues: cosolvents come of age. Recent studies with peptides and proteins." Q Rev Biophys **31**(3): 297-355.

Caselli, R. J., A. C. Dueck, D. E. Locke, M. N. Sabbagh, G. L. Ahern, S. Z. Rapcsak, L. C. Baxter, R. Yaari, B. K. Woodruff, C. Hoffman-Snyder, R. Rademakers, S. Findley and E. M. Reiman (2011). "Cerebrovascular risk factors and preclinical memory decline in healthy APOE epsilon4 homozygotes." Neurology **76**(12): 1078-1084.

Chelius, D., K. Jing, A. Lueras, D. S. Rehder, T. M. Dillon, A. Vizel, R. S. Rajan, T. Li, M. J. Treuheit and P. V. Bondarenko (2006). "Formation of pyroglutamic acid from N-terminal glutamic acid in immunoglobulin gamma antibodies." Anal Chem **78**(7): 2370-2376.

Chen, F., D. David, A. Ferrari and J. Gotz (2004). "Posttranslational modifications of tau--role in human tauopathies and modeling in transgenic animals." Curr Drug Targets **5**(6): 503-515.

Chen, Y. R., H. B. Huang, C. L. Chyan, M. S. Shiao, T. H. Lin and Y. C. Chen (2006). "The effect of Abeta conformation on the metal affinity and aggregation mechanism studied by circular dichroism spectroscopy." J Biochem **139**(4): 733-740.

Chien, D. T., A. K. Szardenings, S. Bahri, J. C. Walsh, F. Mu, C. Xia, W. R. Shankle, A. J. Lerner, M. Y. Su, A. Elizarov and H. C. Kolb (2014). "Early clinical PET imaging results with the novel PHF-tau radioligand [F18]-T808." J Alzheimers Dis **38**(1): 171-184.

Citron, M. (2010). "Alzheimer's disease: strategies for disease modification." Nat Rev Drug Discov **9**(5): 387-398.

Crowther, R. A. and C. M. Wischik (1985). "Image reconstruction of the Alzheimer paired helical filament." EMBO J **4**(13B): 3661-3665.

Cruz, L., B. Urbanc, S. V. Buldyrev, R. Christie, T. Gomez-Isla, S. Havlin, M. McNamara, H. E. Stanley and B. T. Hyman (1997). "Aggregation and disaggregation of senile plaques in Alzheimer disease." Proc Natl Acad Sci U S A **94**(14): 7612-7616.

D'Arrigo, C., M. Tabaton and A. Perico (2009). "N-terminal truncated pyroglutamyl beta amyloid peptide Abetapy3-42 shows a faster aggregation kinetics than the full-length Abeta1-42." Biopolymers **91**(10): 861-873.

De Kimpe, L., E. S. van Haastert, A. Kaminari, R. Zwart, H. Rutjes, J. J. Hoozemans and W. Scheper (2013). "Intracellular accumulation of aggregated pyroglutamate amyloid beta: convergence of aging and Abeta pathology at the lysosome." Age (Dordr) **35**(3): 673-687.

De Meyer, G., F. Shapiro, H. Vanderstichele, E. Vanmechelen, S. Engelborghs, P. P. De Deyn, E. Coart, O. Hansson, L. Minthon, H. Zetterberg, K. Blennow, L. Shaw, J. Q. Trojanowski and I. Alzheimer's Disease Neuroimaging (2010). "Diagnosis-independent Alzheimer disease biomarker signature in cognitively normal elderly people." Arch Neurol **67**(8): 949-956.

De Strooper, B. (2010). "Proteases and proteolysis in Alzheimer disease: a multifactorial view on the disease process." Physiol Rev **90**(2): 465-494.

De Strooper, B., R. Vassar and T. Golde (2010). "The secretases: enzymes with therapeutic potential in Alzheimer disease." Nat Rev Neurol **6**(2): 99-107.

Dickson, D. W. (1997). "The pathogenesis of senile plaques." J Neuropathol Exp Neurol **56**(4): 321-339.

Dong, J., C. S. Atwood, V. E. Anderson, S. L. Siedlak, M. A. Smith, G. Perry and P. R. Carey (2003). "Metal binding and oxidation of amyloid-beta within isolated senile plaque cores: Raman microscopic evidence." Biochemistry **42**(10): 2768-2773.

Duara, R., R. F. Lopez-Alberola, W. W. Barker, D. A. Loewenstein, M. Zatinsky, C. E. Eisdorfer and G. B. Weinberg (1993). "A comparison of familial and sporadic Alzheimer's disease." Neurology **43**(7): 1377-1384.

Dubois, B., H. H. Feldman, C. Jacova, H. Hampel, J. L. Molinuevo, K. Blennow, S. T. DeKosky, S. Gauthier, D. Selkoe, R. Bateman, S. Cappa, S. Crutch, S. Engelborghs, G. B. Frisoni, N. C. Fox, D. Galasko, M. O. Habert, G. A. Jicha, A. Nordberg, F. Pasquier, G. Rabinovici, P. Robert, C. Rowe, S. Salloway, M. Sarazin, S. Epelbaum, L. C. de Souza, B. Vellas, P. J. Visser, L. Schneider, Y. Stern, P. Scheltens and J. L. Cummings (2014). "Advancing research diagnostic criteria for Alzheimer's disease: the IWG-2 criteria." Lancet Neurol **13**(6): 614-629.

Eckert, A., C. A. Marques, U. Keil, K. Schussel and W. E. Muller (2003). "Increased apoptotic cell death in sporadic and genetic Alzheimer's disease." Ann N Y Acad Sci **1010**: 604-609.

Edison, P., H. A. Archer, R. Hinz, A. Hammers, N. Pavese, Y. F. Tai, G. Hotton, D. Cutler, N. Fox, A. Kennedy, M. Rossor and D. J. Brooks (2007). "Amyloid, hypometabolism, and cognition in Alzheimer disease: an [11C]PIB and [18F]FDG PET study." Neurology **68**(7): 501-508.

Fan, J., J. Donkin and C. Wellington (2009). "Greasing the wheels of Abeta clearance in Alzheimer's disease: the role of lipids and apolipoprotein E." Biofactors **35**(3): 239-248.

Fezoui, Y., D. M. Hartley, D. M. Walsh, D. J. Selkoe, J. J. Osterhout and D. B. Teplow (2000). "A de novo designed helix-turn-helix peptide forms nontoxic amyloid fibrils." Nat Struct Biol **7**(12): 1095-1099.

Fezoui, Y. and D. B. Teplow (2002). "Kinetic studies of amyloid beta-protein fibril assembly. Differential effects of alpha-helix stabilization." J Biol Chem **277**(40): 36948-36954.

Findeis, M. A., G. M. Musso, C. C. Arico-Muendel, H. W. Benjamin, A. M. Hundal, J. J. Lee, J. Chin, M. Kelley, J. Wakefield, N. J. Hayward and S. M. Molineaux (1999). "Modified-peptide inhibitors of amyloid beta-peptide polymerization." Biochemistry **38**(21): 6791-6800.

Finder, V. H., I. Vodopivec, R. M. Nitsch and R. Glockshuber (2010). "The recombinant amyloid-beta peptide Abeta1-42 aggregates faster and is more neurotoxic than synthetic Abeta1-42." J Mol Biol **396**(1): 9-18.

Flaherty, D. B., J. P. Soria, H. G. Tomasiewicz and J. G. Wood (2000). "Phosphorylation of human tau protein by microtubule-associated kinases: GSK3beta and cdk5 are key participants." J Neurosci Res **62**(3): 463-472.

Fotuhi, M., V. Hachinski and P. J. Whitehouse (2009). "Changing perspectives regarding late-life dementia." Nat Rev Neurol **5**(12): 649-658.

Fox, N. C., S. Cousens, R. Scahill, R. J. Harvey and M. N. Rossor (2000). "Using serial registered brain magnetic resonance imaging to measure disease progression in Alzheimer disease: power calculations and estimates of sample size to detect treatment effects." Arch Neurol **57**(3): 339-344.

Fox, N. C., W. R. Crum, R. I. Scahill, J. M. Stevens, J. C. Janssen and M. N. Rossor (2001). "Imaging of onset and progression of Alzheimer's disease with voxel-compression mapping of serial magnetic resonance images." Lancet **358**(9277): 201-205.

Friedhoff, P., M. von Bergen, E. M. Mandelkow and E. Mandelkow (2000). "Structure of tau protein and assembly into paired helical filaments." Biochim Biophys Acta **1502**(1): 122-132.

Funke, S., T. van Groen, I. Kadish, D. Bartnik, L. Nagel-Steger, O. Brener, T. Sehl, R. Batra-Safferling, C. Moriscot, G. Schoehn, A. H. Horn, A. Muller-Schiffmann, C. Korth, H. Sticht and D. Willbold (2010). "Oral treatment with the d-enantiomeric peptide D3 improves the pathology and behavior of Alzheimer's Disease transgenic mice." ACS Chem Neurosci **1**(9): 639-648.

Funke, S. A., E. Birkmann, F. Henke, P. Gortz, C. Lange-Asschenfeldt, D. Riesner and D. Willbold (2007). "Single particle detection of Abeta aggregates associated with Alzheimer's disease." Biochem Biophys Res Commun **364**(4): 902-907.

Funke, S. A., L. Wang, E. Birkmann and D. Willbold (2010). "Single-particle detection system for Abeta aggregates: adaptation of surface-fluorescence intensity distribution analysis to laser scanning microscopy." Rejuvenation Res **13**(2-3): 206-209.

Galimberti, D. and E. Scarpini (2012). "Progress in Alzheimer's disease." J Neurol **259**(2): 201-211.

Garai, K., B. Sahoo, P. Sengupta and S. Maiti (2008). "Quasihomogeneous nucleation of amyloid beta yields numerical bounds for the critical radius, the surface tension, and the free energy barrier for nucleus formation." J Chem Phys **128**(4): 045102.

Gatz, M., C. A. Reynolds, L. Fratiglioni, B. Johansson, J. A. Mortimer, S. Berg, A. Fiske and N. L. Pedersen (2006). "Role of genes and environments for explaining Alzheimer disease." Arch Gen Psychiatry **63**(2): 168-174.

Gilman, S., M. Koller, R. S. Black, L. Jenkins, S. G. Griffith, N. C. Fox, L. Eisner, L. Kirby, M. B. Rovira, F. Forette, J. M. Orgogozo and A. N. S. Team (2005). "Clinical effects of Abeta immunization (AN1792) in patients with AD in an interrupted trial." Neurology **64**(9): 1553-1562.

Golde, T. E., L. S. Schneider and E. H. Koo (2011). "Anti-abeta therapeutics in Alzheimer's disease: the need for a paradigm shift." Neuron **69**(2): 203-213.

Gorevic, P. D., F. Goni, B. Pons-Estel, F. Alvarez, N. S. Peress and B. Frangione (1986). "Isolation and partial characterization of neurofibrillary tangles and amyloid plaque core in Alzheimer's disease: immunohistological studies." J Neuropathol Exp Neurol **45**(6): 647-664.

Gunn, A. P., C. L. Masters and R. A. Cherny (2010). "Pyroglutamate-Abeta: role in the natural history of Alzheimer's disease." Int J Biochem Cell Biol **42**(12): 1915-1918.

Guntert, A., H. Dobeli and B. Bohrmann (2006). "High sensitivity analysis of amyloid-beta peptide composition in amyloid deposits from human and PS2APP mouse brain." Neuroscience **143**(2): 461-475.

Haas, C. (2012). "Strategies, development, and pitfalls of therapeutic options for Alzheimer's disease." J Alzheimers Dis **28**(2): 241-281.

Haass, C., A. Y. Hung, M. G. Schlossmacher, T. Oltersdorf, D. B. Teplow and D. J. Selkoe (1993). "Normal cellular processing of the beta-amyloid precursor protein results in the secretion of the amyloid beta peptide and related molecules." Ann N Y Acad Sci **695**: 109-116.

Haass, C. and D. J. Selkoe (2007). "Soluble protein oligomers in neurodegeneration: lessons from the Alzheimer's amyloid beta-peptide." Nat Rev Mol Cell Biol **8**(2): 101-112.

Hardy, J. and D. J. Selkoe (2002). "The amyloid hypothesis of Alzheimer's disease: progress and problems on the road to therapeutics." Science **297**(5580): 353-356.

Hardy, J. A. and G. A. Higgins (1992). "Alzheimer's disease: the amyloid cascade hypothesis." Science **256**(5054): 184-185.

Harigaya, Y., T. C. Saido, C. B. Eckman, C. M. Prada, M. Shoji and S. G. Younkin (2000). "Amyloid beta protein starting pyroglutamate at position 3 is a major component of the amyloid deposits in the Alzheimer's disease brain." Biochem Biophys Res Commun **276**(2): 422-427.

Hartig, W., S. Goldhammer, U. Bauer, F. Wegner, O. Wirths, T. A. Bayer and J. Grosche (2010). "Concomitant detection of beta-amyloid peptides with N-terminal truncation and different C-terminal endings in cortical plaques from cases with Alzheimer's disease, senile monkeys and triple transgenic mice." J Chem Neuroanat **40**(1): 82-92.

He, W. and C. J. Barrow (1999). "The A beta 3-pyroglutamyl and 11-pyroglutamyl peptides found in senile plaque have greater beta-sheet forming and aggregation propensities in vitro than full-length A beta." Biochemistry **38**(33): 10871-10877.

Herard, A. S., L. Besret, A. Dubois, J. Dauguet, T. Delzescaux, P. Hantraye, G. Bonvento and K. L. Moya (2006). "siRNA targeted against amyloid precursor protein impairs synaptic activity in vivo." Neurobiol Aging **27**(12): 1740-1750.

Hoe, H. S., K. J. Lee, R. S. Carney, J. Lee, A. Markova, J. Y. Lee, B. W. Howell, B. T. Hyman, D. T. Pak, G. Bu and G. W. Rebeck (2009). "Interaction of reelin with amyloid precursor protein promotes neurite outgrowth." J Neurosci **29**(23): 7459-7473.

Holmes, C., D. Boche, D. Wilkinson, G. Yadegarfar, V. Hopkins, A. Bayer, R. W. Jones, R. Bullock, S. Love, J. W. Neal, E. Zotova and J. A. Nicoll (2008). "Long-term effects of Abeta42 immunisation in Alzheimer's disease: follow-up of a randomised, placebo-controlled phase I trial." Lancet **372**(9634): 216-223.

Hosoda, R., T. C. Saido, L. Otvos, Jr., T. Arai, D. M. Mann, V. M. Lee, J. Q. Trojanowski and T. Iwatsubo (1998). "Quantification of modified amyloid beta peptides in Alzheimer disease and Down syndrome brains." J Neuropathol Exp Neurol **57**(11): 1089-1095.

Hou, L., H. Shao, Y. Zhang, H. Li, N. K. Menon, E. B. Neuhaus, J. M. Brewer, I. J. Byeon, D. G. Ray, M. P. Vitek, T. Iwashita, R. A. Makula, A. B. Przybyla and M. G. Zagorski (2004). "Solution NMR studies of the A beta(1-40) and A beta(1-42) peptides establish that the Met35 oxidation state affects the mechanism of amyloid formation." J Am Chem Soc **126**(7): 1992-2005.

Huang, Y. and L. Mucke (2012). "Alzheimer mechanisms and therapeutic strategies." Cell **148**(6): 1204-1222.

Huse, J. T., K. Liu, D. S. Pijak, D. Carlin, V. M. Lee and R. W. Doms (2002). "Beta-secretase processing in the trans-Golgi network preferentially generates truncated amyloid species that accumulate in Alzheimer's disease brain." J Biol Chem **277**(18): 16278-16284.

Hutton, M. and J. Hardy (1997). "The presenilins and Alzheimer's disease." Hum Mol Genet **6**(10): 1639-1646.

Ikonomovic, M. D., W. E. Klunk, E. E. Abrahamson, C. A. Mathis, J. C. Price, N. D. Tsopelas, B. J. Lopresti, S. Ziolko, W. Bi, W. R. Paljug, M. L. Debnath, C. E. Hope, B. A. Isanski, R. L. Hamilton and S. T. DeKosky (2008). "Post-mortem correlates of in vivo PiB-PET amyloid imaging in a typical case of Alzheimer's disease." Brain **131**(Pt 6): 1630-1645.

Imtiaz, B., A. M. Tolppanen, M. Kivipelto and H. Soininen (2014). "Future directions in Alzheimer's disease from risk factors to prevention." Biochem Pharmacol **88**(4): 661-670.

Iqbal, K. and I. Grundke-Iqbal (2010). "Alzheimer's disease, a multifactorial disorder seeking multitherapies." Alzheimers Dement **6**(5): 420-424.

Iwatsubo, T., T. C. Saido, D. M. Mann, V. M. Lee and J. Q. Trojanowski (1996). "Full-length amyloid-beta (1-42(43)) and amino-terminally modified and truncated amyloid-beta 42(43) deposit in diffuse plaques." Am J Pathol **149**(6): 1823-1830.

Jack, C. R., Jr., M. S. Albert, D. S. Knopman, G. M. McKhann, R. A. Sperling, M. C. Carrillo, B. Thies and C. H. Phelps (2011). "Introduction to the recommendations from the National Institute on Aging-Alzheimer's Association workgroups on diagnostic guidelines for Alzheimer's disease." Alzheimers Dement **7**(3): 257-262.

Jawhar, S., O. Wirths and T. A. Bayer (2011). "Pyroglutamate amyloid-beta (Abeta): a hatchet man in Alzheimer disease." J Biol Chem **286**(45): 38825-38832.

Kapust, R. B., J. Tozser, T. D. Copeland and D. S. Waugh (2002). "The P1' specificity of tobacco etch virus protease." Biochem Biophys Res Commun **294**(5): 949-955.

Khan, M. V., G. Rabbani, E. Ahmad and R. H. Khan (2014). "Fluoroalcohols-induced modulation and amyloid formation in conalbumin." Int J Biol Macromol **70**: 606-614.

Kirkitadze, M. D., M. M. Condron and D. B. Teplow (2001). "Identification and characterization of key kinetic intermediates in amyloid beta-protein fibrillogenesis." J Mol Biol **312**(5): 1103-1119.

Klunk, W. E., H. Engler, A. Nordberg, Y. Wang, G. Blomqvist, D. P. Holt, M. Bergstrom, I. Savitcheva, G. F. Huang, S. Estrada, B. Ausen, M. L. Debnath, J. Barletta, J. C. Price, J. Sandell, B. J. Lopresti, A. Wall, P. Koivisto, G. Antoni, C. A. Mathis and B. Langstrom (2004). "Imaging brain amyloid in Alzheimer's disease with Pittsburgh Compound-B." Ann Neurol **55**(3): 306-319.

Kokkoni, N., K. Stott, H. Amijee, J. M. Mason and A. J. Doig (2006). "N-Methylated peptide inhibitors of beta-amyloid aggregation and toxicity. Optimization of the inhibitor structure." Biochemistry **45**(32): 9906-9918.

Konno, T., S. Oiki and T. Morii (2007). "Synergistic action of polyanionic and non-polar cofactors in fibrillation of human islet amyloid polypeptide." FEBS Lett **581**(8): 1635-1638.

Kumar, J. and V. Sim (2014). "D-amino acid-based peptide inhibitors as early or preventative therapy in Alzheimer disease." Prion **8**(1): 119-124.

Kumar, S., N. Rezaei-Ghaleh, D. Terwel, D. R. Thal, M. Richard, M. Hoch, J. M. Mc Donald, U. Wullner, K. Glebov, M. T. Heneka, D. M. Walsh, M. Zweckstetter and J. Walter (2011). "Extracellular phosphorylation of the amyloid beta-peptide promotes formation of toxic aggregates during the pathogenesis of Alzheimer's disease." EMBO J **30**(11): 2255-2265.

Kumar, S. and J. B. Udgaonkar (2009). "Structurally distinct amyloid protofibrils form on separate pathways of aggregation of a small protein." Biochemistry **48**(27): 6441-6449.

Kuo, Y. M., M. R. Emmerling, A. S. Woods, R. J. Cotter and A. E. Roher (1997). "Isolation, chemical characterization, and quantitation of A beta 3-pyroglutamyl peptide from neuritic plaques and vascular amyloid deposits." Biochem Biophys Res Commun **237**(1): 188-191.

Lambert, M. P., A. K. Barlow, B. A. Chromy, C. Edwards, R. Freed, M. Liosatos, T. E. Morgan, I. Rozovsky, B. Trommer, K. L. Viola, P. Wals, C. Zhang, C. E. Finch, G. A. Krafft and W. L. Klein (1998). "Diffusible, nonfibrillar ligands derived from Abeta1-42 are potent central nervous system neurotoxins." Proc Natl Acad Sci U S A **95**(11): 6448-6453.

Laske, C., H. R. Sohrabi, S. M. Frost, K. Lopez-de-Ipina, P. Garrard, M. Buscema, J. Dauwels, S. R. Soekadar, S. Mueller, C. Linnemann, S. A. Bridenbaugh, Y. Kanagasingam, R. N. Martins and S. E. O'Bryant (2015). "Innovative diagnostic tools for early detection of Alzheimer's disease." Alzheimers Dement **11**(5): 561-578.

Lawrence, A. D. and B. J. Sahakian (1998). "The cognitive psychopharmacology of Alzheimer's disease: focus on cholinergic systems." Neurochem Res **23**(5): 787-794.

Lemere, C. A. and E. Masliah (2010). "Can Alzheimer disease be prevented by amyloid-beta immunotherapy?" Nat Rev Neurol **6**(2): 108-119.

Liu, G., A. Prabhakar, D. Aucoin, M. Simon, S. Sparks, K. J. Robbins, A. Sheen, S. A. Petty and N. D. Lazo (2010). "Mechanistic studies of peptide self-assembly: transient alpha-helices to stable beta-sheets." J Am Chem Soc **132**(51): 18223-18232.

Lockhart, A., J. R. Lamb, T. Osredkar, L. I. Sue, J. N. Joyce, L. Ye, V. Libri, D. Leppert and T. G. Beach (2007). "PIB is a non-specific imaging marker of amyloid-beta (Abeta) peptide-related cerebral amyloidosis." Brain **130**(Pt 10): 2607-2615.

Luhrs, T., C. Ritter, M. Adrian, D. Riek-Loher, B. Bohrmann, H. Dobeli, D. Schubert and R. Riek (2005). "3D structure of Alzheimer's amyloid-beta(1-42) fibrils." Proc Natl Acad Sci U S A **102**(48): 17342-17347.

Mann, D. M., D. Jones, D. Prinja and M. S. Purkiss (1990). "The prevalence of amyloid (A4) protein deposits within the cerebral and cerebellar cortex in Down's syndrome and Alzheimer's disease." Acta Neuropathol **80**(3): 318-327.

Marr, R. A., E. Rockenstein, A. Mukherjee, M. S. Kindy, L. B. Hersh, F. H. Gage, I. M. Verma and E. Masliah (2003). "Neprilysin gene transfer reduces human amyloid pathology in transgenic mice." J Neurosci **23**(6): 1992-1996.

Marsh, J. A., V. K. Singh, Z. Jia and J. D. Forman-Kay (2006). "Sensitivity of secondary structure propensities to sequence differences between alpha- and gamma-synuclein: implications for fibrillation." Protein Sci **15**(12): 2795-2804.

Masters, C. L., G. Simms, N. A. Weinman, G. Multhaup, B. L. McDonald and K. Beyreuther (1985). "Amyloid plaque core protein in Alzheimer disease and Down syndrome." Proc Natl Acad Sci U S A **82**(12): 4245-4249.

McKhann, G., D. Drachman, M. Folstein, R. Katzman, D. Price and E. M. Stadlan (1984). "Clinical diagnosis of Alzheimer's disease: report of the NINCDS-ADRDA Work Group under the auspices of Department of Health and Human Services Task Force on Alzheimer's Disease." Neurology **34**(7): 939-944.

Mendieta, J., M. A. Fuertes, R. Kunjishapatham, I. Santa-Maria, F. J. Moreno, C. Alonso, F. Gago, V. Munoz, J. Avila and F. Hernandez (2005). "Phosphorylation modulates the

alpha-helical structure and polymerization of a peptide from the third tau microtubule-binding repeat." Biochim Biophys Acta **1721**(1-3): 16-26.

Mihara, H. and Y. Takahashi (1997). "Engineering peptides and proteins that undergo alpha-to-beta transitions." Curr Opin Struct Biol **7**(4): 501-508.

Miller, D. L., I. A. Papayannopoulos, J. Styles, S. A. Bobin, Y. Y. Lin, K. Biemann and K. Iqbal (1993). "Peptide compositions of the cerebrovascular and senile plaque core amyloid deposits of Alzheimer's disease." Arch Biochem Biophys **301**(1): 41-52.

Milton, N. G. (2001). "Phosphorylation of amyloid-beta at the serine 26 residue by human cdc2 kinase." Neuroreport **12**(17): 3839-3844.

Mischo, A., O. Ohlenschlager, K. H. Guhrs and M. Gorlach (2012). "Recombinant production of isotope-labeled peptides and spontaneous cyclization of amino-terminal glutamine into pyroglutamic acid." Chembiochem **13**(10): 1421-1423.

Mori, H., K. Takio, M. Ogawara and D. J. Selkoe (1992). "Mass spectrometry of purified amyloid beta protein in Alzheimer's disease." J Biol Chem **267**(24): 17082-17086.

Morris, J. K., R. A. Honea, E. D. Vidoni, R. H. Swerdlow and J. M. Burns (2014). "Is Alzheimer's disease a systemic disease?" Biochim Biophys Acta **1842**(9): 1340-1349.

Morris, M., S. Maeda, K. Vossel and L. Mucke (2011). "The many faces of tau." Neuron **70**(3): 410-426.

Mucke, L. (2009). "Neuroscience: Alzheimer's disease." Nature **461**(7266): 895-897.

Mullane, K. and M. Williams (2013). "Alzheimer's therapeutics: continued clinical failures question the validity of the amyloid hypothesis-but what lies beyond?" Biochem Pharmacol **85**(3): 289-305.

Murphy, G. M., Jr., L. F. Eng, W. G. Ellis, G. Perry, L. C. Meissner and J. R. Tinklenberg (1990). "Antigenic profile of plaques and neurofibrillary tangles in the amygdala in Down's syndrome: a comparison with Alzheimer's disease." Brain Res **537**(1-2): 102-108.

Nag, S., B. Sarkar, A. Bandyopadhyay, B. Sahoo, V. K. Sreenivasan, M. Kombrabail, C. Muralidharan and S. Maiti (2011). "Nature of the amyloid-beta monomer and the monomer-oligomer equilibrium." J Biol Chem **286**(16): 13827-13833.

Nalivaeva, N. N., C. Beckett, N. D. Belyaev and A. J. Turner (2012). "Are amyloid-degrading enzymes viable therapeutic targets in Alzheimer's disease?" J Neurochem **120 Suppl 1**: 167-185.

Naslund, J., A. Schierhorn, U. Hellman, L. Lannfelt, A. D. Roses, L. O. Tjernberg, J. Silberring, S. E. Gandy, B. Winblad, P. Greengard and et al. (1994). "Relative abundance of Alzheimer A beta amyloid peptide variants in Alzheimer disease and normal aging." Proc Natl Acad Sci U S A **91**(18): 8378-8382.

National Institute of Aging. (2015). "Alzheimer's disease fact sheet." Retrieved 21 Aug, 2015, from https://www.nia.nih.gov/.

Okamura, N., S. Furumoto, M. T. Fodero-Tavoletti, R. S. Mulligan, R. Harada, P. Yates, S. Pejoska, Y. Kudo, C. L. Masters, K. Yanai, C. C. Rowe and V. L. Villemagne (2014). "Non-

invasive assessment of Alzheimer's disease neurofibrillary pathology using 18F-THK5105 PET." Brain **137**(Pt 6): 1762-1771.

Panza, F., V. Solfrizzi, V. Frisardi, C. Capurso, A. D'Introno, A. M. Colacicco, G. Vendemiale, A. Capurso and B. P. Imbimbo (2009). "Disease-modifying approach to the treatment of Alzheimer's disease: from alpha-secretase activators to gamma-secretase inhibitors and modulators." Drugs Aging **26**(7): 537-555.

Perez-Garmendia, R. and G. Gevorkian (2013). "Pyroglutamate-Modified Amyloid Beta Peptides: Emerging Targets for Alzheimer s Disease Immunotherapy." Curr Neuropharmacol **11**(5): 491-498.

Perl, D. P. (2010). "Neuropathology of Alzheimer's disease." Mt Sinai J Med **77**(1): 32-42.

Piccini, A., C. Russo, A. Gliozzi, A. Relini, A. Vitali, R. Borghi, L. Giliberto, A. Armirotti, C. D'Arrigo, A. Bachi, A. Cattaneo, C. Canale, S. Torrassa, T. C. Saido, W. Markesbery, P. Gambetti and M. Tabaton (2005). "beta-amyloid is different in normal aging and in Alzheimer disease." J Biol Chem **280**(40): 34186-34192.

Pike, C. J., M. J. Overman and C. W. Cotman (1995). "Amino-terminal deletions enhance aggregation of beta-amyloid peptides in vitro." J Biol Chem **270**(41): 23895-23898.

Portelius, E., N. Bogdanovic, M. K. Gustavsson, I. Volkmann, G. Brinkmalm, H. Zetterberg, B. Winblad and K. Blennow (2010). "Mass spectrometric characterization of brain amyloid beta isoform signatures in familial and sporadic Alzheimer's disease." Acta Neuropathol **120**(2): 185-193.

Portelius, E., H. Zetterberg, R. A. Dean, A. Marcil, P. Bourgeois, M. Nutu, U. Andreasson, E. Siemers, K. G. Mawuenyega, W. C. Sigurdson, P. C. May, S. M. Paul, D. M. Holtzman, K. Blennow and R. J. Bateman (2012). "Amyloid-beta(1-15/16) as a marker for gamma-secretase inhibition in Alzheimer's disease." J Alzheimers Dis **31**(2): 335-341.

Prelli, F., E. Castano, G. G. Glenner and B. Frangione (1988). "Differences between vascular and plaque core amyloid in Alzheimer's disease." J Neurochem **51**(2): 648-651.

Priller, C., T. Bauer, G. Mitteregger, B. Krebs, H. A. Kretzschmar and J. Herms (2006). "Synapse formation and function is modulated by the amyloid precursor protein." J Neurosci **26**(27): 7212-7221.

Prince, M., R. Bryce, E. Albanese, A. Wimo, W. Ribeiro and C. P. Ferri (2013). "The global prevalence of dementia: a systematic review and metaanalysis." Alzheimers Dement **9**(1): 63-75 e62.

Reitz, C. and R. Mayeux (2014). "Alzheimer disease: epidemiology, diagnostic criteria, risk factors and biomarkers." Biochem Pharmacol **88**(4): 640-651.

Rezaei-Ghaleh, N., E. Andreetto, L. M. Yan, A. Kapurniotu and M. Zweckstetter (2011). "Interaction between amyloid beta peptide and an aggregation blocker peptide mimicking islet amyloid polypeptide." PLoS One **6**(5): e20289.

Russo, C., T. C. Saido, L. M. DeBusk, M. Tabaton, P. Gambetti and J. K. Teller (1997). "Heterogeneity of water-soluble amyloid beta-peptide in Alzheimer's disease and Down's syndrome brains." FEBS Lett **409**(3): 411-416.

Russo, C., S. Salis, V. Dolcini, V. Venezia, X. H. Song, J. K. Teller and G. Schettini (2001). "Amino-terminal modification and tyrosine phosphorylation of [corrected] carboxy-terminal fragments of the amyloid precursor protein in Alzheimer's disease and Down's syndrome brain." Neurobiol Dis **8**(1): 173-180.

Saido, T. C., T. Iwatsubo, D. M. Mann, H. Shimada, Y. Ihara and S. Kawashima (1995). "Dominant and differential deposition of distinct beta-amyloid peptide species, A beta N3(pE), in senile plaques." Neuron **14**(2): 457-466.

Saido, T. C., W. Yamao-Harigaya, T. Iwatsubo and S. Kawashima (1996). "Amino- and carboxyl-terminal heterogeneity of beta-amyloid peptides deposited in human brain." Neurosci Lett **215**(3): 173-176.

Schilling, S., T. Hoffmann, S. Manhart, M. Hoffmann and H. U. Demuth (2004). "Glutaminyl cyclases unfold glutamyl cyclase activity under mild acid conditions." FEBS Lett **563**(1-3): 191-196.

Schilling, S., T. Lauber, M. Schaupp, S. Manhart, E. Scheel, G. Bohm and H. U. Demuth (2006). "On the seeding and oligomerization of pGlu-amyloid peptides (in vitro)." Biochemistry **45**(41): 12393-12399.

Schilling, S., A. J. Niestroj, J. U. Rahfeld, T. Hoffmann, M. Wermann, K. Zunkel, C. Wasternack and H. U. Demuth (2003). "Identification of human glutaminyl cyclase as a metalloenzyme. Potent inhibition by imidazole derivatives and heterocyclic chelators." J Biol Chem **278**(50): 49773-49779.

Schilling, S., C. Wasternack and H. U. Demuth (2008). "Glutaminyl cyclases from animals and plants: a case of functionally convergent protein evolution." Biol Chem **389**(8): 983-991.

Schlenzig, D., R. Ronicke, H. Cynis, H. H. Ludwig, E. Scheel, K. Reymann, T. Saido, G. Hause, S. Schilling and H. U. Demuth (2012). "N-Terminal pyroglutamate formation of Abeta38 and Abeta40 enforces oligomer formation and potency to disrupt hippocampal long-term potentiation." J Neurochem **121**(5): 774-784.

Schwarzinger, S., G. J. Kroon, T. R. Foss, J. Chung, P. E. Wright and H. J. Dyson (2001). "Sequence-dependent correction of random coil NMR chemical shifts." J Am Chem Soc **123**(13): 2970-2978.

Selkoe, D. J. (1997). "Alzheimer's disease: genotypes, phenotypes, and treatments." Science **275**(5300): 630-631.

Selkoe, D. J. (1999). "Translating cell biology into therapeutic advances in Alzheimer's disease." Nature **399**(6738 Suppl): A23-31.

Selkoe, D. J., C. R. Abraham, M. B. Podlisny and L. K. Duffy (1986). "Isolation of low-molecular-weight proteins from amyloid plaque fibers in Alzheimer's disease." J Neurochem **46**(6): 1820-1834.

Serpell, L. C. (2000). "Alzheimer's amyloid fibrils: structure and assembly." Biochim Biophys Acta **1502**(1): 16-30.

Sevalle, J., A. Amoyel, P. Robert, M. C. Fournie-Zaluski, B. Roques and F. Checler (2009). "Aminopeptidase A contributes to the N-terminal truncation of amyloid beta-peptide." J Neurochem **109**(1): 248-256.

Shankar, G. M., S. Li, T. H. Mehta, A. Garcia-Munoz, N. E. Shepardson, I. Smith, F. M. Brett, M. A. Farrell, M. J. Rowan, C. A. Lemere, C. M. Regan, D. M. Walsh, B. L. Sabatini and D. J. Selkoe (2008). "Amyloid-beta protein dimers isolated directly from Alzheimer's brains impair synaptic plasticity and memory." Nat Med **14**(8): 837-842.

Shen, Y., F. Delaglio, G. Cornilescu and A. Bax (2009). "TALOS+: a hybrid method for predicting protein backbone torsion angles from NMR chemical shifts." J Biomol NMR **44**(4): 213-223.

Shibata, M., S. Yamada, S. R. Kumar, M. Calero, J. Bading, B. Frangione, D. M. Holtzman, C. A. Miller, D. K. Strickland, J. Ghiso and B. V. Zlokovic (2000). "Clearance of Alzheimer's amyloid-ss(1-40) peptide from brain by LDL receptor-related protein-1 at the blood-brain barrier." J Clin Invest **106**(12): 1489-1499.

Spencer, B., R. A. Marr, E. Rockenstein, L. Crews, A. Adame, R. Potkar, C. Patrick, F. H. Gage, I. M. Verma and E. Masliah (2008). "Long-term neprilysin gene transfer is associated with reduced levels of intracellular Abeta and behavioral improvement in APP transgenic mice." BMC Neurosci **9**: 109.

Sticht, H., P. Bayer, D. Willbold, S. Dames, C. Hilbich, K. Beyreuther, R. W. Frank and P. Rosch (1995). "Structure of amyloid A4-(1-40)-peptide of Alzheimer's disease." Eur J Biochem **233**(1): 293-298.

Sullivan, C. P., E. A. Berg, R. Elliott-Bryant, J. B. Fishman, A. C. McKee, P. J. Morin, M. A. Shia and R. E. Fine (2011). "Pyroglutamate-Abeta 3 and 11 colocalize in amyloid plaques in Alzheimer's disease cerebral cortex with pyroglutamate-Abeta 11 forming the central core." Neurosci Lett **505**(2): 109-112.

Sun, N., R. Hartmann, J. Lecher, M. Stoldt, S. A. Funke, L. Gremer, H. H. Ludwig, H. U. Demuth, M. Kleinschmidt and D. Willbold (2012). "Structural analysis of the pyroglutamate-modified isoform of the Alzheimer's disease-related amyloid-beta using NMR spectroscopy." J Pept Sci **18**(11): 691-695.

Svedberg, M. M., H. Hall, E. Hellstrom-Lindahl, S. Estrada, Z. Guan, A. Nordberg and B. Langstrom (2009). "[(11)C]PIB-amyloid binding and levels of Abeta40 and Abeta42 in postmortem brain tissue from Alzheimer patients." Neurochem Int **54**(5-6): 347-357.

Tjernberg, L. O., J. Naslund, F. Lindqvist, J. Johansson, A. R. Karlstrom, J. Thyberg, L. Terenius and C. Nordstedt (1996). "Arrest of beta-amyloid fibril formation by a pentapeptide ligand." J Biol Chem **271**(15): 8545-8548.

Trojanowski, J. Q., A. B. Smith, D. Huryn and V. M. Lee (2005). "Microtubule-stabilising drugs for therapy of Alzheimer's disease and other neurodegenerative disorders with axonal transport impairments." Expert Opin Pharmacother **6**(5): 683-686.

Turner, P. R., K. O'Connor, W. P. Tate and W. C. Abraham (2003). "Roles of amyloid precursor protein and its fragments in regulating neural activity, plasticity and memory." Prog Neurobiol **70**(1): 1-32.

Twardzik, D. R. and A. Peterkofsky (1972). "Glutamic acid as a precursor to N-terminal pyroglutamic acid in mouse plasmacytoma protein (protein synthesis-initiation-immunoglobulins-pyrrolidone carboxylic acid)." Proc Natl Acad Sci U S A **69**(1): 274-277.

van Beek, J. D., L. Beaulieu, H. Schafer, M. Demura, T. Asakura and B. H. Meier (2000). "Solid-state NMR determination of the secondary structure of Samia cynthia ricini silk." Nature **405**(6790): 1077-1079.

van Groen, T., I. Kadish, A. Funke, D. Bartnik and D. Willbold (2012). "Treatment with Abeta42 binding D-amino acid peptides reduce amyloid deposition and inflammation in APP/PS1 double transgenic mice." Adv Protein Chem Struct Biol **88**: 133-152.

van Groen, T., I. Kadish, S. A. Funke, D. Bartnik and D. Willbold (2013). "Treatment with D3 removes amyloid deposits, reduces inflammation, and improves cognition in aged AbetaPP/PS1 double transgenic mice." J Alzheimers Dis **34**(3): 609-620.

van Groen, T., I. Kadish, K. Wiesehan, S. A. Funke and D. Willbold (2009). "In vitro and in vivo staining characteristics of small, fluorescent, Abeta42-binding D-enantiomeric peptides in transgenic AD mouse models." ChemMedChem **4**(2): 276-282.

van Groen, T., K. Wiesehan, S. A. Funke, I. Kadish, L. Nagel-Steger and D. Willbold (2008). "Reduction of Alzheimer's disease amyloid plaque load in transgenic mice by D3, A D-enantiomeric peptide identified by mirror image phage display." ChemMedChem **3**(12): 1848-1852.

Venkataramani, V., O. Wirths, H. Budka, W. Hartig, G. G. Kovacs and T. A. Bayer (2012). "Antibody 9D5 recognizes oligomeric pyroglutamate amyloid-beta in a fraction of amyloid-beta deposits in Alzheimer's disease without cross-reactivity with other protein aggregates." J Alzheimers Dis **29**(2): 361-371.

Wang-Dietrich, L., S. A. Funke, K. Kuhbach, K. Wang, A. Besmehn, S. Willbold, Y. Cinar, O. Bannach, E. Birkmann and D. Willbold (2013). "The amyloid-beta oligomer count in cerebrospinal fluid is a biomarker for Alzheimer's disease." J Alzheimers Dis **34**(4): 985-994.

Weber, D. K., M. A. Sani and J. D. Gehman (2014). "A routine method for cloning, expressing and purifying Abeta(1-42) for structural NMR studies." Amino Acids **46**(10): 2415-2426.

Weidemann, A., G. Konig, D. Bunke, P. Fischer, J. M. Salbaum, C. L. Masters and K. Beyreuther (1989). "Identification, biogenesis, and localization of precursors of Alzheimer's disease A4 amyloid protein." Cell **57**(1): 115-126.

Welander, H., J. Franberg, C. Graff, E. Sundstrom, B. Winblad and L. O. Tjernberg (2009). "Abeta43 is more frequent than Abeta40 in amyloid plaque cores from Alzheimer disease brains." J Neurochem **110**(2): 697-706.

Weuve, J., L. E. Hebert, P. A. Scherr and D. A. Evans (2014). "Deaths in the United States among persons with Alzheimer's disease (2010-2050)." Alzheimers Dement **10**(2): e40-46.

Wiesehan, K., J. Stohr, L. Nagel-Steger, T. van Groen, D. Riesner and D. Willbold (2008). "Inhibition of cytotoxicity and amyloid fibril formation by a D-amino acid peptide that specifically binds to Alzheimer's disease amyloid peptide." Protein Eng Des Sel **21**(4): 241-246.

Wiltfang, J., H. Esselmann, M. Bibl, A. Smirnov, M. Otto, S. Paul, B. Schmidt, H. W. Klafki, M. Maler, T. Dyrks, M. Bienert, M. Beyermann, E. Ruther and J. Kornhuber (2002). "Highly conserved and disease-specific patterns of carboxyterminally truncated Abeta peptides 1-

37/38/39 in addition to 1-40/42 in Alzheimer's disease and in patients with chronic neuroinflammation." J Neurochem **81**(3): 481-496.

Wirths, O., T. Bethge, A. Marcello, A. Harmeier, S. Jawhar, P. J. Lucassen, G. Multhaup, D. L. Brody, T. Esparza, M. Ingelsson, H. Kalimo, L. Lannfelt and T. A. Bayer (2010). "Pyroglutamate Abeta pathology in APP/PS1KI mice, sporadic and familial Alzheimer's disease cases." J Neural Transm **117**(1): 85-96.

Wirths, O., H. Breyhan, H. Cynis, S. Schilling, H. U. Demuth and T. A. Bayer (2009). "Intraneuronal pyroglutamate-Abeta 3-42 triggers neurodegeneration and lethal neurological deficits in a transgenic mouse model." Acta Neuropathol **118**(4): 487-496.

Woo, H. N., S. H. Baik, J. S. Park, A. R. Gwon, S. Yang, Y. K. Yun and D. G. Jo (2011). "Secretases as therapeutic targets for Alzheimer's disease." Biochem Biophys Res Commun **404**(1): 10-15.

Xu, S., K. R. Brunden, J. Q. Trojanowski and V. M. Lee (2010). "Characterization of tau fibrillization in vitro." Alzheimers Dement **6**(2): 110-117.

Zhang, H., S. Neal and D. S. Wishart (2003). "RefDB: a database of uniformly referenced protein chemical shifts." J Biomol NMR **25**(3): 173-195.

Zhao, L. N., H. Long, Y. Mu and L. Y. Chew (2012). "The toxicity of amyloid beta oligomers." Int J Mol Sci **13**(6): 7303-7327.

Zhao, L. N., L. Lu, L. Y. Chew and Y. Mu (2014). "Alzheimer's disease--a panorama glimpse." Int J Mol Sci **15**(7): 12631-12650.

Zilka, N., M. Korenova and M. Novak (2009). "Misfolded tau protein and disease modifying pathways in transgenic rodent models of human tauopathies." Acta Neuropathol **118**(1): 71-86.

Zlokovic, B. V. (2004). "Clearing amyloid through the blood-brain barrier." J Neurochem **89**(4): 807-811.

## Danksagung

Mein Dank geht an bei Prof. Dr. Dieter Willbold für die herzliche Aufnahme in seinem Institut am Forschungszentrum Jülich und die Bereitstellung des interessanten und aktuellen Forschungsthemas. Zusätzlich danke ich für die Möglichkeit zum Besuch sowohl nationaler als auch internationaler Konferenzen und Kurse und der der Schaffung exzellenter Forschungsbedingungen.

Ich möchte mich herzlich bei Prof. Dr. Henrike Heise für die Übernahme der Rolle als Mentorin sowie Zweitgutachter bedanken.

Der Graduiertenschule „BioStruct“ danke ich für die finanzielle Unterstützung in Form eines halbjährigen Stipendiums.

Mein ganz besonderer Dank geht an Dr. Melanie Schwarten für die herausragende fachliche Führung und die permanente Hilfestellung, ganz gleich in welcher Situation. Gemeinsame Diskussionen und ein offenes Ohr für jegliche Fragen und Probleme haben mich stets motiviert und maßgeblich zum Gelingen dieser Arbeit beigetragen.

Bei Dr. Lothar Gremer möchte ich mich für die Unterstützung bei langwierigen Experimenten und für fachliche Korrekturen bedanken.

An Dr. Justin Lecher geht mein Dank für die Geduld bei sich häufenden informationstechnischen Fragen und Problemen. Dr. Kerstin Reiß und Dr. Matthias Stoldt danke ich für die fachliche Hilfestellung und begleitende Motivation bei schwierigen Fragestellungen.

Ein großer Dank geht an Maren Thomaier, Tina Dunkelmann, Tamar Ziehm, Kateryna Kravchenko, Antonia Klein und Leonie Leithold für zahlreichen wissenschaftlichen Austausch, Diskussionen von Problemen aller Art und eine tolle Arbeitsatmosphäre.

Besonderer Dank geht an das Service-Team für die Bereitstellung vieler Medien und Puffer, die es mir ermöglicht haben meine Zeit für mein Projekt nutzen zu können. Und natürlich geht ein großer Dank an das komplette ICS-6 Team!

Für ständige moralische Unterstützung und die Begleitung verschiedener „Hochs“ und „Tiefs“ geht ein riesengroßer Dank an meine Familie und insbesondere an meine wunderbaren Eltern sowie meine Schwester! Ihr hab mich während der gesamten Zeit meiner Promotion stets unterstützt - Ohne euch wäre mir dies nicht möglich gewesen.

## Eidesstattliche Erklärung

Hiermit erkläre ich an Eides statt, dass ich die vorliegende Dissertation selbstständig verfasst und keine anderen als die von mir angegebenen Quellen und Hilfsmittel verwendet und Zitate deutlich kenntlich gemacht habe.

Ferner erkläre ich, dass ich in keinem anderen Dissertationsverfahren mit oder ohne Erfolg versucht habe, diese Dissertation einzureichen.

Jülich,

# List of publications

## Publications

2016, “The pyroglutamate amyloid-β(3-42) undergoes amyloid aggregation via an α-helical intermediate”; **Dammers C**, Reiß K, Lecher J, Gremer L, Ziehm T, Schwarten M, Willbold D; *(Journal of biological chemistry, under review)*

2015, “Aβ-directed therapy interferes successfully with pEAβ(3-42) induced degenerative phenotype in transgenic mice”; Dunkelmann T, Teichmann K, Tusche M, **Dammers C**, Jürgens D, Langen K J, Demuth H U., Shah N J, Kutzsche J, Willuweit A, Willbold D; *(to be submitted)*

2015, “Structural analysis and aggregation of pyroglutamate EAβ(3-40) in aqueous triflouroethanol”; **Dammers C**, Gremer L, Reiß K, Neudecker P, Klein AN, Schwarten M, Willbold D

2015, “Purification and characterization of recombinant N-terminally pyroglutamate-modified amyloid-β variants and structural analysis by solution NMR spectroscopy”; **Dammers C**, Gremer L, Neudecker P, Schwarten M, Willbold D; PLOS ONE

2014, “Rapid detection of different human anti-HCV immunoglobulins on electrical biochips”; Blohm L, Püttmann C, Holz S, Piechotta G, Albers J, **Dammers C**, Kleines M, Krüttgen A, Melmer G, Nähring J, Barth S, Nebling E; peer-reviewed article, Antibody Technology Journal, Volume 2014:4, Pages 23-32

**Conference presentations**

2015, “Structural analysis of pyroglutamate amyloid-β by NMR spectroscopy”; **Christina Dammers**, Kerstin Reiß, Lothar Gremer, Philipp Neudecker, Melanie Schwarten, Dieter Willbold; Conference poster presentation Düsseldorf-Jülich Symposium on Neurodegenerative Diseases (Germany, Düsseldorf)

2015, “Interaction studies of amyloid beta and therapeutic peptides by NMR spectroscopy”; Kerstin Reiss, **Christina Dammers**, Tamar Ziehm, Lothar Gremer, Philipp Neudecker, and Dieter Willbold; Conference poster presentation Düsseldorf-Jülich Symposium on Neurodegenerative Diseases (Germany, Düsseldorf)

2015, “Structural analysis of pyroglutamate amyloid-β(3-42) by solution state NMR spectroscopy”; **Christina Dammers**, Kerstin Reiß, Lothar Gremer, Philipp Neudecker, Melanie Schwarten, Dieter Willbold; Conference poster presentation EUROMAR 2015 (Prague, Czech Republic)

2015, “Selection and characterization of tau binding D-enantiomeric peptides for therapeutic applications in neurodegenerative diseases”; **Christina Dammers**, Deniz Yolcu, Marcus Pickhardt, Dieter Willbold, Eckhard Mandelkow, Susanne Aileen Funke; Conference poster presentation Alzheimer’s and Parkinson’s Diseases Congress – AD/PD (Nizza, France)

2013, “Selection and characterization of tau binding D-enantiomeric peptides for therapeutic applications in neurodegenerative diseases”; Susanne Funke, **Christina Dammers**, Dennis Yolcu, Laura Kukuk, Stephan Rudolph, Dieter Willbold; Alzheimer’s & Dementia, Volume 9 Issue 4 Supplement, July 2013, Pages P330

2012, “Hepatitis C Virus diagnosis on the basis of Core, NS3 and NS4A”; **Christina Dammers**, Christiane Püttmann, Alexandre Krüttgen, Stefan Barth, Jörg Nähring; Conference poster presentation Biomedica 2012 (Liège, Belgium)